Quasi-static cyclic tests on RC bridge piers with detailing deficiencies

Institut für Baustatik und Konstruktion, ETH Zürich

Quasi-static cyclic tests on RC bridge piers with detailing deficiencies

Pia Hannewald
Martin Bimschas
Alessandro Dazio

IBK Bericht Nr. 352, Dezember 2013

KEYWORDS:
RC bridge piers, wall-type, quasi-static cyclic tests, inelastic deformation behavior, detailing deficiencies, lap-splice, inelastic shear strength

Pia Hannewald, Martin Bimschas, Alessandro Dazio:
Quasi-static cyclic tests on RC bridge piers with detailing deficiencies

Bericht IBK Nr. 352, Dezember 2013

Sie finden das Verzeichnis der IBK-Publikationen auf unserer Homepage unter:
The catalogue of IBK publications is available on our homepage at:
www.ibk.ethz.ch/publications

Die meisten Berichte von Nr. 270 bis Nr. 333 sind auch noch in gedruckter Form unter Angabe der ISBN-Nr. erhältlich bei:
Most reports from No. 270 to No. 333 can still be purchased in printed form by indicating the ISBN number from:

AVA Verlagsauslieferung AG
Centralweg 16
CH-8910 Affoltern am Albis

Tel. ++41 44 762 42 00
Fax ++41 44 762 42 10
e-mail: avainfo@ava.ch

Berichte ab Nr. 334 sind nur noch in elektronischer Form verfügbar. Sie finden die entsprechenden Dateien in der e-collection der ETH Bibliothek unter http://e-collection.library.ethz.ch oder über die Links auf unserer Homepage.
Reports from No. 334 onwards are only available in electronic form. The respective files can be found in the e-collection of the ETH Library at http://e-collection.library.ethz.ch or through the links on our homepage.

Quasi-static cyclic tests on RC bridge piers with detailing deficiencies

Pia Hannewald
Martin Bimschas
Alessandro Dazio

Institute of Structural Engineering
Swiss Federal Institute of Technology

Zürich
Dezember 2013

Preface

The quasi-static cyclic tests on four reinforced concrete bridge piers representative of the Swiss building tradition from the 1960s and 1970s presented in this report are part of a broader research effort funded by the Swiss Federal Roads Office (ASTRA) aiming to provide the bases for a rational displacement-based assessment strategy of the seismic safety of all highway bridges in the country.

The large scale (1:2) test units represent existing bridge piers with wall-type rectangular cross-section and relatively low slenderness. Such piers are commonly used to brace continuous girder bridges in the transverse direction and despite the low to moderate seismicity of Switzerland they were identified as potentially critical, especially because of their inherent seismic deficiencies, such as very low transverse reinforcement ratios and lap-splices in potential plastic regions, typical of the considered historical period, during which the majority of the existing bridges was designed.

The thorough description of the observed behaviour and the extensive measurements of both local and global deformation quantities up to total failure allow a comprehensive understanding of the phenomena influencing the force-deformation behaviour of the test units. The results indicate that despite the significant structural deficiencies, the piers were able to sustain quite large inelastic deformations, even though their hysteretic behaviour is characterised by important softening effects. Nevertheless, as long as the axial load carrying capacity is not affected, as it was the case for the tested piers, it is believed that explicitly considering the softening phase of single piers during the assessment of bridges is a viable strategy to verify more realistically their adequate structural safety, thus avoiding expensive and unnecessary retrofit interventions.

In a next phase, the test results will be used to support the development of mechanical models for the reliable estimation of the force-deformation behaviour of RC bridge piers incorporating structural deficiencies. Such models are an indispensable condition for the attainment of the final goal of the research effort.

Pavia, 2013 Alessandro Dazio

Summary

This report documents the tests on four wall-type reinforced concrete bridge piers, that were tested in the framework of a research project funded by the Federal Roads Office (FEDRO). Seven piers were tested in total during this research, the first three are already documented in [Bim10]. This test series aimed at providing some insight into the cyclic behavior of existing bridge piers which were not designed to withstand earthquakes. For this reason, the detailing of the test units corresponded to detailing that is often found in reality but not permissible according to modern seismic design codes, such as low transverse reinforcement ratios and lap-splices at the base of the pier.

The test units in 1:2 scale were tested quasi-statically under single curvature bending with increasing displacement amplitudes up to failure. Measurements included the top displacement and the elongation along the sides of the test units as well as the deformation on the surface of the test units. The lateral displacements and vertical elongation along the sides were measured by means of LVDTs. The deformations on the surface, were typically measured by means of targets that were glued in a 150 mm $\times$ 150 mm grid and tracked by an optical measurement system. These measurements allowed for determining displacement and strain fields.

In this report, the results of the measurements on the four tests are documented and shown graphically. The graphs include the measured load-deformation relationships, the moment-curvature relationships and strain fields of selected load steps. Furthermore, the most important observations that were made during the tests are reported.

Zusammenfassung

Dieser Bericht dokumentiert die Versuche an vier wandartigen Stahlbeton-Brückenstützen, die im Rahmen eines von dem Bundesamt für Strassen (ASTRA) finanzierten Forschungsprojektes durchgeführt wurden. Insgesamt wurden im Rahmen dieses Projektes sieben Versuchskörper getestet, die ersten drei davon werden in [Bim10] dokumentiert. Ziel der Versuchsreihe war es, Einblicke in das zyklische Verhalten von bestehenden Brückenstützen, die nicht für eine Erdbebeneinwirkung bemessen wurden, zu bekommen. Aus diesem Grund hatten die Versuchskörper konstruktive Details, die zwar bei bestehenden Stützen häufig zu finden sind, aber gemäss heutiger seismischer Normen nicht zulässig wären, wie zum Beispiel geringe Querbewehrungsgehalte und Bewehrungsstösse am Stützenfuss.

Die Versuchskörper im Massstab 1:2 wurden als Kragarme unter quasi-statischer Belastung mit ansteigender Kopfauslenkung bis zum Versagen getestet. Die Messungen umfassten die Horizontalverschiebungen, die Verformungen entlang der Seiten sowie die Verformungen auf der Oberfläche der Versuchskörper. Die Horizontalverschiebungen und Vertikalverformungen entlang der Seite wurden mittels Weggebern gemessen. Um das Verformungsfeld zu messen kam in der Regel ein optisches Messsystem zum Einsatz, mit dem die Verschiebungen von Messpunkten, die in einem 150 mm × 150 mm aufgebracht wurden, gemessen wurden. Diese Messungen konnten zur Bestimmung von Verschiebungs- und Dehnungsfeldern verwendet werden.

In dem vorliegenden Bericht werden die Messergebnisse der vier Versuchskörper dokumentiert und graphisch dargestellt. Es werden unter anderem die gemessenen Last - Verformungskurven, Momenten - Krümmungskurven und Dehnungsfelder aller Versuchskörper bei ausgewhlten Laststufen wiedergegeben. Ausserdem werden die wichtigsten Beobachtungen, die während der Versuchsdurchführungen gemacht wurden, dokumentiert.

Contents

1 Introduction

1.1 Problem Statement

Before modern seismic codes were introduced, bridges were often built with reinforced concrete piers featuring detailing characteristics which are nowadays avoided in seismic design. In Switzerland, many bridges were built prior to 1989 when such codes were introduced and therefore feature for example lap splices in potential plastic hinge regions, low transverse reinforcement ratios and no confining reinforcement. With these detailing characteristics a ductile behavior cannot be ensured and brittle failure of the structure might occur.

To predict the actual displacement capacity of both existing and new structures, reliable models are needed. When an existing structure is assessed, reliable models are important, since the predicted capacity will form the basis on which the decision on whether retrofitting is necessary is made. Underpredicting the capacity could in this case lead to uneconomical retrofitting measures, whereas overpredicting the capacity would underestimate the risk and yield unconservative results. However, a reliable prediction of the force-displacement relationship and hence the displacement capacity is still a challenging endeavor, especially for existing structures. One reason for the latter arises from the fact that many predictive models were calibrated against tests with detailing according to modern seismic codes and consideration of detailing deficiencies is not included. Moreover, experimental data on piers with detailing deficiencies is scarce and the validation of existing models for this type of piers hence difficult.

1.2 Objective and Scope of the Test Program

The objective of this test program is to provide high quality experimental evidence on the behavior of piers with the above mentioned detailing deficiencies. The data obtained from these tests can then be used in a next step to develop and validate mechanical models describing the force-deformation behavior as well as to determine the failure limits and thereby eventually the displacement capacity.

The overall test campaign includes two parts. In a first part, which is presented in [Bim10], three piers with low transverse reinforcement ratios, no confining reinforcement and, in one case, a lap splice in the plastic hinge region were tested. However, some parameters, namely the transverse reinforcement ratio and the aspect ratio, whose influence on the failure mode and the deformation behavior is generally considered to be significant, were not varied. In order to provide a more comprehensive set of data, including the mentioned parameters, a second part of the test campaign was initiated, which is presented in this report.

The experimental data collected in this test campaign contributes to closing the previously mentioned gap among existing experimental evidence. A large number of force and deformation quantities were measured to describe the global as well as the local behavior of the test units. Eventually, these tests contribute to providing a more comprehensive basis for the development of improved mechanical models needed for a rational displacement-based assessment.

1.3 Test Program

To investigate the load-deformation behavior up to the point of failure of existing bridge piers incorporating structural deficiencies, a total of seven piers was tested at scale 1:2. The test units were subjected to single bending under reversed cyclic loading with increasing target displacements until either the axial force bearing capacity was lost or a residual shear force resistance was reached. To provide an overview of the entire program, the characteristics of all test units, presented in [Bim10] and in this report, are summarized in Table 1.1.

Part	Test unit	Shear span a	Aspect ratio (a/d)	Longitudinal reinforcement ratio	Lap splice	Transverse reinforcement ratio
1*	VK1	3.30 m	2.2	$\varrho_l = 0.82\%$	no splice	$\varrho_t = 0.08\%$
	VK2	3.30 m	2.2	$\varrho_l = 0.82\%$	$\sim 43d_l$	$\varrho_t = 0.08\%$
	VK3	3.30 m	2.2	$\varrho_l = 1.23\%$	no splice	$\varrho_t = 0.08\%$
2	VK4	3.30 m	2.2	$\varrho_l = 1.23\%$	$\sim 43d_l$	$\varrho_t = 0.08\%$
	VK5	4.50 m	3.0	$\varrho_l = 1.23\%$	$\sim 43d_l$	$\varrho_t = 0.08\%$
	VK6	4.50 m	3.0	$\varrho_l = 1.23\%$	no splice	$\varrho_t = 0.08\%$
	VK7	3.30 m	2.2	$\varrho_l = 1.23\%$	no splice	$\varrho_t = 0.22\%$

Table 1.1: Dimensions and reinforcement of the test units of the entire test program ([*] reported in [Bim10]).

In the second part of the test program which is presented in this report, all piers had the same rectangular cross section dimensions of 35 cm width and 150 cm length, as well as the same longitudinal reinforcement ratio of $\varrho_l = 1.23\,\%$ provided by $\mathrm{d_l} = 14$ mm bars. Transverse reinforcement ratios varied between $\varrho_t = 0.08\,\%$ and $\varrho_t = 0.22\,\%$ and were provided by bars that were not anchored in the core concrete. Confining reinforcement was not provided, as well. Two piers with a shear-span-to-depth ratio of $a/d = 2.2$ and two piers with $a/d = 3.0$ were tested. The difference between the two piers with $a/d = 3.0$ was a lap splice of the longitudinal reinforcement at the bottom of one pier. A splice length of 60 cm corresponding to $43d_l$ was chosen, which is in the range of the shortest length ever allowed by the Swiss design codes. One of the piers with $a/d = 2.2$ (VK4) also had a splice with the same length at the bottom of the pier, the other one (VK7) had no splice and was the only pier tested with a higher transverse reinforcement ratio. For the longitudinal reinforcement hot-rolled ductile reinforcement with 521 MPa yield stress and 609 MPa ultimate strength was used. The piers were all constructed with the same type of concrete, with a strength varying between 32 to 44 MPa at the day of testing.

As it can be seen from Table 1.1, the characteristics of the test units tested within the first part of the program - i.e. VK1, VK2 and VK3 - were similar to those of the units tested within the second part. The first two test units had a lower longitudinal reinforcement ratio of $\varrho_l = 0.82\,\%$, while the characteristics of the lap splices, i.e. a length of 60 cm, were the same as those in the second part of the test program

1.4 Outline of the Report

Chapter 2 contains detailed information on the test units. The technical drawings of test units VK4 to VK7 are presented along with an overview of the varied parameters. The chapter also provides information on the construction of the test units as well as on the material, i.e. the concrete and steel mechanical properties. In Chapter 3 the test setup and the testing procedure are described. Drawings of the test setup are provided together with description of how the test units were mounted in the test stand. Detailed information on the measurement setups, which comprise hard-wired measurements along the sides of the test units, manual and optical measurements over the longitudinal faces of the test units and crack width determination, can be found in Section 3.2 alongside drawings of the measurement setup. Background information on the chosen load history is given in Section 3.3. In Chapter 4 the results of all tests are presented. Section 4.1 contains a description of how each type of data is processed and presented in the report. In the following Sections 4.2 through 4.5 the observations and data of the experiments are presented. Each section follows the same outline. First, the observations made during the test are described. Then, graphs presenting the hard-wired measurement data, the optical or manual measurement data as well as crack widths are included. In the last part of the chapter the deformation components, namely sliding, shear, flexural and fixed-end deformation, are presented.

2 Test Units

2.1 Dimensions and Reinforcement

Four piers, whose dimensions and reinforcement details are listed in Table 2.1, were constructed for this test series. The design of the piers was based on four sample piers of existing Swiss bridges built between 1965 and 1971, whose detailing was typical of piers constructed in this time period. Background information on the choice of the sample piers and the chosen layout for the test units can be found in [Bim10], which also contains information about the testing of units VK1 to VK3. Piers VK4 to VK7 (VK: **V**ersuchs**k**örper = Test Unit) are variations of these test units.

Test unit	VK4	VK5	VK6	VK7
Total height	3.70 m	4.85 m	4.85 m	3.70 m
Shear span a	3.30 m	4.50 m	4.50 m	3.30 m
Longitudinal reinforcement	42 × d14 mm	42 × d14 mm	42 × d14 mm	42 × d14 mm
Longitudinal reinforcement ratio	$\varrho_l = 1.23\%$	$\varrho_l = 1.23\%$	$\varrho_l = 1.23\%$	$\varrho_l = 1.23\%$
Lap splice	600 mm $\sim 43d_l$	600 mm $\sim 43d_l$	no splice	no splice
Transverse reinforcement	$d_t = 6$ mm, s=200 mm	$d_t = 6$ mm, s=200 mm	$d_t = 6$ mm, s=200 mm	$d_t = 6$ mm, s=75 mm
Transverse reinforcement ratio	$\varrho_t = 0.08\%$	$\varrho_t = 0.08\%$	$\varrho_t = 0.08\%$	$\varrho_t = 0.22\%$

Table 2.1: Dimensions and reinforcement of the test units.

All piers had the same width of 35 cm and length of 150 cm, whereas the height and thereby the shear-span-to-depth-ratio a/d varied. Test units VK4 to VK7 had the same longitudinal reinforcement, consisting of 42 bars of diameter $d_l = 14$ mm, which resulted in a geometric reinforcement ratio of $\varrho_l = 1.23\%$. The longitudinal reinforcement was anchored at the bottom of the foundation with a 200 mm long 90° hook. Two of the test units had 600 mm $\sim 43d_l$ long straight lap-splices at the bottom of the pier. According to SIA162:1968 [SIA68] and SIA162:1989 [SIA93], splice lengths of at least $45d_l$ and $40d_l$, respectively, were required in general and lengths of $65d_l$ and $60d_l$, respectively, for splices in regions with tensile stress. Before these two generations of codes, in SIA162:1956 [SIA56], provisions were only made for

splices with hooks. The splice length chosen for the test units is therefore in the range of the shortest splice length ever allowed in Switzerland for straight bars.

A transverse reinforcement ratio of $\varrho_t = 0.08\%$, adopted from one of the reference piers, was chosen for all piers except VK7. From 1968 on, a ratio this low was no longer allowed and a minimum transverse reinforcement ratio of 0.15 % first [SIA68] and 0.2 % later [SIA93], was required. VK7 was designed for shear according to [SIA03] and [SIA93]. For the shear design, the maximum value obtained from the pier's moment capacity, considering overstrength, and the previous test data [Bim10] was considered. This led to a reinforcement ratio of $\varrho_t = 0.22\%$. The transverse reinforcement of all piers consisted of $d_t = 6$ mm stirrups featuring 100 mm long 90° hooks, meaning that the hooks were not anchored in the core concrete. The stirrups of VK4 through VK6 were spaced s=200 mm apart ($\varrho_t = 0.08\%$) and those of VK7 s=75 mm ($\varrho_t = 0.22\%$). At the top part of the pier, where the horizontal and vertical forces were applied, the stirrup spacing was always 75 mm. The transverse reinforcement had a clear concrete cover of $c_{nom,t} = 20$mm resulting in $c_{nom,l} = 26$mm clear cover of the longitudinal reinforcement.

All foundations were 300 cm long, 144 cm wide and 90 cm high. As the foundations were later fixed to the strong floor with six prestressed bars of diameter 42 mm their dimensions were partly determined by the tie-down pattern. Four additional bars were used for horizontal prestressing of the foundation. Two Deha 6351-12.5-550 socket lifting anchors were provided at the top of the pier and two to four Deha 6000-10-340 lifting anchors in the foundation for transportation. The technical drawings, elevation and cross section, of the piers' reinforcement layouts and dimensions are shown in Figures 2.1 to 2.4. Technical drawings of the foundations, which were merely designed as a stiff bearing for the pier, are not included in this report.

2.2 Construction

The piers were built by Stüssi AG in Dällikon (ZH) between September 2009 and July 2010. The date of construction of the test units as well as the time range during which the test units and the concrete material samples were tested are summarized in Table 2.2.

test unit	VK4	VK5	VK6	VK7
Casting of foundation	23.09.09	26.10.09	22.01.10	13.07.10
Casting of pier	29.09.09	06.11.09	05.02.10	16.07.10
Start of test	23.11.09	18.03.10	12.05.10	18.08.10
End of test	17.12.09	29.03.10	01.06.10	01.09.10
Duration of test	25 days	12 days	21 days	15 days
Material tests	10.12.09 & 11.03.10	11.03. & 08.04.10	14.05. & 04.06.10	03.09.10

Table 2.2: Dates of construction as well as testing of the test units and the concrete material samples.

Construction of each pier began with the foundation including the longitudinal reinforcement bars. The reinforcement bars on which strain gauges were applied were arranged so that the center of the gauge was 90 cm above the bottom plate of the formwork, where the construction joint would later be, see also Figure 3.4. After the concrete was poured and compacted, the top surface of the foundation was only planed outside the core area of the pier. If necessary, the core area was roughened by stirring up the fresh concrete on the surface moving a trowel along a zigzag pattern. Pictures of this joint surface are provided in Figure 2.5. No other special measures were taken to roughen the concrete before casting of the pier.

When the foundation was completed, the rest of the longitudinal reinforcement, if the reinforcement was spliced, and the stirrups were added. As the casting direction and height influences properties such as bond conditions or concrete compaction, all piers were cast upright, to obtain realistic characteristics. A Doka Framax XLife formwork was used, which allowed casting even the taller piers in one single step. Concrete was pumped into the formwork up to a height of about 0.5 to 1.0 m and compacted, then the next load of concrete was pumped in up to a height of about 2.0 m and compacted and so forth until the pier was finished. Casting and compacting of the piers lasted about half an hour each time. When the concrete works were finished, the top of the pier was sealed with a plastic cover and the pier remained in the formwork for about a week to minimize cracking due to shrinkage. Piers were turned horizontally for transportation and turned back up for testing using the provided anchors.

Some problems occurred with the formwork, especially during construction of the first test unit, as extra boards had to be inserted in the formwork at the narrow (lateral) faces of the pier. The couplings which would later support the LVDTs (see Section 3.2.1) were fixed to those boards. Thereby the connection to the formwork panels of the wide (longitudinal) faces was apparently weakened and the panels were pushed outwards on each end of the pier, resulting in widths larger than 35 cm. Some cement leaked through the construction joints of the formwork panels of VK4, hence the aggregate was visible along these joints after stripping. To create an even surface, the joints were repaired with a high strength mortar. The dimensions of all piers measured after delivery to the laboratory are displayed in Figure 2.6. In the middle, the width of the piers was measured through the holes of the formwork anchors, so they could not be measured as accurately as on the wall faces. The dimensions were measured about every meter starting from the pier base or where the holes of the anchors and formwork joints were. The lengths of the piers were usually rather exact, varying only by about ± 5 mm. VK6 was only measured along the sides, as the wall surface was even.

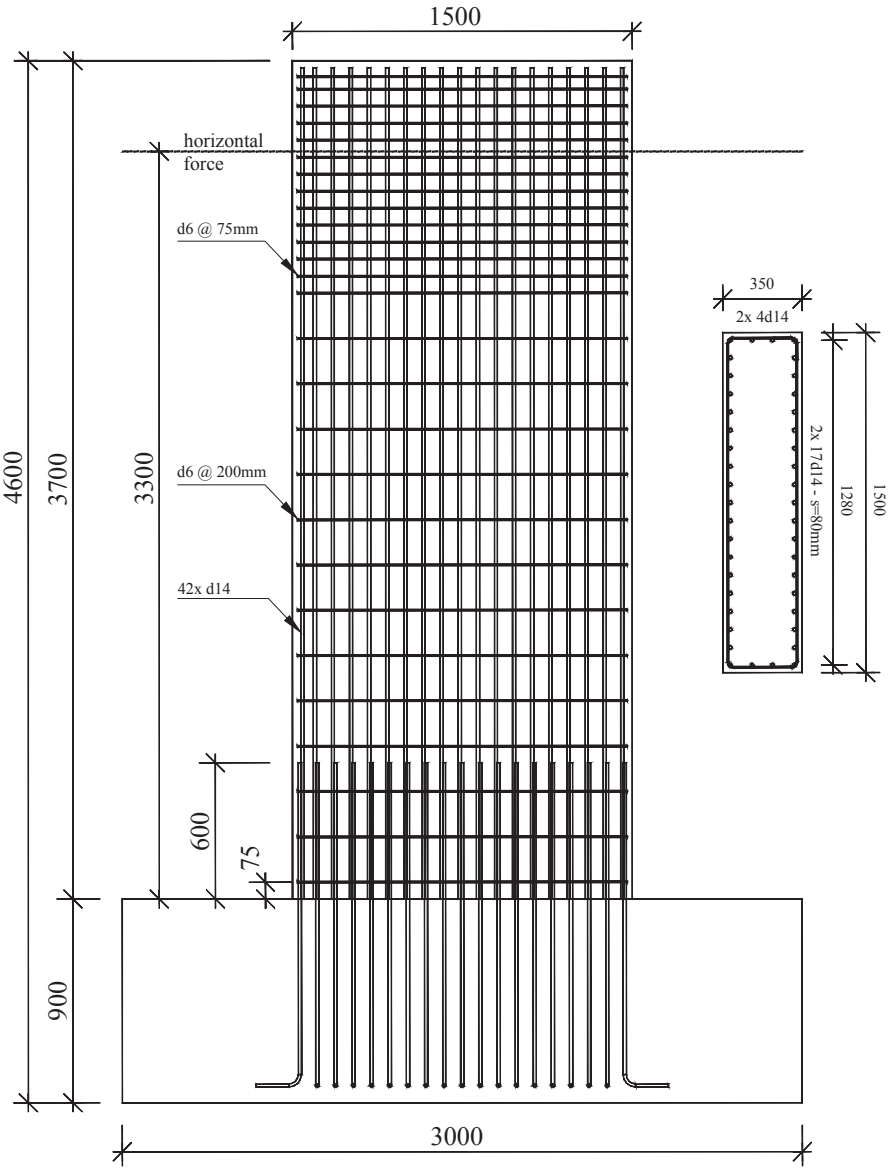

Figure 2.1: Reinforcement layout - elevation and cross section of test unit VK4. All dimensions in [mm].

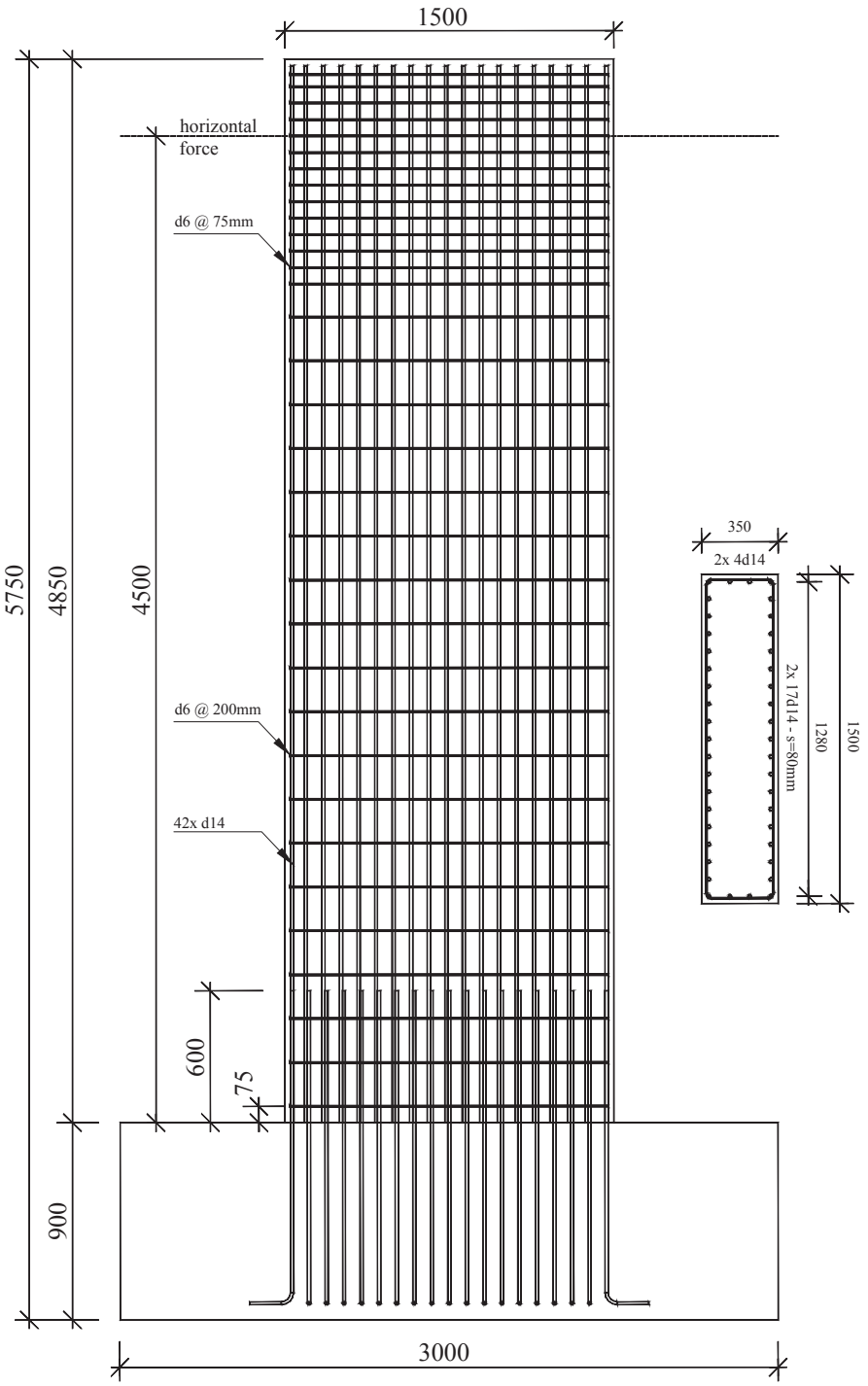

Figure 2.2: Reinforcement layout - elevation and cross section of test unit VK5. All dimensions in [mm].

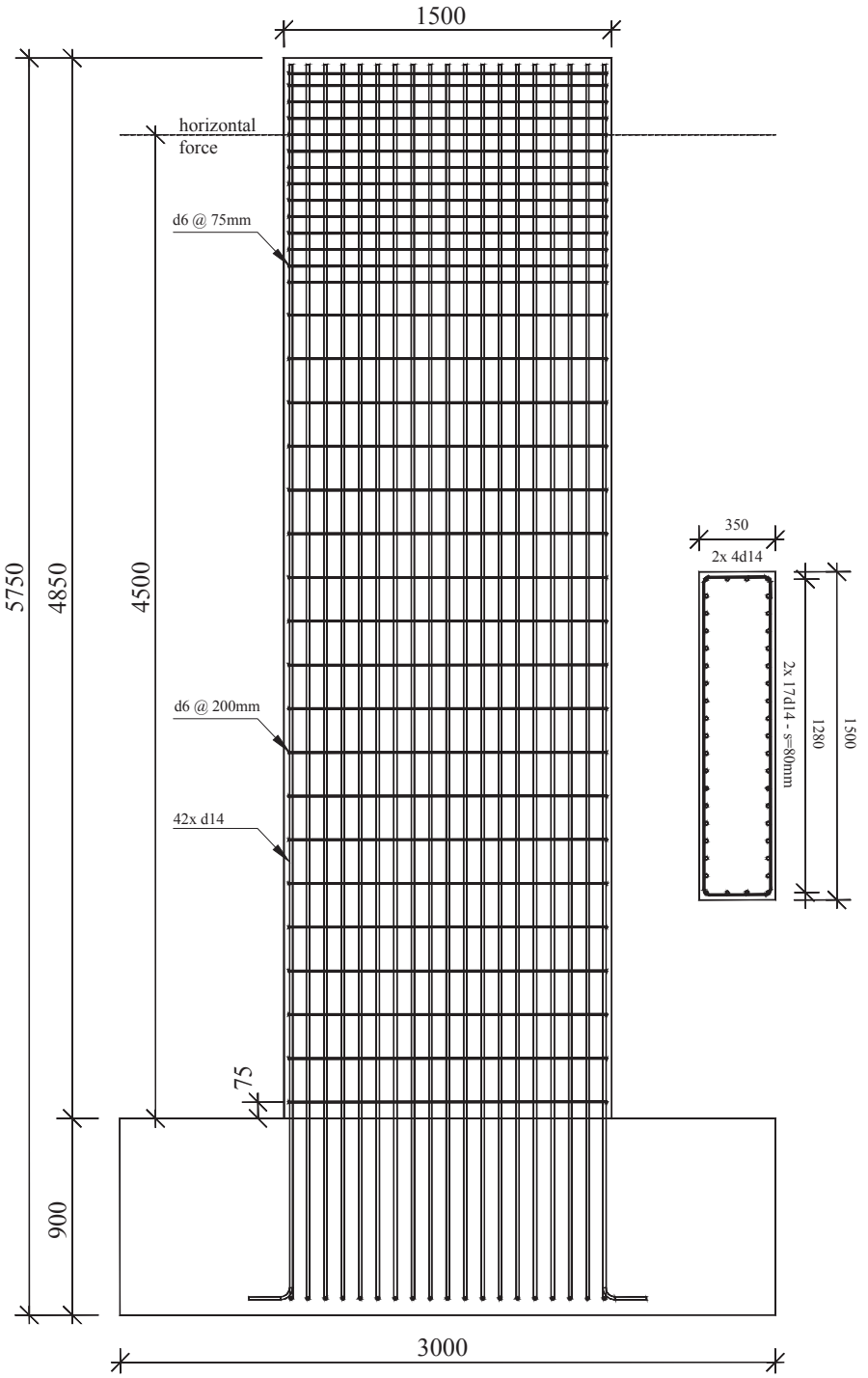

Figure 2.3: Reinforcement layout - elevation and cross section of test unit VK6. All dimensions in [mm].

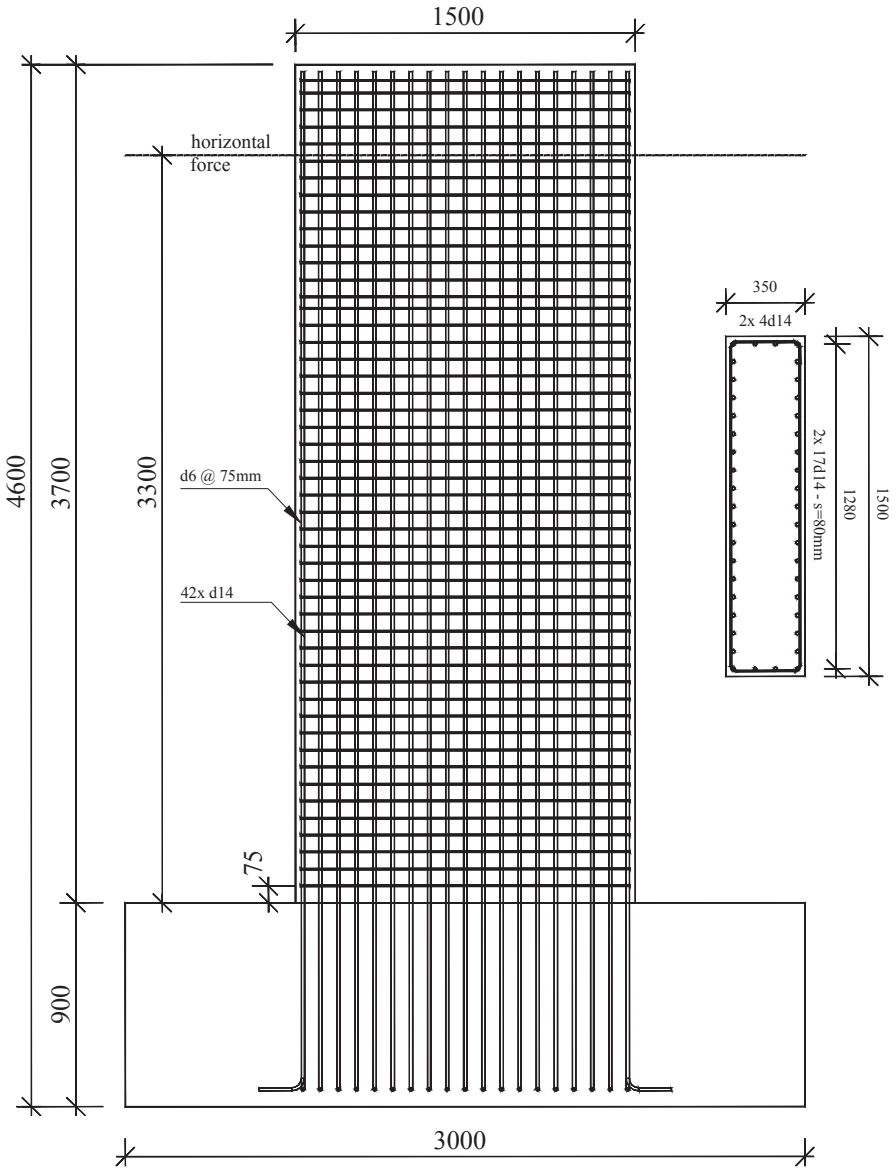

Figure 2.4: Reinforcement layout - elevation and cross section of test unit VK7. All dimensions in [mm].

Figure 2.5: Pictures of the construction joints of VK4 (left) and VK5 (right). Construction joints of VK6 an VK7 were treated in the same manner.

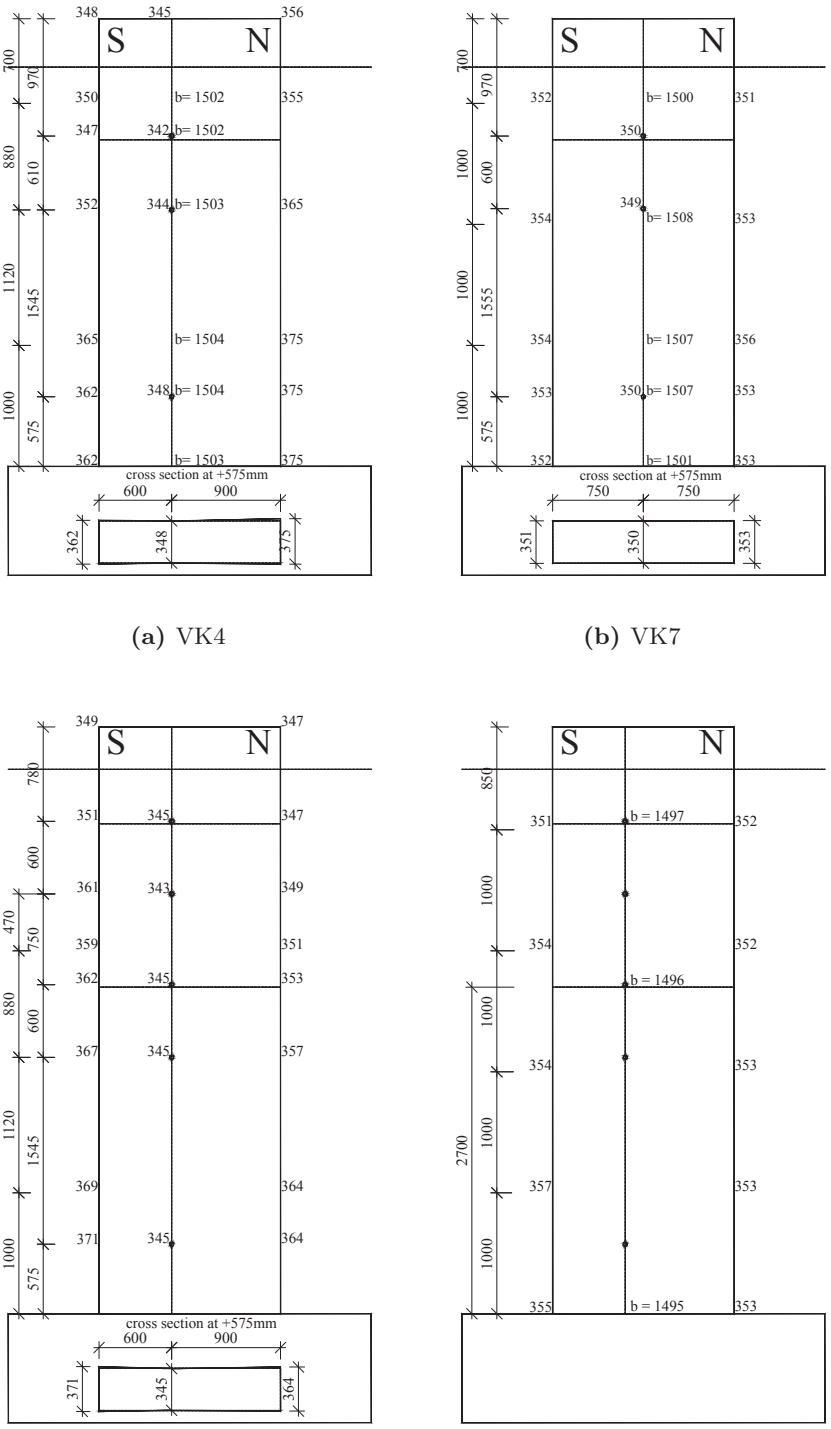

(a) VK4 **(b)** VK7

(c) VK5 **(d)** VK6

Figure 2.6: Dimensions of the test units measured after delivery to the laboratory. The dimensions are written next to the location were they were measured, formwork joints and anchor holes are indicated in the drawings. All dimensions in [mm].

2.3 Material

2.3.1 Concrete

Two different kinds of concrete were used for construction of the test units. The foundation concrete was a standard mix made by Stüssi AG while the concrete used for the piers was concrete no. A153 with the mix design according to Table 2.3 from Holcim AG. During the construction period of the piers, the mixture of the concrete was varied slightly. Cement was changed from Normo4 (VK4) to Fluvio4 (VK5, VK6) and eventually Optimo4 (VK7), all of compressive strength class 42.5N. In this section, the dates and results of the concrete material tests performed right before or after completion of the pier tests are provided.

Aggregate 0/16	1847 kg
Maximum grain size	16 mm
Cement minimum	308 kg
Water cement ratio w/c_{eq}	$\sim$ 0.58 to 0.62
Compressive strength class (according to SN EN 206-1)	C25/30

Table 2.3: Pier concrete mix design as provided by Holcim AG.

The following values were determined in the material tests:

$f_{c,cube}$ Concrete cube strength (cube: 150 × 150 × 150 mm).

$f_{c,cyl}$ Concrete cylinder strength (cylinder: diameter = 150 mm, height = 300 mm).

$f_{ct,3Pb}$ Tensile strength of concrete determined from a three-point bending test on a 300 mm long beam with a square cross section (sidelength 120 mm).

$f_{ct,dp}$ Tensile strength of concrete determined from double-punch tests according to Equation 2.1 [CY80]

$$f_{ct,dp} = \frac{F}{\pi(1.2rh - a^2)} \tag{2.1}$$

with the punching force F, cylinder height $h = 145$ mm and radius $r = 75$ mm and the steel punch radius $a = 19$ mm.

$E_{c,SIA}$, $E_{c,\sigma-\varepsilon}$ modulus of elasticity determined according to [SIA89] and from $\sigma - \varepsilon$ curve, respectively.

$\varepsilon_{c,cu}$ Strain at compressive strength of concrete.

ρ Density calculated from weight and dimensions of all cylinders tested for each unit.

The standard wall test series comprised three cylinders ($f_{c,cyl}$, $\varepsilon_{c,cu}$, E_c) and cubes ($f_{c,cube}$), four double punch tests ($f_{ct,dp}$), cut out of two cylinders, as well as four three point bending tests on prisms ($f_{ct,3Pb}$). Material tests of the foundation concrete were kept to a minimum and only three cubes were tested each time to determine the strength at the day of testing.

Additional tests were made as listed in Table 2.4. All tests were conducted on a Walter+Bai testing machine.

The tests to determine the stress-strain relationships were run displacement controlled with a velocity corresponding to a strain increase of 0.02‰/s. In most cases, $f_{c,cyl}$ was calculated from the peak load obtained from these stress-strain curves. If cylinder compressive tests were made, they were run in force control with a loading velocity corresponding to a stress increase of 0.6 MPa/s, equal to the velocity used in the cube tests. The three-point-bending tests were loaded with 0.05kN/s, the double punch tests with a velocity corresponding to a compressive strain increase of 0.02MPa/s, referring to the complete cross section.

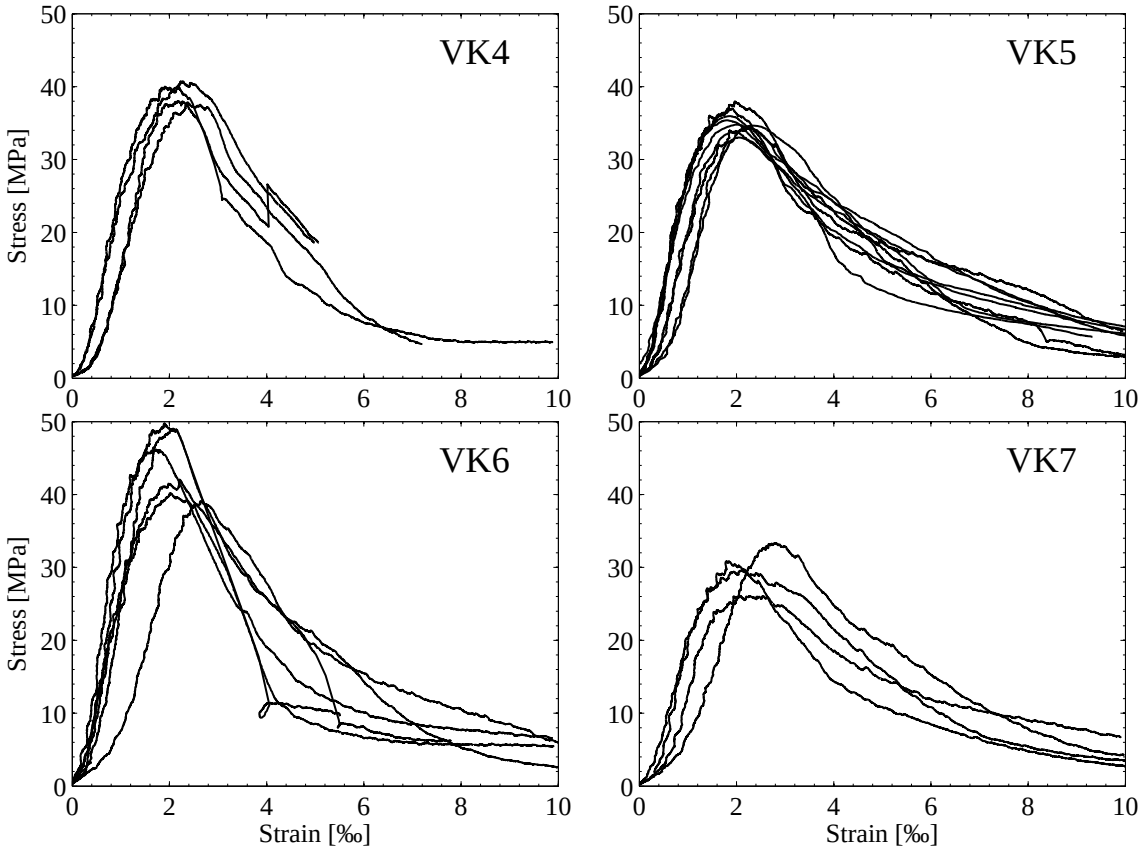

Figure 2.7: Concrete stress-strain relationships obtained from cylinder tests and strains determined from piston stroke.

Two different approaches were used to determine the modulus of elasticity E_c. It was determined as both the secant modulus in the third loading cycle, $E_{c,SIA}$ according to SIA162/1 [SIA89] and as secant modulus on the first loading branch $E_{c,\sigma-\varepsilon}$. In general, three cylinders were used to determine $E_{c,SIA}$, while $E_{c,\sigma-\varepsilon}$ was determined on all six material samples.

$E_{c,SIA}$ was determined in the third loading cycle between a bottom stress of 0.5 MPa and a peak stress of 14 MPa, corresponding to approximately $1/3 f_{c,cube}$. The stress and strain differences between 2 MPa and 13 MPa (instead of 0.5 MPa and 13 MPa) in that third cycle were used to calculate $E_{c,SIA}$, since the stress-strain relationship was almost straight in that area. In these tests, two extensometers with 150 mm base length, clamped to the cylinders, measured

the strains. Those measurements were also used to calibrate the piston stroke, which is affected by the machine's stiffness otherwise. The calibrated piston stroke was later needed to calculate the strains when the stress-strains relationships were determined. After the test to determine $E_{c,SIA}$ was completed, the cylinder had to be taken out of the machine to remove the device carrying the extensometers and was then put back in to determine the complete stress-strain relationship.

From the stress-strain relationships, the cylinder compressive strength $f_{c,cyl}$, the corresponding strain $\varepsilon_{c,cu}$ as well as the modulus of elasticity on the initial loading branch $E_{c,\sigma-\varepsilon}$ were determined. Usually, the cylinders were loaded until the strain was about 10 ‰ but some tests were stopped earlier. If the cylinder was one of the three used to determine $E_{c,SIA}$, then $E_{c,\sigma-\varepsilon}$ was determined in the first of the three cycles as secant modulus between 2 MPa and 13 MPa on the initial loading branch using the strains obtained from the extensometer readings. If it was one of the other three cylinders, $E_{c,\sigma-\varepsilon}$ was determined from the piston stroke. The cylinder strength $f_{c,cyl}$ and the corresponding stress $\varepsilon_{c,cu}$ were always obtained from the stress-strain relationship. Hence, $E_{c,\sigma-\varepsilon}$ was determined three times using the extensometer readings and three times by means of the piston stroke, whereas $\varepsilon_{c,cu}$ was determined from the piston stroke each time. In Table 2.4 only the mean value of all six $E_{c,\sigma-\varepsilon}$ is given and no distinction is made between the two different sources of the strains. However, it can be noted that the coefficient of variation is larger for the values determined from the piston stroke, since it is not as accurate as the extensometer readings. In Figure 2.7 the stress-strain relationships as determined from the calibrated piston stroke and the machine's internal load-cell signal are presented. In the graphs it can be seen that the relationships determined with the piston stroke have an initial offset and a remaining influence of the machine's stiffness. As the offset usually was in the range of 0.1-0.2 ‰ at 2 MPa and could only be estimated for those cylinders used for determination of $E_{c,SIA}$, i.e. when the extensometer measurements were made, it was not subtracted from any of the results.

During the large scale test of unit VK4, three cylinders were tested, but the $\sigma-\varepsilon$ relationship was not determined. Therefore, those tests have been conducted later with the remaining cylinders. The values from these tests are given in the second column of VK4 in Table 2.4. In the case of VK5 and VK6, only one value is presented for each quantity, since the material tests were conducted right before and after the pier test in each case and one mean value of each quantity was deemed appropriate to characterize the properties of the pier.

One curve of the cylinders of VK4 has an inexplicable jump after the peak and two of the curves of VK6 contain sudden stress drops, but the data is presented in the graphs nevertheless. For some reason, the concrete cylinder strength is greater than the cube strength measured in the VK6 material tests. One explanation might be that two of three cubes, as well as two of the four prisms had to be taken out of the formwork very early. In the case of the cubes, this might have caused some damage to the specimen. Two concrete cylinders of VK7 were tested much later than the others, because there was some problem with the extensometers during the first tests. Therefore, $E_{c,SIA}$ was only determined in two tests.

	VK4		VK5	VK6	VK7
	value & # tests	value & # tests	value & # tests	value & # tests	value & # tests
Pier					
sample age [d]	72	163	125 & 153	98 & 119	49
$f_{c,cube}$	41.7 ± 1.8%		44.3 ± 4.9%	37.1 ± 9.7%	38.9 ± 3.4%
[MPa]	3		6	3	6
$f_{c,cyl}$	34.6 ± 0.5%	39.2 ± 3.5%	35.2 ± 4.4%	44.4 ± 10.3%	30.0 ± 10.1%
[MPa]	3	4	9	6	4
$f_{ct,3Pb}$	4.1 ± 10.8%		6.34 ± 1.3%	4.89 ± 6.1%	4.90 ± 10.0%
[MPa]	4		4	4	4
$f_{ct,dp}$	3.02 ± 10.2%		3.30 ± 8.4%	3.52 ± 8.7%	2.46 ± 15.2%
[MPa]	4		4	6	6
$E_{c,SIA}$	27.6 ± 5.7%	27.8	27.6 ± 2.7%	32.1 ± 5.9%	26.4
[GPa]	3	2	3	3	2 (133d old)
$E_{c,\sigma-\varepsilon}$	26.5 ± 5.7%	24.9 ± 14.7%	23.7 ± 19.7%	26.0 ± 29.8%	18.7 ± 29.5%
[GPa]	3	4	9	6	4
$\varepsilon_{c,cu}$		2.19 ± 9.4%	2.02 ± 8.8%	2.1 ± 15.4%	2.21 ± 18.8%
[‰]		4	9	6	4
ρ	2290 ± 1.1%		2291 ± 0.4%	2314 ± 0.6%	2292 ± 0.3%
$[\frac{\text{kg}}{\text{m}^3}]$	10		9	6	6
Foundation					
sample age [d]	78		164	112	52
$f_{c,cube}$	54.1 ± 4.6%		56.5 ± 4.5%	49.5 ± 4.4%	39.7 ± 1.0%
[MPa]	3		3.0	3	3
$f_{c,cyl}$	43.5 ± 4.1%			44.4 ± 3.3%	
[MPa]	3			3	
$E_{c,\sigma-\varepsilon}$				28.7 ± 13.6%	
[GPa]				3	
$\varepsilon_{c,cu}$				2.05 ± 10.0%	
[‰]				3	
$f_{ct,dp}$				3.48 ± 12.9%	2.87 ± 1.0%
[MPa]				4	3

Table 2.4: Concrete properties of test units VK4 to VK7, mean values and coefficient of variation in the first rows, and number of tests in the second.

2.3.2 Steel

Two different kinds of reinforcing steel produced by Stahl Gerlafingen AG were used for the test units. The longitudinal reinforcement consisted of hot-rolled, ductile reinforcing bars type "topar-S 500C" with 14 mm diameter. For the stirrups micro-alloyed cold-formed bars with 6 mm diameter were used. All steel tests were conducted on a servo-hydraulic testing machine type Schenk ± 480 kN before construction of the test units. The results of the tests are presented in Table 2.5.

The following values were determined in the material tests:

E_s	Modulus of elasticity; determined as secant modulus in the elastic range using 1/3 and 2/3 of $f_{s,y,dyn}$ or $R_{p,0.2}$ with the related strain values.
$f_{s,y,dyn}$, $f_{s,y,stat}$	Dynamic and static yield strength, respectively.
$R_{p,0.2}$	Proof strength at 0.2 % non-proportinal extension determined by drawing a line parallel to the stress-strain curve between 1/3 and $2/3R_{p,0.2}$ in the elastic range. The initial loading branch appeared rather straight and was therefore used as reference for the parallel line. $R_{p,0.2}$ is defined as the stress value at the intersection between the inserted parallel line and the $\sigma - \varepsilon$ curve. This value was determined for the d6 bars which have no yield plateau.
$\varepsilon_{s,y}$	Yield strain, calculated from extensometer readings.
$\varepsilon_{s,h}$	Strain at onset of hardening, calculated from extensometer readings.
$f_{s,u,dyn}$, $f_{s,u,stat}$	Dynamic and static tensile strength, respectively. The static tensile strength was not measured but calculated assuming the same stress drop as measured while dismounting the extensometer.
A_{gt}	Percentage elongation at maximum force, determined from calibrated piston stroke when maximum force was reached first.
A_t	Percentage total elongation at fracture, determined from calibrated piston stroke at about 550 MPa for d14 bars and >600 MPa for d6 bars.

For the steel tests, six 1 m long pieces were cut from six different bars of each type of reinforcement steel. To determine the effective area, these test pieces were weighed and the effective area was calculated assuming a material density of 7.85g/cm^3. Stresses listed in Table 2.5 refer to the nominal area, however. When they were clamped to the testing machine, the d14 mm bars had a free length of 757 mm and the d6 mm bars one of 820 mm. As the d14 mm bars have a pronounced yield plateau whereas the d6 mm bars do not, the used loading protocol differed.

The d14 mm test pieces had a free length of 757 mm. In the elastic range, the loading velocity corresponded to a strain increase of 0.05 ‰/s, in the plastic range to 0.5 ‰/s. After reaching the yield plateau the test was stopped about two minutes to determine the static yield strength. Afterwards it was continued with the higher loading velocity until fracture. Initially, strains were determined using an extensometer type MFI-40 with 300 mm base length. Since the measurement range of this device is not large enough to measure the strains up to fracture, the tests had to be stopped a second time in the hardening range at about 50 ‰ to dismount the

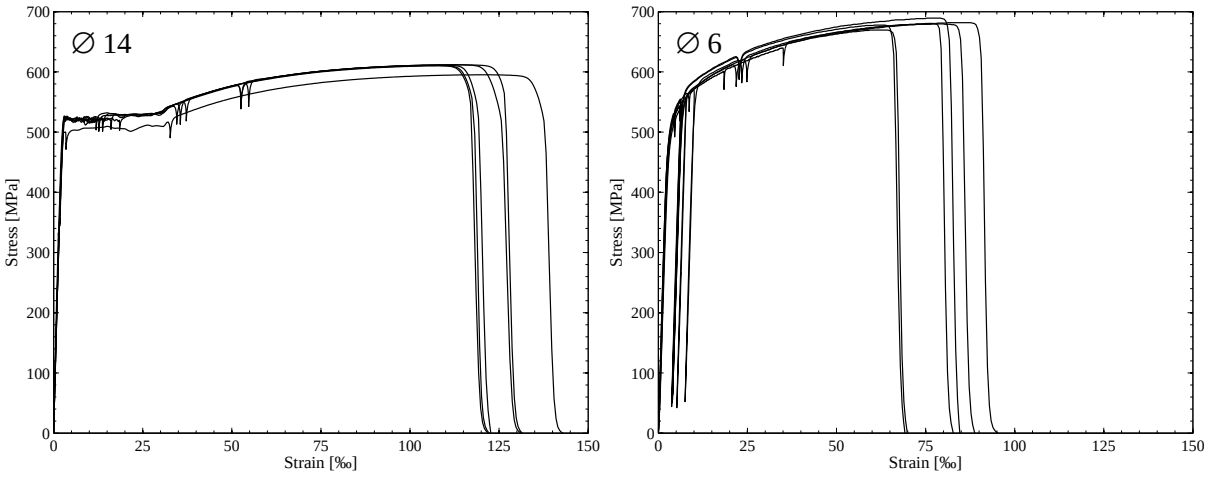

(a) Reinforcement d14 mm **(b)** Reinforcement d6 mm

Figure 2.8: Reinforcement stress-strain diagrams with strains determined from piston stroke.

extensometer. The stress drop recorded during this second stop was used to estimate the static tensile strength. Strain values listed in Table 2.5 are taken from extensometer readings except for the elongation at maximum force and the total elongation, which are calculated from the piston stroke, calibrated considering the testing machine's stiffness.

The d6 mm test pieces were loaded with 0.05 ‰/s until the stress was lowered to about 10% of $R_{p,0.2}$. Unloading to $0.1R_{p,0.2}$ started at approximately 7 ‰ strain. Afterwards, the test was continued with ten times the velocity (i.e. 0.5 ‰/s) until fracture. At about 5 ‰ and then again in the hardening range at about 25 ‰ the test was stopped approximately two minutes to determine the difference between dynamic and static stress at both loading velocities. The static values were calculated by subtracting these stress drops from the dynamic values. One test was completely run with 0.5 ‰/s and one with 0.05 ‰/s up to 3.5 %, accidentally. In Figure 2.8 the curves determined from the piston stroke are plotted.

number of samples		d14 mm 6		d6 mm 6	
property		mean value	CoV [%]	mean value	CoV [%]
A_{eff}	mm^2	153	0.08	28.4	0.3
E_s	[GPa]	202	1.27	197	2.65
$f_{s,y,dyn}$	[MPa]	521	1.93		
$f_{s,y,stat}$	[MPa]	498	2.52		
$\varepsilon_{s,y}$	[‰]	2.58	3.52		
$\varepsilon_{s,h}$	[‰]	28.6	4.50		
$R_{p,0.2,dyn}$	[MPa]			528	1.38
$R_{p,0.2,stat}$	[MPa]			504	1.53
$f_{s,u,dyn}$	[MPa]	609	1.08	680	0.97
$f_{s,u,stat}$	[MPa]	580	1.33	646	0.72
$\frac{f_{s,u,dyn}}{f_{s,y,dyn}}$ or $\frac{f_{s,u,dyn}}{R_{p,0.2,dyn}}$	[-]	1.17		1.29	
A_{gt}	[‰]	110	4.48	71.2	13.36
A_t	[‰]	123	6.10	78.2	12.64

Table 2.5: Mean values and coefficient of variation (CoV) of steel properties of test units VK4 to VK7.

3 Test Setup and Procedure

3.1 Test Setup

A picture of the test setup is shown in Figure 3.1 while drawings of the plan view and the elevation of the test setup are presented in Figures 3.2 and 3.3. After the test units were delivered to the laboratory, they were first measured, painted and instrumented with the studs for the manual measurements (see Section 3.2.3) or the steel plates for the optical measurements (see Section 3.2.2). The steel plates to which the actuator was later connected were also mounted while the test units were still in horizontal position. When these works were completed, the test units were erected and the horizontal prestressing of the foundation was applied. Before they were fixed to the strong floor in the test stand, the piers were aligned perpendicular to the floor by means of three small stacks of metal plates placed under the foundation. The gap between foundation and floor was then grouted to ensure support of the test units over the entire foundation area. Six vertical openings were provided in the foundation to fasten the test units to the floor with diameter 42 mm tensioning rods. After the mortar had hardened, the vertical tensioning rods were inserted and prestressed. To provide a horizontal shear support, steel plates were mounted between the foundation and the feet of the four vertical columns of the steel frame. Horizontal forces were thereby directly transferred to the strong floor via the steel column footings.

The steel frame served as horizontal support to prevent tilting of the pier to the side. To provide a horizontal sliding support with low friction, steel plates with a teflon coating were mounted on the two horizontal steel beams, parallel to the test unit and metal plates were glued to the pier. Initially, the teflon supports had about 0.5 cm distance to the metal plates, so the piers were only supported horizontally at the top after tilting slightly. The steel columns on the East and West side of the test stand were connected with two C-shaped steel-profiles to make the frame stiffer and distribute potential horizontal forces to all columns. All steel columns were clamped to the floor with tensioning rods and mechanical shear keys. At the southern side of the test stand, steel columns with no connection to the steel frame were positioned to serve as reference columns for the horizontal deformation measurements (HorDisp_1 to _6 and _FoundationSouth, see Section 3.2.1). The Linear Variable Differential Transformers (LVDT), with which these measurements were made, were fastened to horizontal steel profiles mounted on the reference columns and connected to the test units with invar-wire.

The two steel plates, which were previously clamped to the top of the pier by means of ten d13 Stahlton rods, each prestressed to 100 kN, served as connection plates for the horizontal actuator. A Walter+Bai AG servo-hydraulic actuator with ± 1000 kN force and 1200 mm total displacement capacity was used to apply the horizontal force and displacement. The actuator was equipped with both load cell and displacement transducer, used to control the deformation rate, as loading always was applied in displacement control. Since small deformations are imposed on the reaction wall and the hinges of the actuator have some backlash, which are both part of the

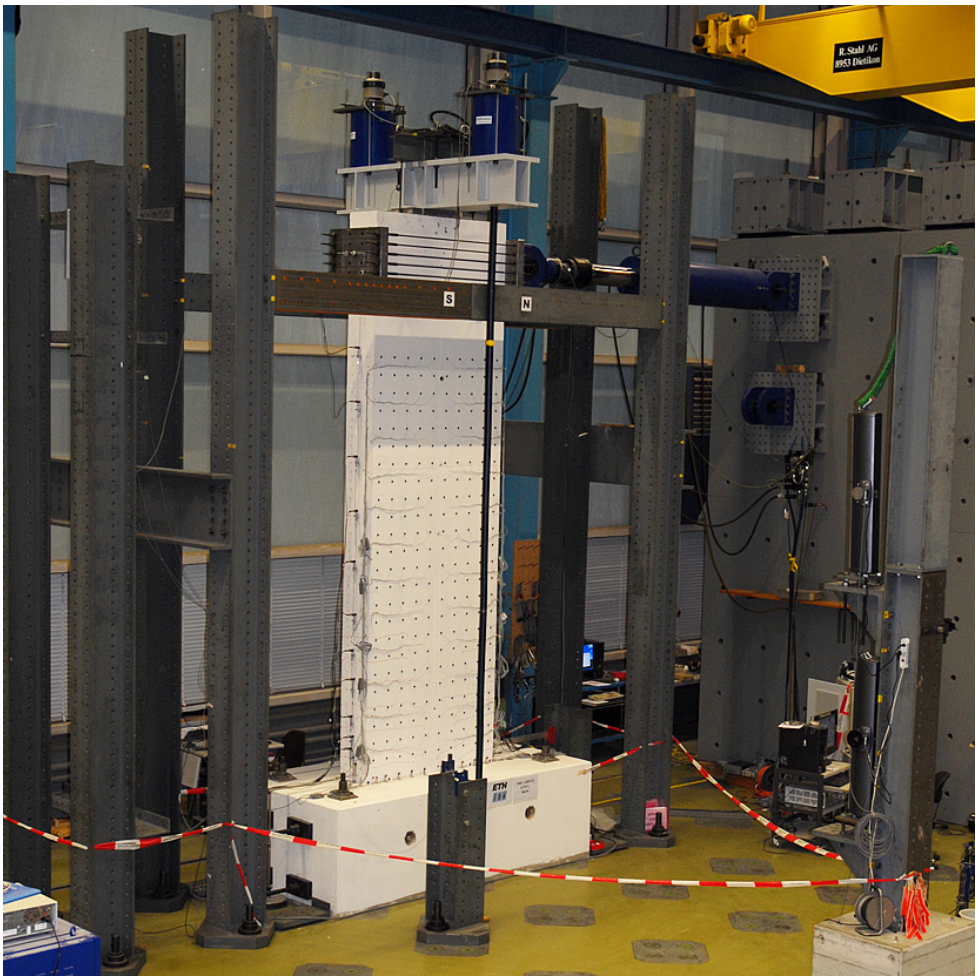

Figure 3.1: Picture of test unit VK6 before testing.

deformation measured by the actuator's internal transducer, LVDTs were used to measure the top displacement of the test units. Two pressure transducers were connected to the actuator's chambers to calculate the applied forces from the pressure in the chambers and thereby double-check the force signal of the load cell. Since the two chambers have different piston areas, 1000 kN pushing force are obtained with 141.5 bar pressure in the back chamber and 1000 kN pulling force with a pressure of 254.5 bar in the front chamber.

The vertical force, simulating the axial load on the bridge pier, was applied by means of two prestressed tendons of type Stahlton BBRV 1000, made of 22 wires d7 mm, with a maximum characteristic force of $1.0P_k = 1414$ kN each. A transverse steel beam supporting two hollow core jacks was centrically aligned on top of the pier and the tendons were fastened on top of the jacks. Load-cells were inserted to control the force of each tendon in addition to a pressure transducer measuring the oil pressure of the hydraulic circuit including both jacks. Each tendon was prestressed to 650 kN resulting in a total force of 1300 kN. During the test, the forces were monitored and the oil pressure manually adjusted, so the total force could be kept in a range of about 1300 ± 10 kN most of the time.

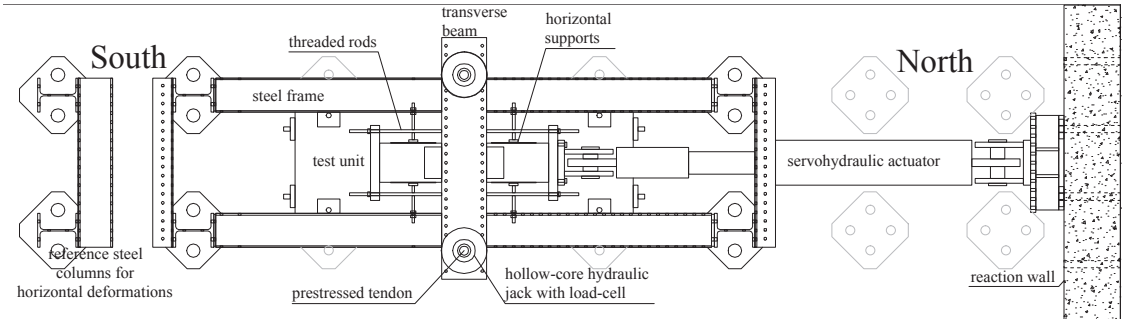

Figure 3.2: Plan view of the test setup.

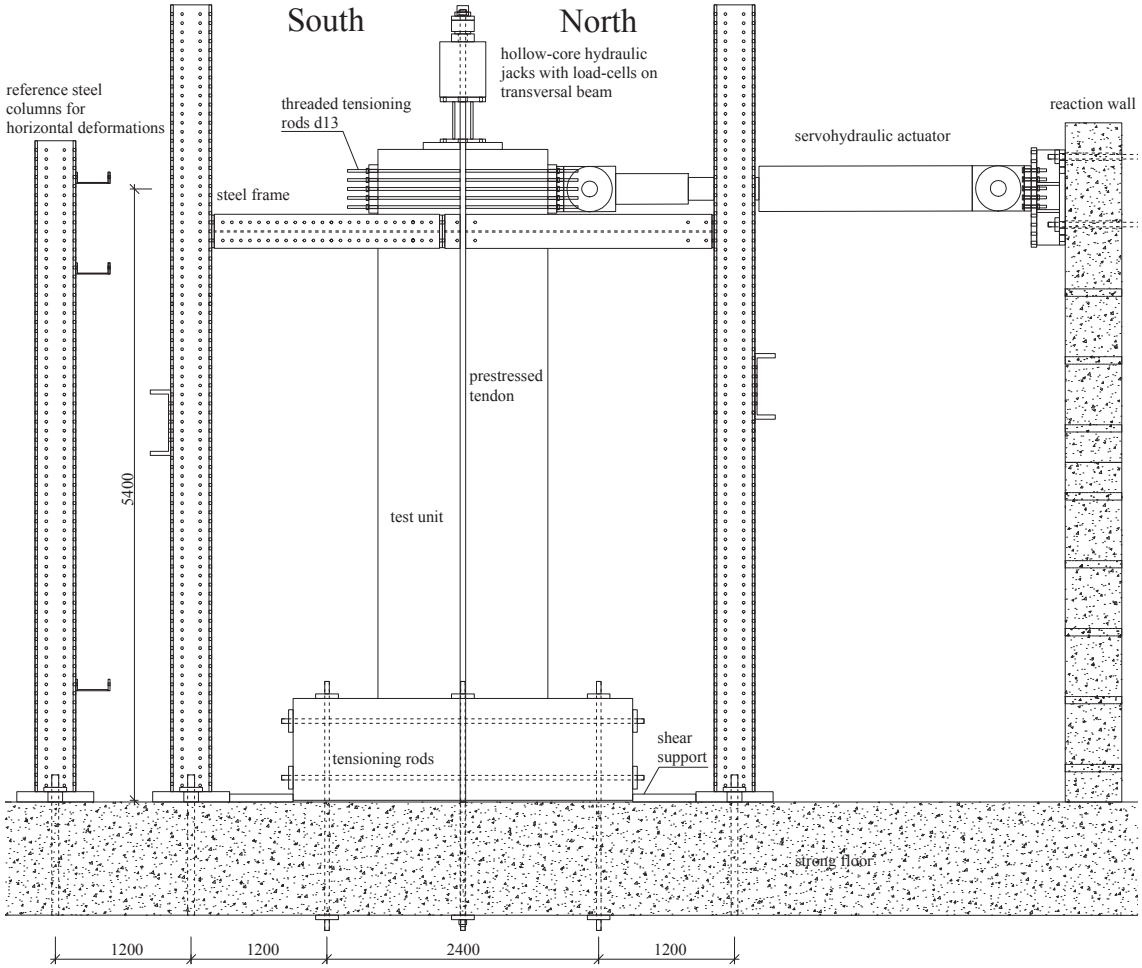

Figure 3.3: Test Setup, view from the East side. All dimensions in [mm].

3.2 Measurements

3.2.1 Hard-wired Measurements

During the tests, up to 52 hard wired measurements were recorded with a frequency of 0.5 Hz. An overview of all hard wired measurements is presented in Table 3.1 and drawings of the setup are presented Figures 3.5 through 3.7. Depending on the height, 10 to 13 LVDTs were mounted along the sides of the piers. They were fastened to 180 mm long bolts embedded in the concrete and measured the vertical deformations 22 mm away from the pier's surface. Three LVDTs were used to measure the vertical and horizontal deformations of the foundation. The horizontal deformation was measured against the reference column at the top of the foundation. The devices measuring the vertical displacement were mounted at the South and North face of the foundation of VK4, directly above the floor. Thereby uplift at the bottom of the foundation was measured and the rotation at the pier footing, i.e. the top of the foundation, was only measured with the optical system (see Section 3.2.2). In all other tests, the LVDTs measuring the foundation uplift were fastened to special brackets and measured the uplift relative to the strong floor at the top of the foundation against the plates also used for VertDef_S01 and _N01. Ten of the longitudinal reinforcement bars were instrumented with strain gauges as shown in Figure 3.4. The center of the gauges was approximately located in the construction joint between foundation and pier, where the base crack typically develops and hence the largest steel strains are expected.

Horizontal deformations of the pier were measured at three different locations: 50 mm above the base, at the top end of the optical or manual measurement grid and at the height of horizontal force application. HorDisp_1 measured the displacement just above the pier base and HorDisp_4 served as control measurement for the horizontal displacement determined by the optical system or manual measurements. When VK4 was tested, the latter measured the deformation 2.75 m above the foundation. Because the optical measurements could not, as initially planned, be made up to that height, the LVDT was moved downwards for VK7.

At the top, two to three LVDTs were used, to have redundant measurements of this important value. HorDisp_5 and _6 measured the displacement at the height of the actuator and were able to cover a range of ±100 mm. Therefore, they had to be adjusted at some stage during the tests, when displacements larger than ±100 mm were applied. Up to this point, displacements were

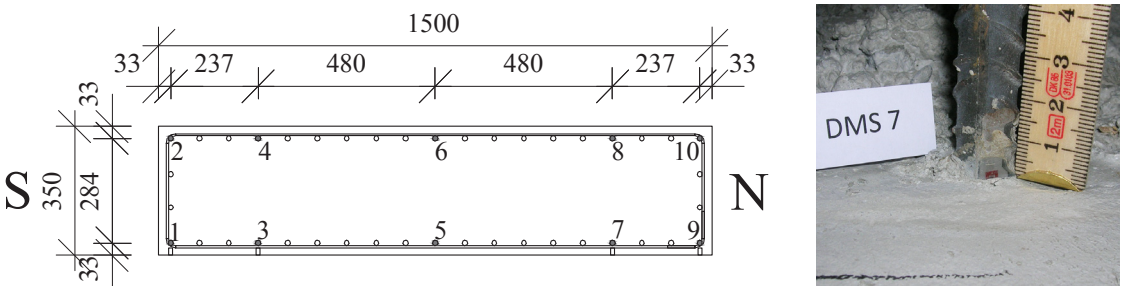

Figure 3.4: Strain gauges applied on the vertical reinforcement bars in the construction joint between foundation and pier. Drawing of the cross section with numbers of the strain gauges written next to the corresponding bar (filled in grey), to the left. Picture of a gauge after construction of the foundation, to the right.

always measured by both devices but from then on, larger deformations were only measured by one of them while the other one was out of range. To double check the deformation, especially because of the necessary adjusting process, an additional LVDT, which could cover the entire deformation range, was used for VK5 and VK6. Since the accuracy of that device is less than that of HorDisp_5 and _6, it served mainly as control unit during the test. Because adjusting was no problem, the additional LVDT was not used for VK7.

All forces were measured with load-cells. The horizontal force was measured by the internal load cell of the actuator and double-checked using the force calculated from the measurements of the pressure transducers connected to the actuator's chambers. Those pressure transducers were not planned initially, but added while testing VK4. One load cell was mounted on top of each of the hollow-core jacks, by which the vertical force was applied. The vertical force was double-checked using a pressure transducer to measure the oil pressure in the circuit to which both jacks were connected.

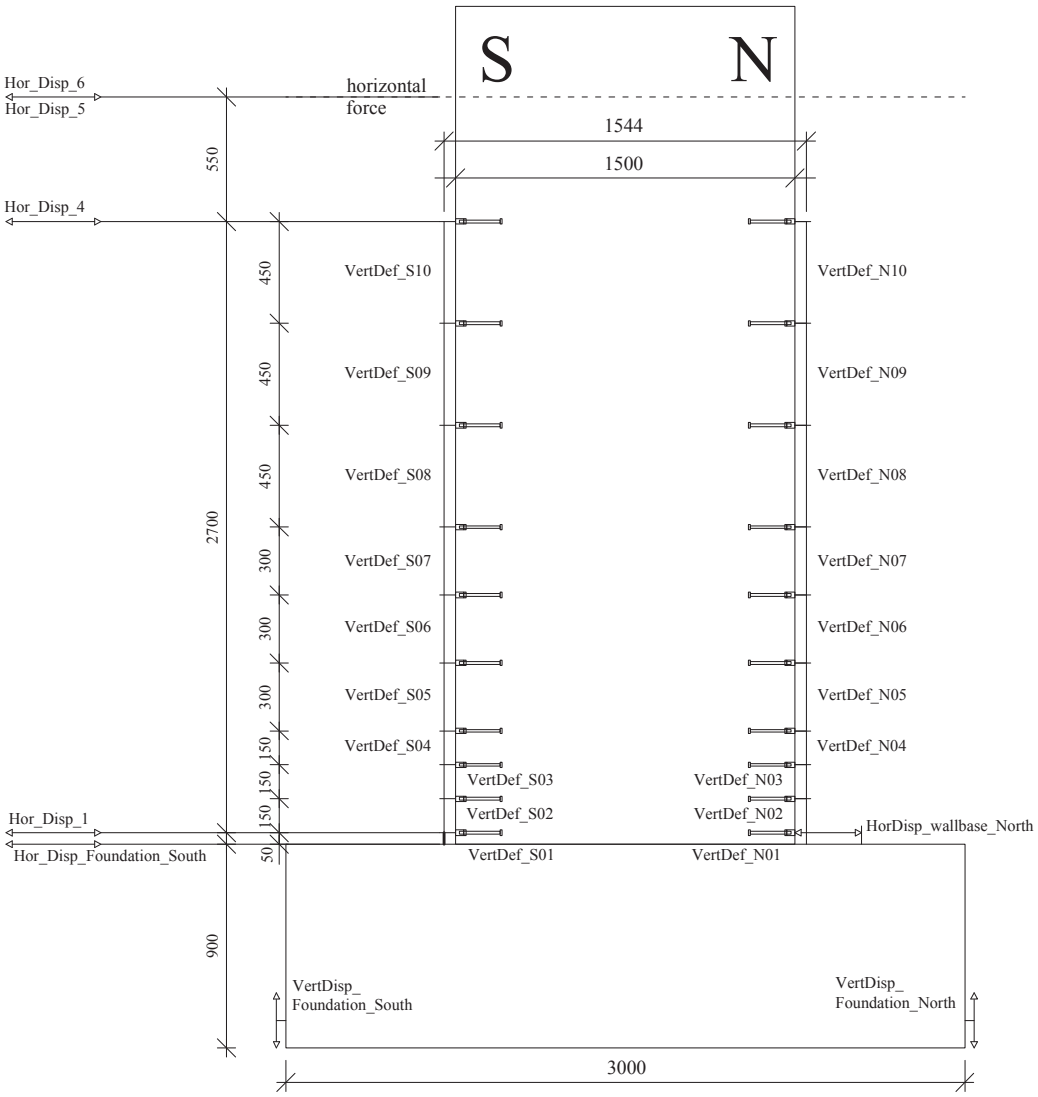

Figure 3.5: Hard-wired measurements (LVDTs only) of test unit VK4. All dimensions in [mm]. LVDTs VertDisp_Foundation_North and VertDisp_Foundation_South are assumed to measure deformations at the North and South face of the foundation even though their center lines have a small distance to the foundation's surface.

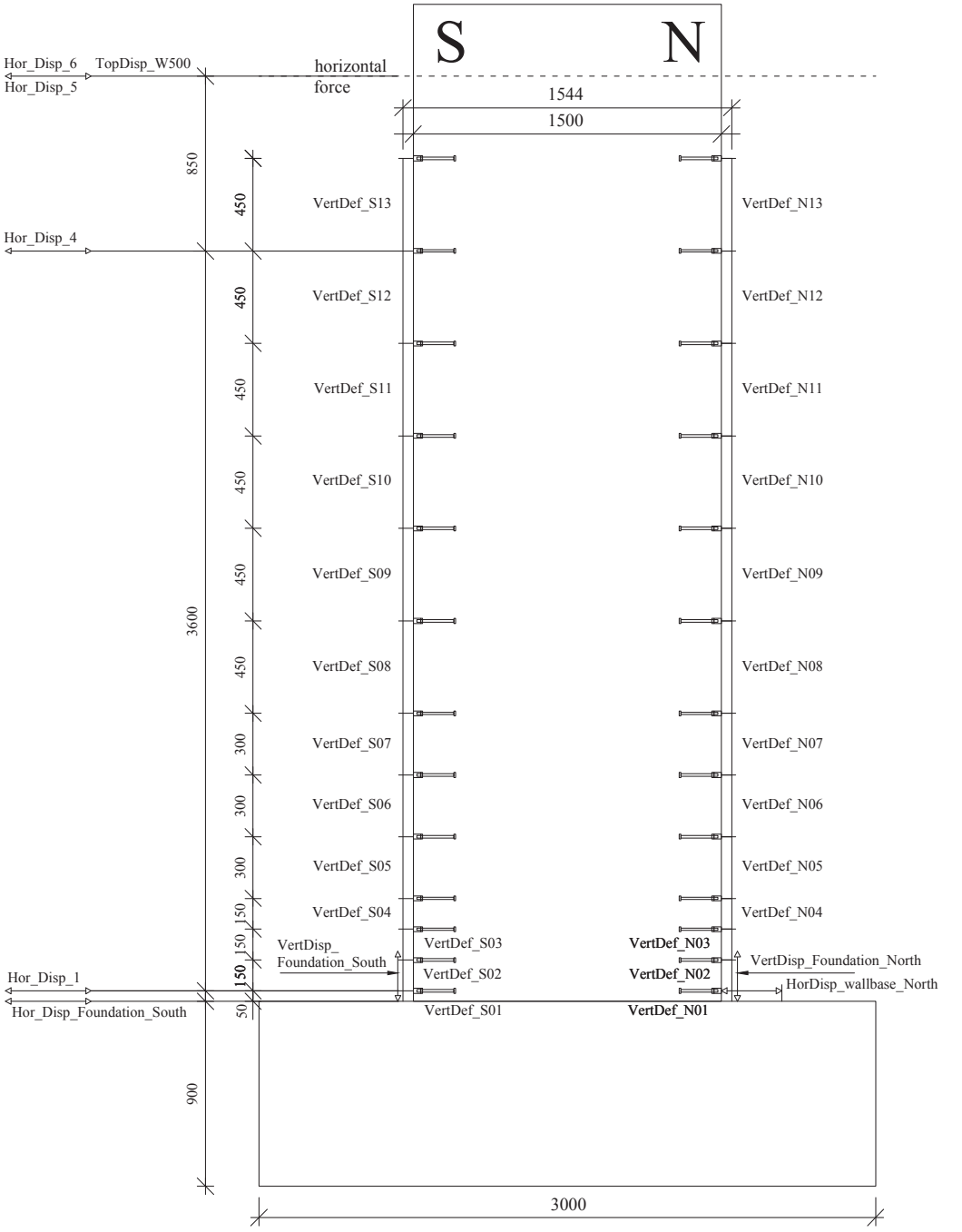

Figure 3.6: Hard-wired measurements (LVDTs only) of test units VK5 and VK6. All dimensions in [mm]. VertDisp_Foundation_North and VertDisp_Foundation_South measure the uplift of the base plates of VertDef_S01 and _N01. Since the uplift of a plate is assumed constant over its surface the LVDTs are supposed to measure the uplift under _S01 and _N01 regardless of their actual distance.

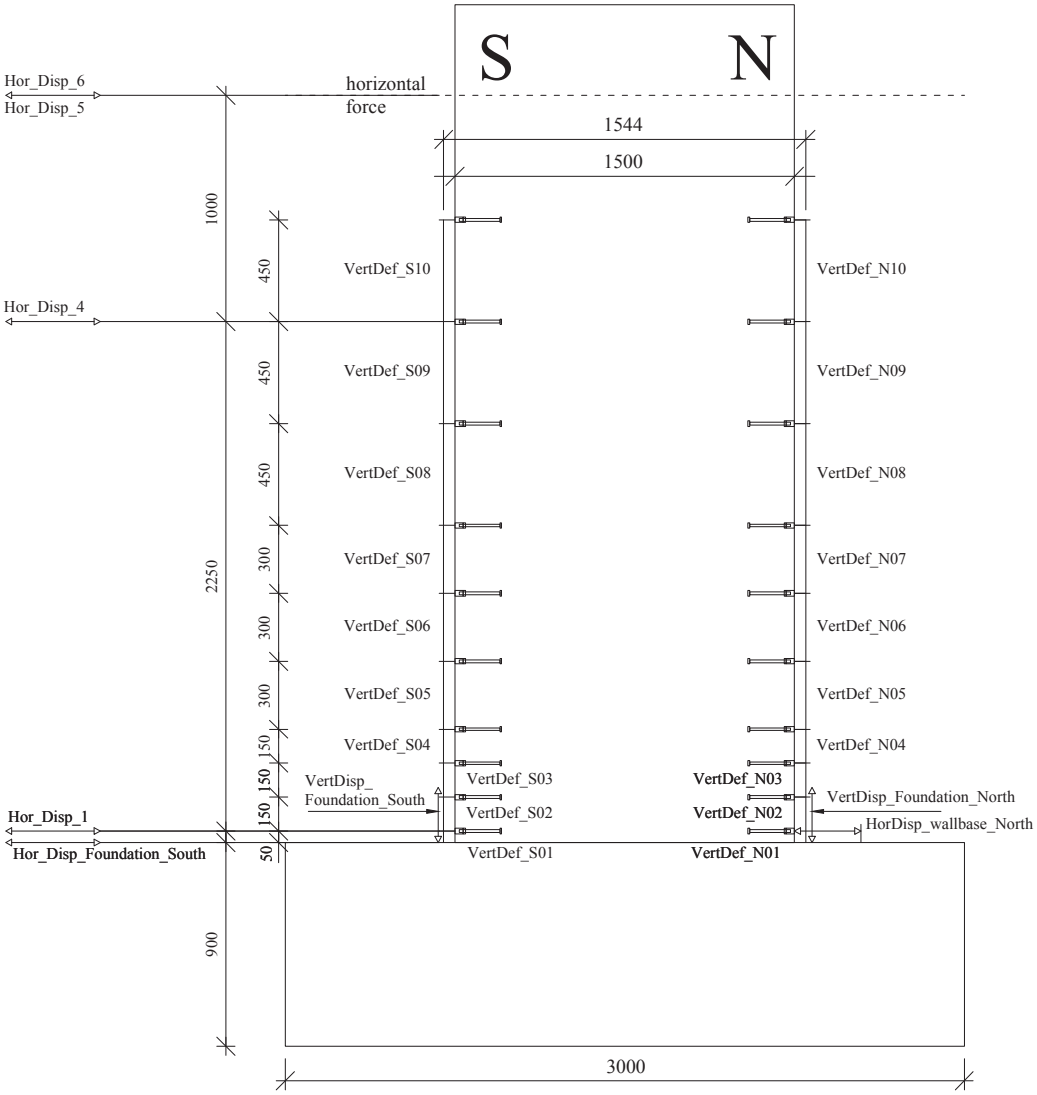

Figure 3.7: Hard-wired measurements (LVDTs only) of test unit VK7. All dimensions in [mm]. VertDisp_Foundation_North and VertDisp_Foundation_South measure the uplift of the base plates of VertDef_S01 and _N01. Since the uplift of a plate is assumed constant over its surface the LVDTs are supposed to measure the uplift under _S01 and _N01 regardless of their actual distance.

Name	Base length	Range	Comment
HorActForce HorActDisp		± 1000 kN 1200 mm	Internal load-cell and displacement transducer of the horizontal actuator
VertForceEast VertForceWest Druckgeber		1000 kN 1000 kN 500 bar	load-cells measuring the force of each tendon and pressure transducer measuring the pressure applied to both hollow-core jacks
Zylinderdruck ... _Druck _Zug		 500 bar 500 bar	pressure transducers connected to chambers of horizontal actuator
VertDef ... _S01, N01 _S02, N02 _S03, N03 _S04, N04 _S05, N05 _S06, N06 _S07, N07 _S08, N08 _S09, N09 _S10, N10	 50 mm 150 mm 150 mm 150 mm 300 mm 300 mm 300 mm 450 mm 450 mm 450 mm	 ±25 mm ±25 mm ±10 mm ±10 mm ±25 mm ±10 mm ±10 mm ±10 mm ±10 mm ±10 mm	LVDTs measuring the elongations along the South and North side of the specimen up to 2.75 m
_S11, N11 _S12, N12 _S13, N13	450 mm 450 mm 450 mm	±10 mm ±10 mm ±10 mm	Additional LVDTs used for the larger test units VK5 and VK6 to measure the elongations up to 4.10 m
HorDisp_6 HorDisp_5 TopDisp_W500		±100 mm ±100 mm 500 mm	LVDTs measuring top displacement, i.e. horizontal displacement at 3.30 m and 4.50 m respectively. W500 was only used in the tests of VK5 and VK6
HorDisp... _4 _1		 ±100 mm ±20 mm	LVDTs measuring the horizontal displacement of the pier 50 mm above the base and at the top of the optical and manual measurement grid
HorDisp _Wallbase_North		±10 mm	LVDT measuring horizontal deformations of the wallbase relative to the foundation
HorDisp _Foundation_South VertDisp... _Foundation_South _Foundation_North		±10 mm ±10 mm ±10 mm	LVDTs measuring the horizontal and vertical displacements of the foundation
DMS1 to DMS10		3 %	strain gauges on reinforcement

Table 3.1: Overview of all hard-wired measurement devices.

3.2.2 Optical Measurements

Deformations of the wall surface were measured along a 150 mm by 150 mm grid over almost the entire pier surface using the optical measurement system NDI Optotrak Certus HD [NDI09]. To carry out the measurements, infrared light emitting diodes (LED), whose positions are tracked by a position sensor during the tests, were glued on small metal plates along a square grid on the Eastern face of the wall. A drawing of the measurement grid of the test units is presented in Figure 3.8.

Four LED markers were attached directly to longitudinal reinforcement bars. Therefore, small styrofoam pieces were glued on the foundation concrete in front of the rebar before the piers were cast. In the laboratory, these styrofoam pieces were removed so that the reinforcement bars were visible and could be instrumented with the LEDs. To measure the deformations of the foundation, L-shaped brackets instrumented with LEDs were glued to the foundation in front of the pier. These measurements were needed to eventually be able to determine the pier's deformations relative to the foundation. Additional LEDs, serving as reference points to check the sensor position, were glued to two reference steel columns with fixed position.

One (VK4 & VK7) or two (VK6) position sensors were used to track and record the position of the LEDs. The x-, y- and z-coordinates of all markers, relative to the position sensors' center, were tracked one after the other by the sensor. The optical measurements were recorded during all loading phases. Additionally, the positions of the LEDs were measured during a two minutes long time frame while the top displacement of the test units was kept constant. This measurement phase was introduced as an attempt to increase the accuracy of the measurements through averaging of the readings. The setup used for the optical measurements is summarized in Table 3.2. Since the necessary second position sensor was not available in the time period during which VK5 was tested, manual measurements were made instead on that pier.

Test unit	VK4, VK7	VK6
Shear span	3.30 m	4.50 m
Grid size	1.35 × 2.50 m	1.35 × 3.60 m
No of LEDs in grid	10 × 18 = 180	10 × 25 = 250
No of LEDs on rebar	4	4
Measurement frequency	3 Hz	3 Hz
No of sensors	1	2
Distance between sensor and pier surface	6.0 m	4.50 m

Table 3.2: Characteristics of the optical measurement setup.

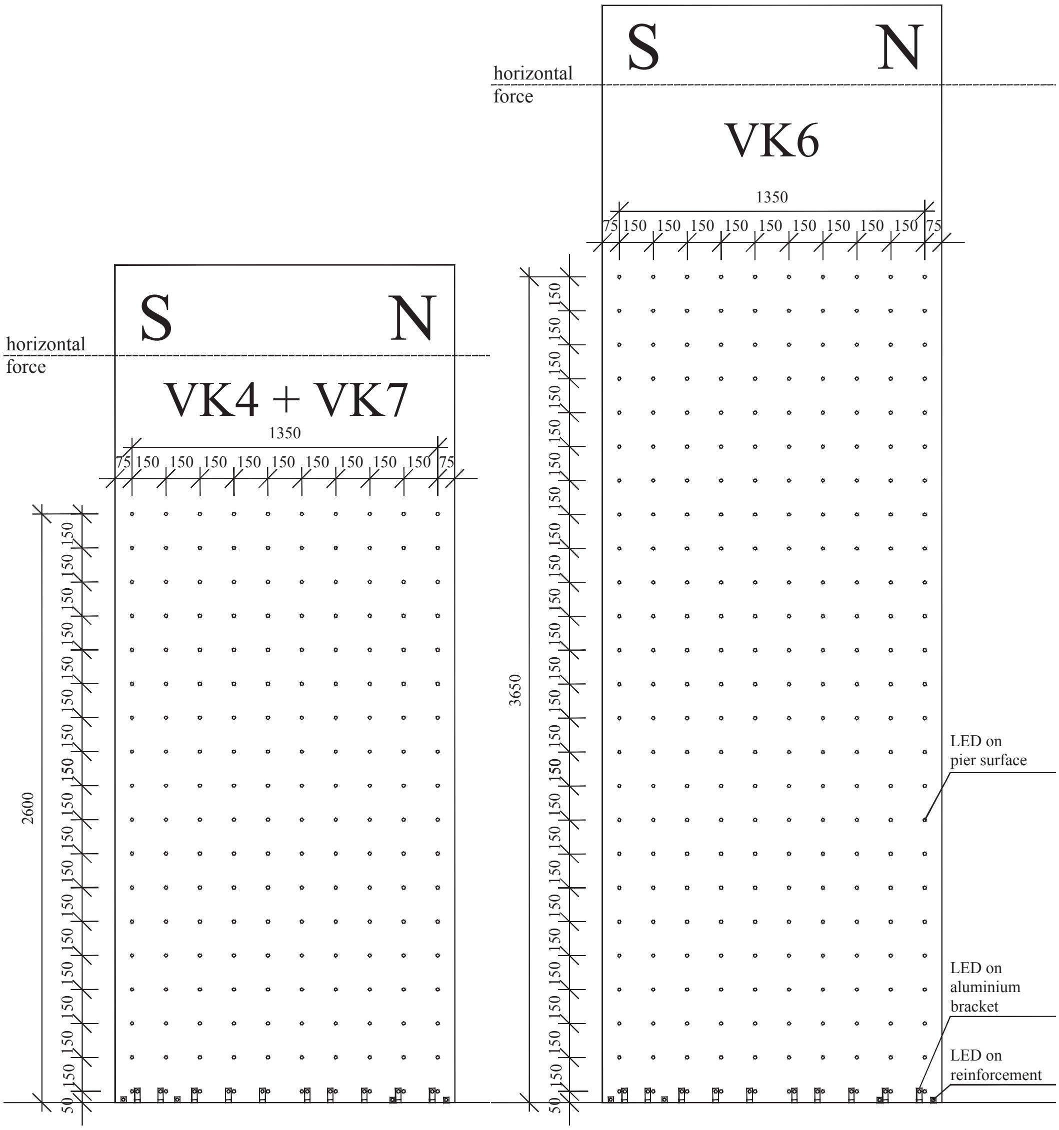

Figure 3.8: Positions of the LED for optical measurements with the Optotrak System on the East face of the pier. All dimensions in [mm].

3.2.3 Manual Measurements

Manual measurements were made to supplement optical and hard-wired measurements and even replace the optical measurements in the case of VK5. For these measurements, aluminium studs with a circular notch in the center were glued to the concrete surface along a square grid with 150 mm spacing on the back, i.e. West face, of the pier. The distance between the studs is measured using an extensometer with two pins fitting into the notches. All horizontal and vertical distances, as well as all diagonals from the lower right to the upper left of the squares were measured manually, one after the other. The diagonals serve as redundant measurements to account for errors and thereby increase accuracy.

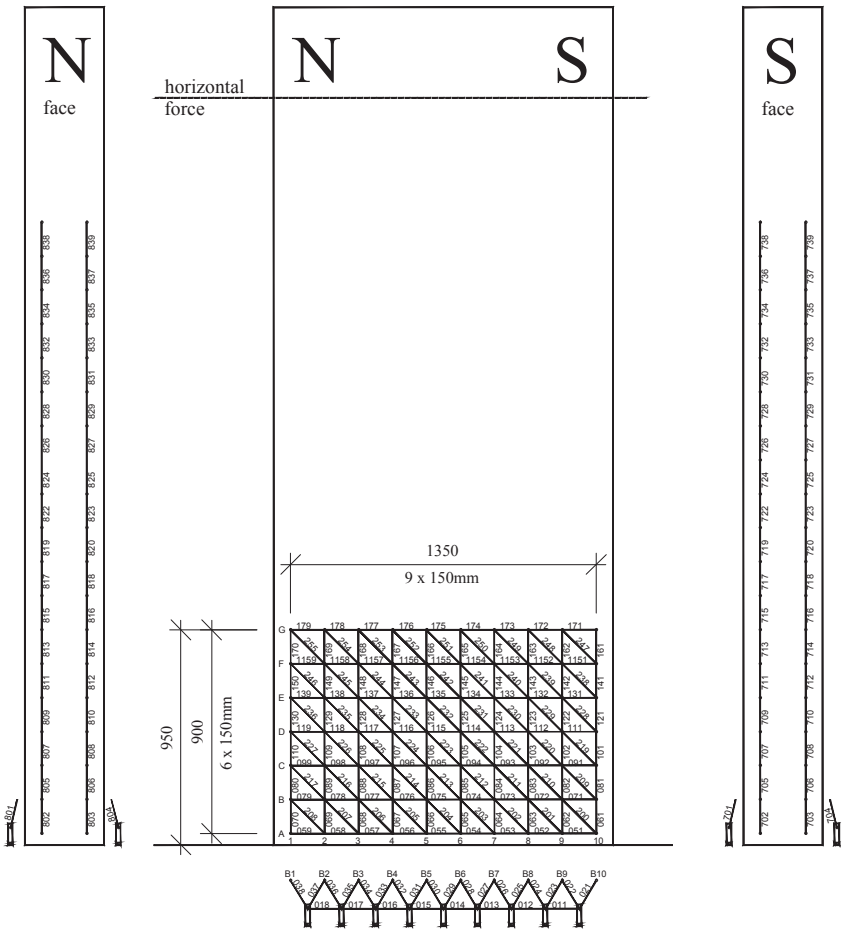

Figure 3.9: Manual measurements of VK4 on the North, West and South face of the pier. All dimensions in [mm].

Two columns of studs with 150 mm spacing were glued along the North and South faces of the test units, to supplement the hard-wired measurements at certain load steps. As the studs are rather flat (approximately 2 mm), the deformations are measured much closer to the surface than with the LVDTs. Therefore, the measured deformations can be assumed to be wall surface deformations, whereas the LVDT measurements would have to be interpolated to project them to the wall surface. To measure the distance between the second row of studs and the foundation L-shaped brackets with studs were glued to the foundation. These measurements served to determine the deformation pattern of the pier relative to the "fixed" foundation later on.

The patterns and numbers of the measurements carried out on test units VK5 and VK6 can be seen in Figure 3.10. On the West face of VK4, measurements were only made up to a height of 950 mm, Figure 3.9, to gather additional strain measurements in the lower part of the wall where the longitudinal reinforcement was spliced. As the second optical position sensor was not available when VK5 was tested, manual measurements were made over almost the entire wall surface, up to a height of 3.65 m. Due to some technical difficulties arising from the use of two position sensors, the same measurements were made as backup up to load step $\mu_\Delta = 3.0$ when

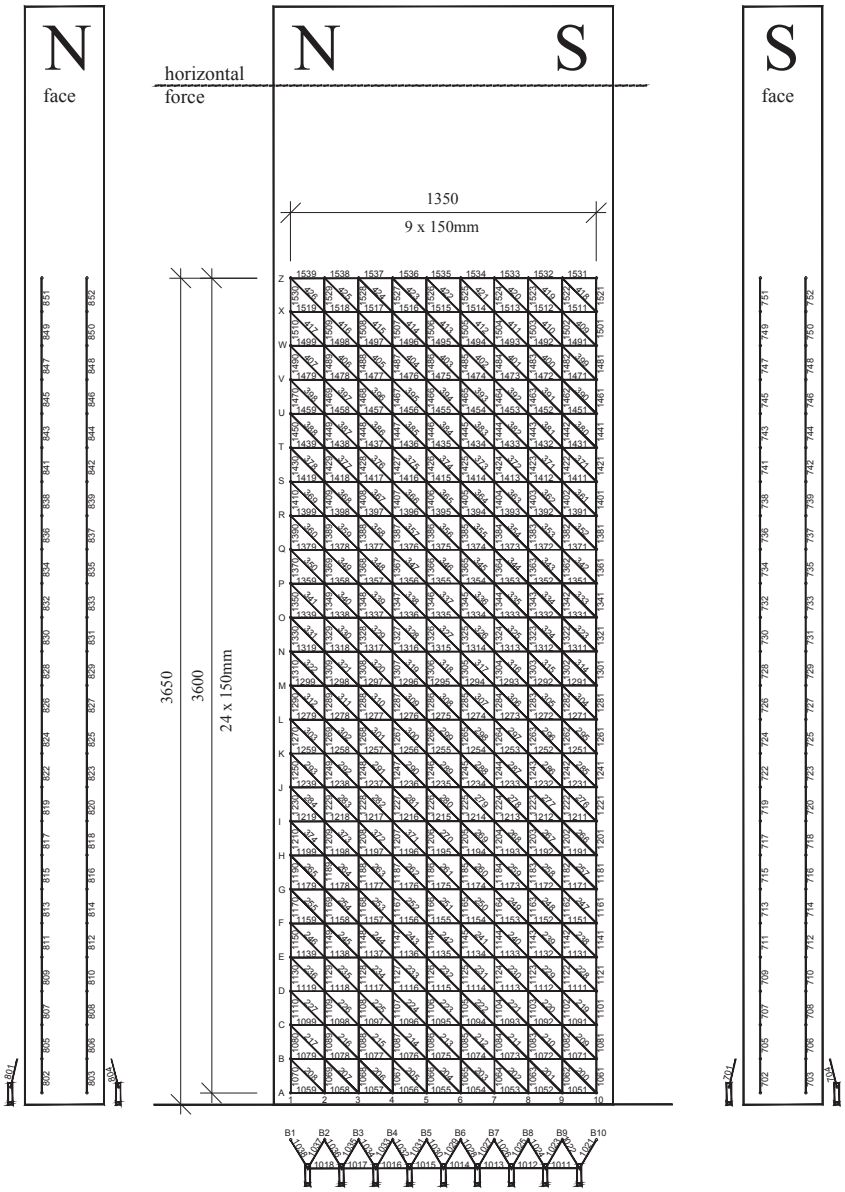

Figure 3.10: Manual measurements of VK5 and VK6 on the North, West and South face of the pier. All dimensions in [mm].

VK6 was tested. Since a preliminary data check before testing VK7 indicated that the optical measurements were sufficiently accurate, no manual measurements were made in the last test.

Extensometers with two base lengths were used for the manual measurements in all tests.

- Extensometer with 150 mm base length, range ± 6 mm
- Extensometer with 212 mm base length, range ± 6 mm

Two sets of manual measurements were made before the vertical load was applied, the latter to ensure that the measurement of the unloaded test unit, serving as reference for all following

measurements, was accurate. Another measurement was carried out after application of the vertical load. From then on, one measurement was taken at every first cycle at load stages $\pm 0.5F'_y$, $\pm 1.0F'_y$, $\mu_\Delta = \pm 1.0$, $\mu_\Delta = \pm 1.5$, $\mu_\Delta = \pm 2.0$ and so forth (see also Figure 3.11), as long as there was a sufficient number of studs at the bottom of the pier, i.e. as long as enough cover concrete was intact. The pattern on the back of the specimen was first measured from bottom to top with the extensometer with 150 mm base length and then with the one with 212 mm base length. Both sides were also measured in one run with the device with 150 mm base length only. After about every 10 to 20 measurements, a calibration measurement on an invar-bar was made to correct for the influence of temperature.

3.2.4 Crack Widths

From the first cycle to 1.0 F'_y on (VK4: from $\mu_\Delta = 1.0$ North on), the widths of some cracks were determined manually at chosen load steps with a crack-width comparator. About ten cracks, whose widths were measured along five sections distributed over the wall surface, were chosen in each loading direction. Whenever possible, the widths were determined at the marked location. If measuring at that place was difficult due to a formwork construction joint with uneven surface, the width was measured at the closest possible location. If cracks were diverging, the width was either measured before the opening of the different branches, or multiple widths were determined.

3.3 Testing Procedure

All tests were quasi-static cyclic experiments subjected to the same type of standardized load history, displayed in Figure 3.11. Before the tests started, all reference measurements were made while the test units were still unloaded. After that, the vertical load was applied and the manual measurements, if any were planned for the test unit, were made. Once the measurements were completed, the servohydraulic horizontal actuator was connected and application of the cyclic loading was started. Some load steps (LS), in which manual measurements were made or crack widths were tracked are indicated in Figure 3.11. Numbering of the load steps started with LS000 & LS001 (two manual measurements) for the unloaded test unit and LS2 for the test unit subjected to axial load. From then on, each target amplitude and center position were subsequently numbered. At target load level $0.25F'_y$ and $0.75F'_y$ .1 and .2 are appended to the load step numbers to indicate the first and second cycle. The second cycle at these load levels was not conducted from the beginning, but added starting with VK2 [Bim10]. To keep the numbers consistent, the appended numbers were kept and load steps were not renumbered in this test campaign.

A reversed cyclic loading history, which was applied in deformation control, was chosen for all tests. The loading velocity was adjusted to the amplitude of the cycles so that loading from one peak of the cycle to the opposite peak lasted about 15-20 minutes each time. In the first phase of each test, i.e. in the elastic range, fractions of the theoretical first yield force F'_y, i.e. ± 0.25, ± 0.50, ± 0.75 and $\pm 1.0F'_y$, were defined as target amplitudes. The theoretical first yield force was defined as the force at onset of yielding of the outermost longitudinal bars and determined by means of moment-curvature analysis. In the inelastic range, multiples of a previously defined theoretical nominal yield displacement, i.e. nominal ductilities $\mu_\Delta = \pm 1.0$ ± 1.5, ± 2.0, ± 3.0

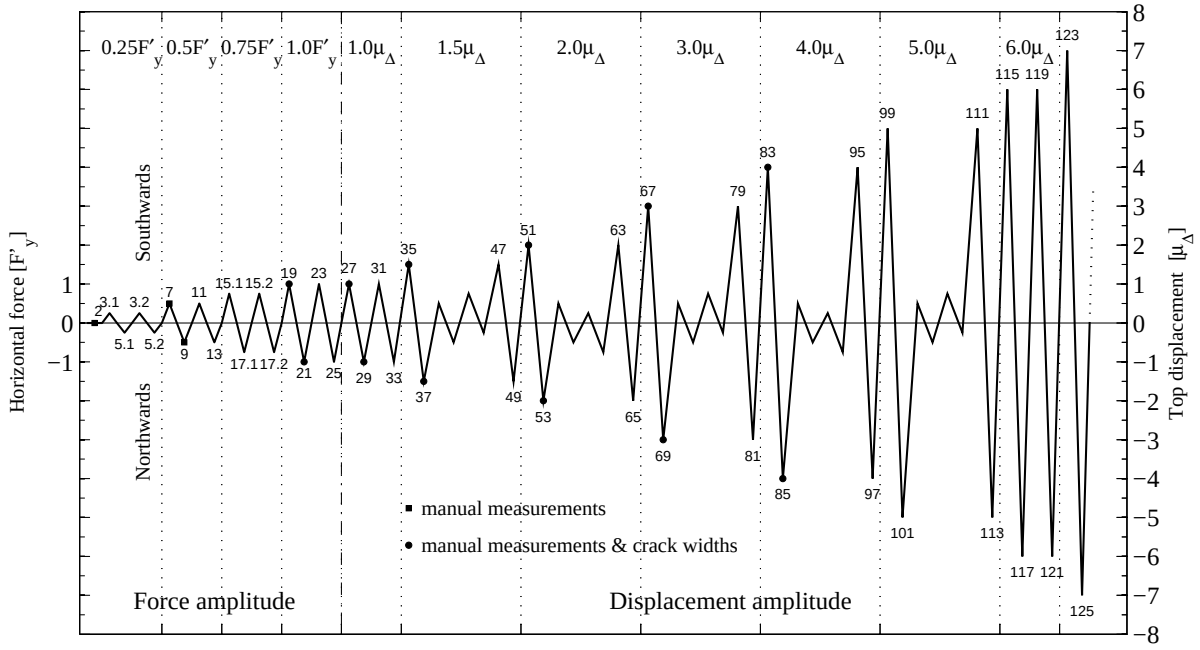

Figure 3.11: Standardized loading history used for all test units.

and so forth, were defined as target displacements. Two cycles were conducted to each target force and displacement, respectively. Starting at $\mu_\Delta = \pm 1.5$, a set of small cycles was inserted in between the two cycles to full ductility. Each set of small cycles comprised a symmetric one with amplitudes $\pm 0.5\mu_\Delta$ and an asymmetric cycle with either $+0.75/-0.25\mu_\Delta$, or $+0.25/-0.75\mu_\Delta$ target displacement. The latter was chosen to assure a more or less symmetric damaging of the test unit. The very first set of small cycles applied to VK4 had featured force amplitudes, but because of the decreasing resistance of the piers during the tests, it was deemed more appropriate to chose displacement amplitudes also for the small cycles from then on. The small cycles were inserted with the objective to investigate the energy dissipated due of these, because in regions of moderate seismicity structures are expected to be subjected to many cycles with smaller amplitudes during an earthquake [Bim10].

The theoretical first yield force F_y' and nominal yield force F_n were calculated before the test by means of a moment-curvature (M-ϕ) analysis. For this analysis, the dynamic steel properties $f_{y,dyn}$ and $f_{u,dyn}$ with the related strains and E_s, listed in Table 2.5, as well as the cylinder concrete strength $f_{c,cyl}$, see Table 2.4, were used. The tensile strength of concrete was assumed zero and the strain at peak stress $\varepsilon_{c,cu} = 0.002$. A bilinear steel stress-strain-curve without yield-plateau and a linear hardening branch, from the yield to the ultimate strength, was used. A positive influence of confinement was not considered, because of the low transverse reinforcement ratio. A normal force of N=1370 kN was applied in all M-ϕ-analysis, because 1300 kN axial load was applied at the top of the pier and the weight of the steel beam including the hollow core jacks used to apply the load as well as the weight of the pier amounts to roughly 70 kN. Nominal values were calculated with the serviceability limit strains $\varepsilon_{nom,steel} = 0.015$ or $\varepsilon_{nom,concrete} = 0.004$, whichever occurred first, and the ultimate values with the strains $\varepsilon_{u,steel} = 0.6A_t$ or $\varepsilon_{u,concrete} = 0.004$, whichever occurred first, according to [PCK07]. Since no confining effect was considered, nominal and ultimate concrete strains were equal. M-ϕ-analyses

were conducted with the SeismoStruct [Sei07] software.

From the analytically obtained first yield curvature ϕ'_y the theoretical first yield displacement Δ'_y can be calculated according to [PCK07] as follows

$$\Delta'_y = \phi'_y \frac{(a + L_{sp})^2}{3} \tag{3.1}$$

with the shear span length a and the strain penetration length $L_{sp} = 0.022 f_y d_l = 160\,\text{mm}$. From the first and nominal yield moments and the first yield displacement, the nominal yield displacement can be obtained according to the following equation:

$$\Delta_y = \Delta'_y \frac{M_N}{M'_y} \tag{3.2}$$

In general, a procedure like this was applied to determine the nominal yield displacements before the start of the entire test campaign, see [Bim10]. The only main difference was that in [Bim10] the strain hardening was neglected in the $M - \phi$ analysis because of the pronounced yield plateau of the longitudinal reinforcement bars. Before the hardening branch of the steel is reached, the stress-strain relationship is elastic-perfectly plastic and since the hardening strain is very high, large curvatures are needed to actually reach the hardening branch. Typically, in this kind of tests, the average of the displacements measured at $\pm 1.0 F'_y$ are defined as experimental first yield displacement, which is used to calculate the nominal yield displacement according to Equation (3.2). However, during the first test campaign, it was decided to use the same theoretical nominal yield displacement as target displacement for all tests units VK1 to VK3 to allow for a more straightforward comparison of the measured hysteretic behavior [Bim10]. For the same reason, the same target forces and displacements as used for VK3 were also used for VK4 and VK7, since the cross sections were the same and differences in F'_y and Δ'_y therefore would merely have depended on varying material properties.

As new target displacements needed to be determined for the taller piers and the first results of the material tests on the type of concrete used for VK4-VK7 were available by then, a new section-analysis was made to calculate the first yield moment of VK5 and VK6. When VK5 was tested, the experimental first and nominal yield displacements could be determined after the elastic cycles were completed. The obtained nominal yield displacement was compared to the displacement obtained by multiplying the theoretical nominal yield displacement used for the shorter test units with the squared relation of the shear spans according to the following equation:

$$\Delta_{y,tall} = \Delta_{y,short} \left(\frac{a_{tall}}{a_{short}} \right)^2 \tag{3.3}$$

With this equation, deformations due to strain penetration and shear displacements are neglected. Since the displacements obtained from the experimentally determined first yield displacement and Equation (3.2) were similar to those obtained with Equation (3.3), the latter was chosen for two reasons. On the one hand, it was directly related to the previously used target

Shear span length	a	3.30 m	4.50 m
First yield moment	M'_y [kNm]	2124*	2137
First yield curvature	ϕ'_y [km^{-1}]	2.54*	2.54
First yield force	F'_y [kN]	644*	475
First yield displacement	Δ'_y [mm]	10.1*	18.4
Nominal yield moment	M_n [kNm]	2808*	2852
Nominal yield curvature	ϕ_y [km^{-1}]	3.36*	3.39
Nominal to first yield ratio	[-]	1.32	1.34
First yield force used to run all tests	F'_y [kN]	641	475
Nominal yield displacement used to run all tests	Δ_y [mm]	10.5*	19.5

Table 3.3: Results of the M-ϕ-analysis with numerically computed displacements and chosen load stages for each aspect ratio. Analysis results marked with * are taken from [Bim10].

displacements and on the other hand VK5 had a lap splice at the pier base, which was expected to influence the stiffness of the pier and thereby its displacements. Therefore, compared to VK6, test unit VK5 seemed to be less suitable to determine the experimental nominal yield displacement, since it was again planned to use the same load steps for both test units.

Important results of the M-ϕ analysis as well as the target forces and displacements used for the experiments are summarized in Table 3.3.

4 Results

4.1 Evaluation and Presentation of Data

4.1.1 Hard-Wired Measurements

Data Processing

The hard-wired channels were recorded by a computer and their data was exported to ascii as well as excel files at the end of each load step. The measurements of each channel during the entire test were then concatenated and checked for obvious errors and disturbances, such as jumps in the readings when a device was touched while marking cracks, for instance, which were corrected. All measurements which were taken while the displacement was kept constant at a particular load step (LS) and during nights or weekends were afterwards disregarded and the remaining data was reduced by removing every second value. All values corresponding to the maximum horizontal force as well as maximum displacement of each cycle were kept in every case. Initially, a sampling frequency of 0.5 Hz was chosen during the cycles and the final data, after removal of every second value, is hence sampled with a frequency of 0.25 Hz.

All LVDTs were set to zero before the application of the vertical load and were already used for measurements during this load application. The signal of the actuator's internal load-cell was set to zero before the actuator was connected to the test unit while the signal of the internal displacement transducer was zeroed afterwards. During the post-processing of the data, it was checked, whether the values at the beginning of the measurements really were zero. If they slightly deviated from zero, the measured values, i.e. the offsets that the measurements still had, were subtracted.

The forces calculated from the measurements by the pressure transducers were compared to the measurements taken by the load-cells, but not processed further if the comparison showed that all forces were correct. To obtain the horizontal force from the pressure transducer readings, the force was calculated according to Equation (4.1a) using the measured pressures in the front and back chamber ($P_{front\,chamber}$ and $P_{back\,chamber}$) and the transformation values from the piston's data sheets. The pressure measured by the pressure transducer connected to the circuit for the vertical load ($P_{Druckgeber}$) was employed to double-check the vertical load applied by each tendon, i.e. the signals of the two load-cells on top of the hollow core jacks, according to Equation (4.1b). The horizontal force was not corrected for the eccentricity of the vertical load. Because the tendons were fixed at the center of the pier at the bottom of the strong floor the eccentricity at the bottom of the pier was regarded as rather small.

$$F_h = \left(\frac{P_{back\,chamber}}{141.5\text{bar}} - \frac{P_{front\,chamber}}{254.5\text{bar}} \right) \cdot 1000\text{kN [kN]} \tag{4.1a}$$

$$F_v = \frac{P_{Druckgeber}[\text{bar}]}{100} \cdot 659.7\text{cm}^2 \text{ [kN]} \tag{4.1b}$$

The top displacement has been corrected according to Equation (4.2) by subtracting the horizontal deformations of the foundation, as well as the deformation resulting from foundation rotation. The latter was determined from the measured uplift of the plates on top of the foundation block against which the measurements of LVDTs VertDef_S01 and VertDef_N01 were also taken ($\Delta_{v,FS}$ and $\Delta_{v,FN}$) and the distance between the LVDTs (L_{dist}) as well as the length of the shear span a. In general, the average of the measurements HorDisp_5 and HorDisp_6 ($\Delta_{HorDisp\_5/6}$) was taken as top displacement up to the point when they had to be rearranged. As described in Section 3.2.1, one of the LVDTs went out of range during the tests when very large horizontal displacements were imposed. When this occurred only the reading of the other device was used to define the top displacement.

$$\Delta_{top} = \Delta_{HorDisp\_5/6} - \Delta_{HorDisp\_Foundation} - \frac{\Delta_{v,FN} - \Delta_{v,FS}}{L_{dist}} a \tag{4.2}$$

Data Presentation

In the following sections, important data stemming from the hard-wired measurements is summarized. First, the global load deflection curves are presented. To better visualize the influence of strength degradation caused by the second cycle with the same target amplitude, plots emphasizing the first and second cycles separately are included as well.
Furthermore, the measured moment curvature relationships along the wall are presented. The curvatures were determined from the data of the LVDTs mounted along the side faces of the test units. To compute the curvature, a distance of $L = 1.544\,\text{m}$ was assumed between the devices, since the center lines of the LVDTs were mounted 22 mm away from the pier's surface, see Figures 3.5 through 3.7. The strain profiles determined from these LVDTs at selected load steps are also presented. To obtain the strains, the measurements were divided by the base lengths of the LVDTs and then projected to the pier's surface with the assumption that plane sections remain plane. That means they were obtained from linear interpolation of the strains at the center line of the LVDTs.
Strain gauge measurements are also presented at selected load steps mainly in the elastic range, since the measurements sometimes appeared to be unreliable at the load steps in the inelastic range.
In all plots, the indicated first and nominal yield forces and moments are not the ones calculated specifically for each test unit, but the ones given in Table 3.3.

4.1.2 Optical Measurements

Data Processing

As explained in Section 3.2.2, optical measurement data was collected both during all loading phases as well as during a two minutes long time frame while the actuator position was kept constant at the end of each loading phase. The measured x-, y- and z- coordinates of all LEDs were stored in separate .csv files for each data collection. The measurements taken over a two minute interval while the top displacement was kept constant at the cycles peak position were processed by reading all coordinates, computing their mean values and transforming those to the wall surface. By default, the coordinate systems origin is located at the center of the position sensor. When the data was processed, the origin of the system was shifted to the left bottom corner of the wall and the axis rotated so that the pier's surface lay in the x-y plane with the x-axis pointing to the right and the y-axis upwards. The x-axis was set along the markers on the brackets, so that the rotation of the foundation is eventually not considered and the deformation of the markers in the transformed coordinate system describes the deformation of the wall only. As the nodes are automatically numbered by the measurement system according to the order in which the LEDs are plugged in, they were renumbered according to their position on the pier's surface to make them easier to use, starting at the left bottom corner of the pier. Only the x- and y-coordinates were used for further processing, since only deformations and strains in-plane are of interest.

Data Presentation

Plots of the strains computed from the measured coordinates at selected load steps are presented in the results sections of the test units. Strain plots were chosen over deformation plots, because the calculated strains are not influenced by the coordinate transformation and it appears useful to know the strain distribution for many purposes.

The mean element strains $\varepsilon_{x,m}$, $\varepsilon_{y,m}$ and $\gamma_{xy,m} = 2\varepsilon_{xy,m}$ were calculated as mean of the strains along all element edges and transformed to the principal strains $\varepsilon_{1,m}$ and $\varepsilon_{2,m}$, according to Equations (4.3) and (4.4). The equations are given for an element k, subjected to strains in x- and y-direction as well as shear. Strains are calculated based on the actually measured base length at the reference load step, that means, the fact that the LEDs are not spaced exactly 150 mm apart is taken into account. In the equations, an upper index of 0 denotes the coordinates measured during the reference load step, i.e. while the test unit was still unloaded (LS001, see Section 3.3), a lower index m denotes the mean strain of the element and Δ is the difference between the current load step coordinate and the reference load step coordinate. In the equations, u and v describe deformations in x-direction and y-direction, respectively, and the indices b,t,l and r indicate whether the strain was determined along the bottom, top, left or right edge of the element.

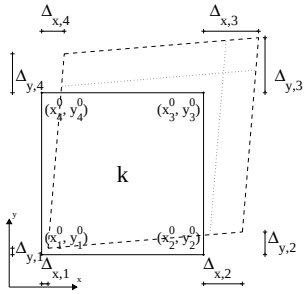

$$\varepsilon_{x,k,m} = 0.5\left(\frac{\partial u_t}{\partial x_t} + \frac{\partial u_b}{\partial x_b}\right) = 0.5\left(\frac{\Delta_{x,2} - \Delta_{x,1}}{x_2^0 - x_1^0} + \frac{\Delta_{x,3} - \Delta_{x,4}}{x_3^0 - x_4^0}\right) \tag{4.3a}$$

$$\varepsilon_{y,k,m} = 0.5\left(\frac{\partial v_l}{\partial y_l} + \frac{\partial v_r}{\partial y_r}\right) = 0.5\left(\frac{\Delta_{y,4} - \Delta_{y,1}}{y_4^0 - y_1^0} + \frac{\Delta_{y,3} - \Delta_{y,2}}{y_3^0 - y_2^0}\right) \tag{4.3b}$$

$$\begin{aligned}\gamma_{xy,k,m} &= 0.5\left[\left(\frac{\partial u_l}{\partial y_l} + \frac{\partial v_t}{\partial x_t}\right) + \left(\frac{\partial u_r}{\partial y_r} + \frac{\partial v_b}{\partial x_b}\right)\right] \\ &= 0.5\left(\frac{\Delta_{x,4} - \Delta_{x,1}}{y_4^0 - y_1^0} + \frac{\Delta_{y,3} - \Delta_{y,4}}{x_3^0 - x_4^0} + \frac{\Delta_{x,3} - \Delta_{x,2}}{y_3^0 - y_2^0} + \frac{\Delta_{y,2} - \Delta_{y,1}}{x_2^0 - x_1^0}\right)\end{aligned} \tag{4.3c}$$

$$\varepsilon_{1,2,m} = \frac{\varepsilon_{x,m} + \varepsilon_{y,m}}{2} \pm \sqrt{\left(\frac{\varepsilon_{x,k,m} - \varepsilon_{y,k,m}}{2}\right)^2 + \left(\frac{\gamma_{xy}}{2}\right)^2} \tag{4.4a}$$

$$\text{if } \varepsilon_{x,k,m} > \varepsilon_{y,k,m} : \varphi = \frac{1}{2}\arctan\frac{\gamma_{xy}}{\varepsilon_{x,k,m} - \varepsilon_{y,k,m}} \tag{4.4b}$$

$$\text{if } \varepsilon_{x,k,m} < \varepsilon_{y,k,m} : \varphi = \frac{\pi}{2} + \frac{1}{2}\arctan\frac{\gamma_{xy}}{\varepsilon_{x,k,m} - \varepsilon_{y,k,m}} \tag{4.4c}$$

Deformation components, i.e. sliding (sl), shear (s), fixed-end deformation resulting from the opening of the base crack (bc) and flexural deformation (fl), were also calculated by means of the optical measurement data up to the top end of the grid. The plots in Sections 4.2 to 4.5 contain the various displacements determined at each first and second cycle as long as enough LEDs were visible in the bottom region of the pier to calculate meaningful deformation components. The sum of these components was calculated at the top end of the grid, corresponding to the height of the LVDT HorDisp_4 (see Figure 3.6), and at the end of the shear span *a*. The sum of the components at each heigth was compared to the horizontal deformation measured by the LVDTs. The horizontal displacements measured by the LVDTs were corrected according to Equation (4.2). To calculate the deformation components at the end of the shear span the strains were extrapolated. Above the measurement grid, a constant shear strain, equal to the average shear strain of the last two measurement rows, was assumed. The curvature distribution was assumed linear between the end of the shear span and the center of the two top rows of the measurement grid. The average strains of the last two rows were used to increase accuracy because the strains at the top of the pier were rather small in general and therefore might have reached the limits of the accuracy of measurement systems. In this report, the components at the end of the shear span are presented together with the deformation measured by the LVDTs.

The mean horizontal deformation of all LEDs in the bottom row located 50 mm above the foundation was assumed to represent the sliding deformation Δ_{sl}. All other deformation components were calculated from the coordinates of the LED columns along the edges of the pier, i.e. the first and last column of the measurement grid. The vertical displacements of the two LEDs at the bottom were used to determine the fixed-end component, stemming from the opening of the base crack. The top displacement Δ_{bc} was obtained by multiplying the base rotation calculated from the difference of the two vertical displacements with the height, see Equation (4.5a). At later load steps during the test, when the markers in the bottom corners were missing because the concrete had spalled off, the next visible markers were used.

To obtain the flexural displacement Δ_{fl} the curvatures were double - integrated over the height. To calculate the curvature, the strains were determined from the change in distance between the markers above each other and divided by the distance between the markers in the same row.

The shear displacements Δ_s were calculated along the grid according to Equation (4.5b), where $h_E = 150\,\text{mm}$ is the height of one row and $b_E = 1350\,\text{mm}$ the width of the grid, and summed up over the height of the grid. The length of the diagonals D_1 and D_2 was calculated from the measured coordinates of all four nodes.

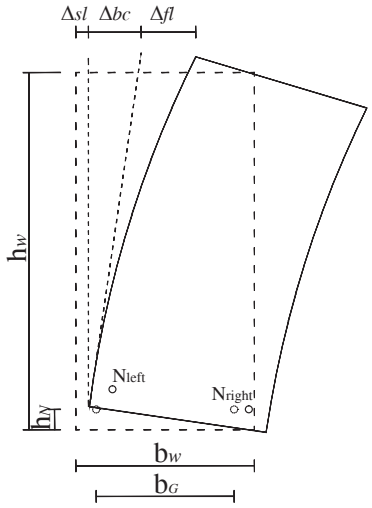

$$\Delta_{bc} = \frac{\Delta_{vert,Nleft} - \Delta_{vert,Nright}}{b_G}\,(h_W - h_N) \tag{4.5a}$$

$$\Delta_s = \frac{D_1^2 - D_2^2}{4b_E} \tag{4.5b}$$

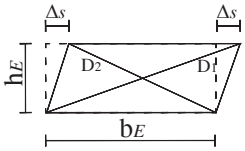

Figure 4.1: Illustration of the sliding, fixed-end and flexural deformation components to the left and of the shear deformation to the right. The diagonals needed to calculate the shear displacement are indicated in the figure to the right.

The data obtained from the optical measurements is also used in combination with data from the hard-wired measurements to show the anchorage slip of some longitudinal reinforcement bars against the strain, measured with a strain gauge attached to the same bar. As shown in Figure 3.8, four longitudinal reinforcement bars were instrumented with one LED each, right above the foundation. More precisely, the center of the LEDs was located at about 10-15 mm above the foundation. The difference in the vertical displacement of the LEDs on the reinforcement and on the brackets next to that reinforcement bar (compare Figure 3.8) corresponds to the slip. In the following sections, the slip is plotted against the strain obtained from the strain gauges that were glued to the reinforcement bars right underneath the LED, i.e. strain gauges 1, 3, 7 and 9 shown in Figure 3.4. These plots are only provided for VK6 and VK7, as the strain gauges of VK4 did not work properly and the optical measurements were replaced with manual measurements in the test of VK5. Furthermore, the slip of the outer reinforcement bars is plotted against the displacement ductility for all test units except for VK5. The displacement ductility was determined according to [PCK07], i.e. it was determined based on the nominal yield displacement according to Equation (3.2) with the experimentally determined displacement at first yield force.

4.1.3 Manual Measurements

Data Processing

In a first step, all manual measurement values were corrected using the calibration measurements on the invar bar, to minimize temperature influence. These calibration measurements were then subtracted from the actual measurements, assuming a linear distribution between the calibrations. Afterwards, the differences between the measurements at the load steps and the second reference measurement (LS001) was calculated to identify and remove obviously erroneous values.

As the measurement grid contains redundant values, a correction, related to a least-squares error compensation, was made by modeling the grid as a linear elastic, externally isostatic 2D truss on which the strains, calculated from all measured deformations and grid base-lengths, were applied as load. The resulting normal forces relate to the measurement errors. Since the same absolute accuracy is assumed for both extensometers, the same axial stiffness EA/l, with the modulus of elasticity E, the truss area A and truss length l, was used for all truss elements. The truss was modeled with the Sofistik finite-element-software [Sof10]. The difference of the truss' nodal displacements between each load step and the reference load step was calculated afterwards and used for further processing.

Data Presentation

Deformations and strains along the measurement grid were determined using the manual measurements. The deformations, i.e. the nodal displacements, result directly from the truss model while the strains were calculated from these deformations, according to Equations (4.3) and (4.4). Strain plots of selected load steps are included in the result sections of the test units.

Deformation components were also determined from the manual measurements the same way as for the optical measurements, see Section 4.1.2.

4.1.4 Crack Widths

Data Presentation

Plots of all monitored cracks, which indicate also the numbers of the cracks and the pattern along which the widths were measured, are presented in the result section of each test unit. Photos of the test units at load step $\mu_\Delta = 3.0$ were used as reference for the plots, since the crack pattern was usually fully developed by then and degradation had not yet initiated. Tables containing the widths of selected cracks at a number of load steps are also included in these sections.

4.2 Test Unit VK4

4.2.1 Test Observations

Test unit VK4 was equal to the previously tested unit VK3 [Bim10], except for a 60 cm long lap splice at the bottom of the pier. Testing began on November 26^{th}, 2009 by applying the vertical load and ended on December 17^{th}, 2009. Before the vertical load was applied, all the reference measurements, including optical and manual measurements, were taken and the hard-wired devices were set to zero. The vertical load of 1300 kN was then slowly applied and the next measurements were taken. The next day, the vertical load was released to 256 kN and then reapplied, because of an error in the optical measurements, to take new measurements with and without axial load. The load could not be lowered further without completely releasing pressure from the circuit, which could possibly have meant that also the anchors of the tendons had to be readjusted before the new load application. Therefore, the new reference measurements were made with this load, which corresponds to an average compressive stress of only 0.5 MPa over the entire cross section.

On December 1^{st} the actuator was connected and the first horizontal loading was applied. It should be noted that an error in the signal of the horizontal force became obvious during the test. However, this was not noticed in the beginning, since the deformations are rather small during the first cycles and the test unit merely appeared to be a bit stiffer than expected. Since a force could only be applied and measured when cycling, it took a few cycles until the force could correctly be determined from the pressure in the piston chambers and the error subsequently identified and fixed. From the small cycles between the first and second large cycle to $\mu_\Delta = 2.0$ onwards, the load-cell worked correctly. Before that, the measured force was 29.7 % too high because of a wrong connection in the cable's plug, which added electrical resistance. Therefore, the horizontal forces which were actually applied during the cycles in the elastic range were lower than intended. Another problem occurred with the strain gauges, whose measurements were unusable, because, as discovered later, there was an incorrect assembly in the connecting box.

During the first load cycles to $(0.25/1.297)F'_y = 0.19F'_y$ the test unit nearly remained without cracks, except for very fine ones, which were starting to develop at the base. At LS007 and LS009, $0.39F'_y$ South 1^{st} and North 1^{st} the first cracks developed in the pier, mainly at the height of the second stirrup above the base. After cycling from LS009 to LS010, the LVDT VertDef_N02 had to be replaced because of a noisy signal during the cycle. At LS015.1 and LS017.1, $(0.75/1.297)F'_y = 0.58F'_y$ South and North 1^{st}, flexural cracks developed primarily up to 95 cm and the widths of the cracks at the bottom and top end regions of the splice, were in the range of 0.05 mm. When $1.0/1.297 = 0.77F'_y$ horizontal force was reached, there were cracks up to 2.30 m and their ends began pointing downwards. Testing was completed that day with the second cycles to this target load.

Because of the error in the force readings, deformations were rather small up to this load step and continuing with load step $\mu_\Delta = 1.0 = 10.5$ mm would have meant almost doubling the horizontal displacement, an additional load step $F'_{y,E}$ was added to the loading history. The cycles peak forces were $F = 609$ kN and $F =$ -613 kN in positive and negative loading direction, and hence still slightly lower than the theoretical yield force $F'_y = 641$ kN. Initially, the intention

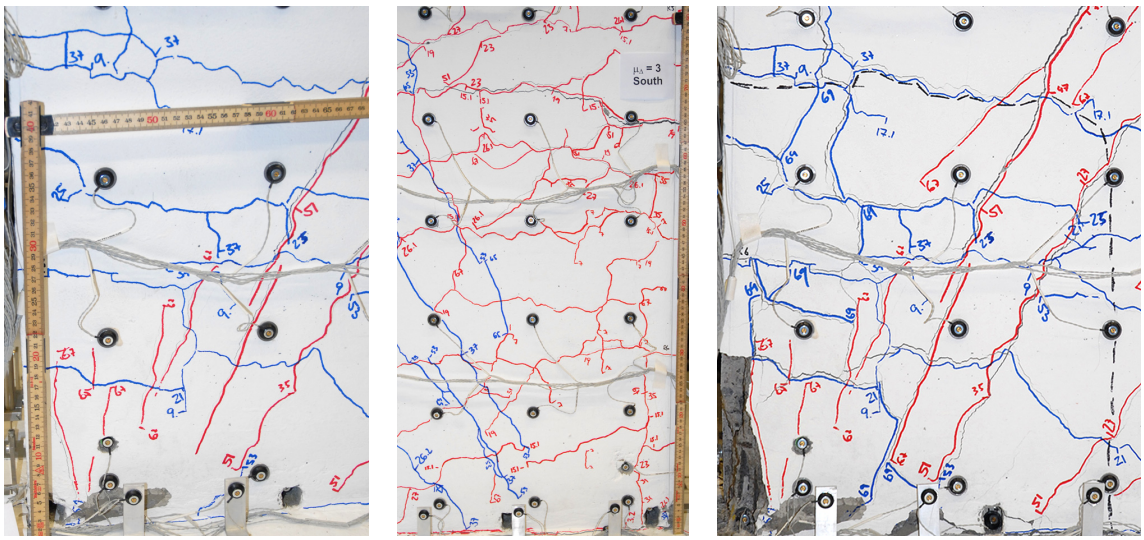

(a) $\mu_\Delta = 3.0$ S 1^{st} **(b)** $\mu_\Delta = 3.0$ S 1^{st} **(c)** $\mu_\Delta = 3.0$ N 1^{st}

Figure 4.2: Front view of the Southern (a) and Northern (b) bottom part of the pier at load step $\mu_\Delta = 3.0$ South and North 1^{st}, as well as the Southern bottom part of the pier at load step $\mu_\Delta = 3.0$ North 1^{st} (c). The dashed line indicates the area with internal cracks in the splice region, which sounded hollow.

was to load until the strain gauges indicated yielding of the longitudinal reinforcement, but since the measured strains were unreasonably low and, as discovered later, false, loading was simply stopped between F'_y and $\mu_\Delta = 1.0$. Cracks formed up to 1.85 m with a main crack distance of 20 cm, equal to the stirrup spacing, and grew clearly steeper at their ends towards the center of the pier. After this additional cycle was completed, the normal loading history was resumed by applying the target displacement of $\mu_\Delta = 1.0$ South 1^{st}. At this load step, the lengths of the cracks increased and widths of 0.15 mm were determined, but crack width determination along a certain pattern was only started at $\mu_\Delta = 1.0$ North 2^{nd} in this test. Besides opening of the cracks, slip along the cracks was observed. In this cycle, the first yield force $F'_y = 641$ kN was actually exceeded the first time in each direction, with peak horizontal forces of 647 kN and -657 kN at LS019 and LS021, respectively.

Before the next cycles were conducted the following day, pressure transducers were connected to the valve controlling the pressure in both chambers of the horizontal actuator to measure the pressure in each chamber and thereby check the applied horizontal force. At the first deflection to $\mu_\Delta = 1.5$ South a vertical crack formed between two horizontal ones in the upper part of the lap splice. After completing the measurements at $\mu_\Delta = 1.5$ North, the pier was unloaded horizontally and all hydraulic devices turned off for the night. The next day, testing was started with small cycles - which contained an extra loop due to a still valid threshold value which shut the actuator down - followed by the second cycle to $\mu_\Delta = 1.5$. The base crack was ~ 0.5 mm and 0.6 mm wide, respectively, when the peak displacements of the second cycle were applied. When both cycles to $\mu_\Delta = 1.5$ were completed, new shear cracks had formed up to almost 2.50 m and some of the previous grew longer and reached to about 20 cm from the opposite edge of the pier in each direction.

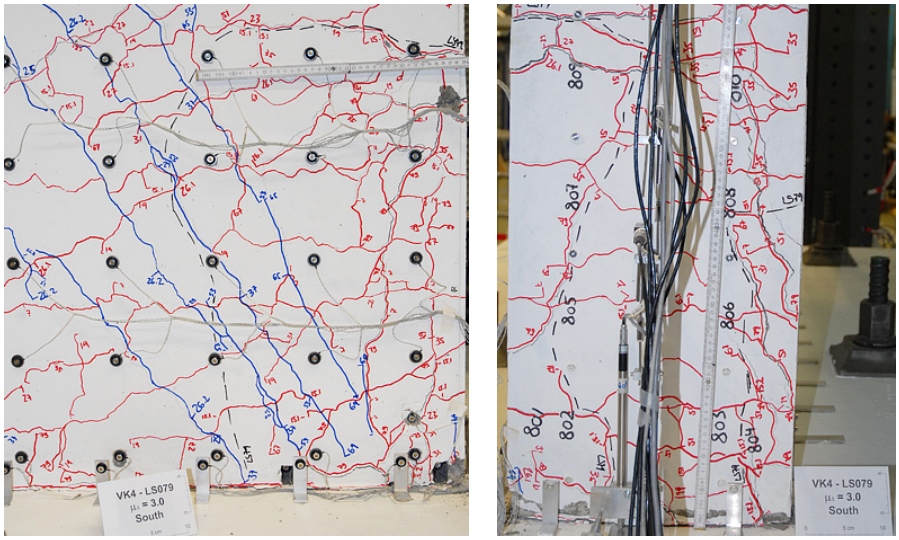

(a) $\mu_\Delta = 3.0$ South 2^{nd} **(b)** $\mu_\Delta = 3.0$ South 2^{nd}

Figure 4.3: Front view of the Northern part of the pier (a) and North face of the pier at the second cycle to $\mu_\Delta = 3.0$ South (b).

After these cycles the source of the error in the horizontal force signal was found and fixed. Two small cycles were inserted to check the signal, before the test was continued with the planned load steps. Since the signal was correct then, loading continued with LS051 $\mu_\Delta = 2.0$, where crack widths were determined and manual measurements made. A previously not monitored crack located above the lap splice at 65 cm height, which was subsequently tracked instead of the previously tracked crack laying above, opened up to 0.6 mm. The base crack opened up to 0.6 - 0.7 mm and on the pier's surface, where new cracks developed up to 2.80 m height, widths of up to 0.8 mm were measured. Crack spacing was mostly between 15 to 20 cm, i.e. in the range of the stirrup spacing. The displacement along the cracks could clearly be observed along the vertical and horizontal lines of the manual measurement grid on the back of the test unit, where a horizontal displacement of about 0.5 mm along a crack crossing measurement no. 126 could be determined. As the foundation had slid southwards by about 1 mm on the strong floor at this load step, additional metal plates were inserted at the horizontal support on the North side. The new location of the test unit was considered in the application of the top displacements in the following cycles.

At the reversed load step at $\mu_\Delta = 2.0$ North 1^{st}, a horizontal crack at 57 cm height, right below a monitored one, was up to 0.35 mm wide and the base crack up to 0.85 mm, whereas the widths of the cracks in between, i.e. in the area with the lap splice, were significantly smaller. Other observations regarding the cracks were similar to those described above. The test unit's peak horizontal load in the negative loading direction, $F_{min} = -871$ kN, was applied during this cycle. When all measurements were finished, the small cycles load steps were applied, followed by the second cycle to $\mu_\Delta = 2.0$. Small cycle load steps were defined by target displacements from this point onwards. At the second peak deflection at $\mu_\Delta = 2.0$ South, the base crack opened up to about 1 - 1.1 mm.

At LS067, $\mu_\Delta = 3.0$ South, the maximum horizontal force $F_{max} = 913$ kN was applied. Cracks formed up to about 2.90 m and grew longer, reaching deep down in the South part of the pier.

In the compression zone on the South, vertical cracks formed to approximately 25 cm height in the outer 13 cm of the pier, see Figure 4.2a. At the Northern part of the pier, the width of the previously mentioned crack above the splice was measured at the pier's edge and 15 cm from the edge. It was 2.5 mm wide at the edge and 1.4 mm wide 15 cm from the edge (Figure 4.2a). This crack was followed subsequently, since the other one above was almost closed then. The base crack was up to 1.6 mm wide. After load reversal, while the top displacement was increased to $\mu_\Delta = 3.0$ North for the first time, there was a clicking sound and the horizontal load dropped 140 kN at -19 mm top displacement due to some failing splices. The previously applied horizontal peak force in the negative loading direction was not reached at this load step, with an eventual horizontal force capacity of 600 kN, i.e. 313 kN less than at $\mu_\Delta = 3.0$ South. By knocking on the pier surface, the area where internal cracks and thereby splice damage occurred could be determined by the hollow sound it produced in these regions. On the front face, damage was detected up to the third column of markers (see Figure 4.2c), i.e. the fifth splice, and on the back up to approximately 95 cm from the pier's Southern edge, i.e. beyond the pier's center line. Additional vertical cracks had also developed in this area during loading. In the corners on the South face, where the concrete had spalled off, about 1 cm relative displacement between the spliced bars was measured by means of a ruler. Hardly any changes were visible in the rest of the crack pattern and the compression zone hardly seemed damaged in compression. At the second peak at $\mu_\Delta = 3.0$ South, some splices at the North side of the pier had also failed, which was also noticeable in a drop of the horizontal force accompanied by a corresponding sound. A 1 mm wide vertical crack had developed on the East face close to the N-E corner of the pier and the cover concrete sounded hollow in a region spanning from the edge up to about the fifth splice from the edge, see Figure 4.3a. Another vertical crack at the North face, close to the N-W corner, was 2 mm wide (Figure 4.3a). On the back (West face) of the pier, the concrete cover was loose at least up to 35 cm height over the entire pier surface and visibly pushed outwards. At the center part of the North face the concrete covering the two central splices seemed less damaged, because it did not appear to be as loose as it was at the back side of the pier. Not much additional damage seemed to occur while cycling to $\mu_\Delta = 3.0$ North the second time. The horizontal force capacity had meanwhile dropped significantly to F = -448 kN which is 51 % of the maximum force value applied in this direction. Manual measurements were taken at the second deflections to $\mu_\Delta = 3.0$ instead of at the first. When that cycle was completed, hydraulics were turned off for the night.

The next day, testing started by increasing the top displacement to $\mu_\Delta = 4.0$ for the first time. During load application, the test had to be stopped to remove some cover concrete pieces pushing against VertDef_S01 and _S02 and to fix their support which had loosened a bit. At the South edge of the pier, which was under compression, some more cover concrete at the front seemed to be loose, possibly due to a buckling bar. At the opposite (North) edge enough cover concrete was missing to measure the relative displacement between the spliced bars, which was 1.3 to 1.5 cm. At LS085, $\mu_\Delta = 4.0$ North, all cover concrete along the splices sounded hollow. In both directions, South and North, the crack widths were determined. In each case, the cracks that had developed at the reversed load step also opened up wide, i.e. the cracks that had formed in positive loading direction also opened up in negative loading direction and vice versa. Therefore, the widths of the cracks stemming from both loading directions were measured at each load step. In the second cycle to $\mu_\Delta = 4.0$, which was conducted during this and the following test day, the horizontal force level was already rather low and the main increase and decrease of horizontal force occurred between about $\pm$ 11 mm. Outside this range, the force-displacement curve was

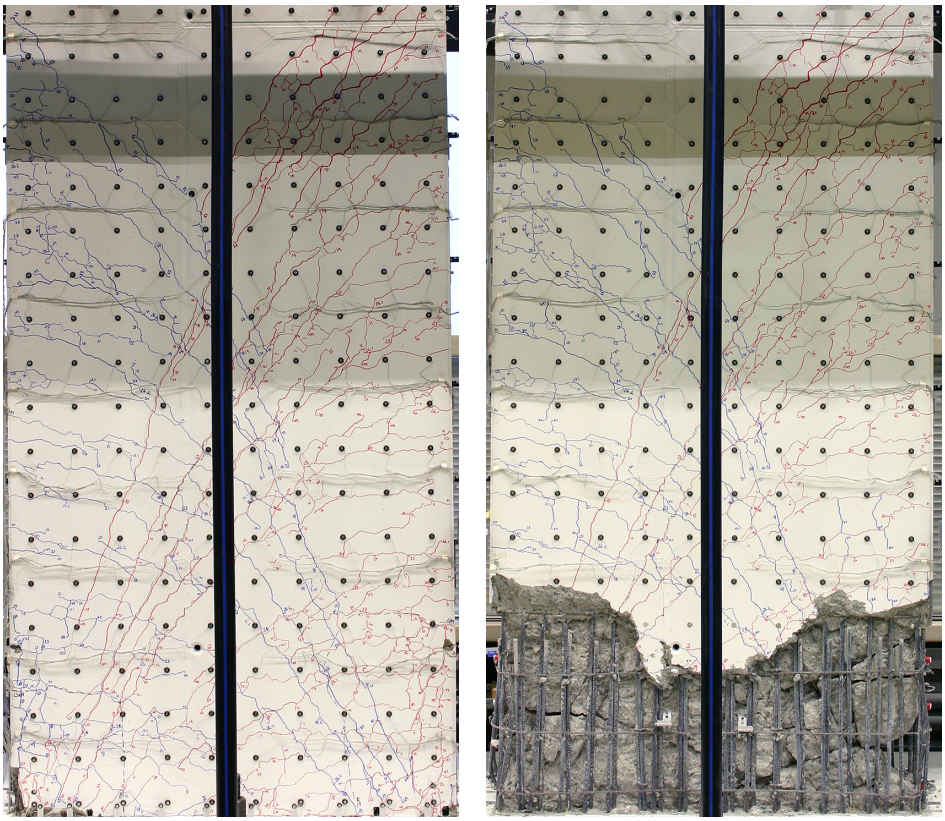

(a) $\mu_\Delta = 3.0$ South 2^{nd}

(b) center position at cycle $\mu_\Delta = 10.0$

Figure 4.4: Test unit VK4: Front view of the pier at $\mu_\Delta = 3.0$ South 1^{st} and at last cycle to $\mu_\Delta = 10.0$ North, i.e. shortly before the test was ended.

rather flat. During the cycles to $\mu_\Delta = 5.0$ and the small cycles in between, some cover concrete became loose enough to be removed and the test had to be stopped once to remove concrete pieces which would otherwise have disturbed LVDTs VertDef_S02 and _S03. Since the lap splice was almost completely damaged before the cycles at $\mu_\Delta = 5.0$, not much additional damage occurred and the horizontal peak force only slightly dropped further in each subsequent load step. At LS115, $\mu_\Delta = 6.0$ South 1^{st} the actuator was stopped too late accidentally. No small cycles were conducted anymore and the observations were similar to those at $\mu_\Delta = 5.0$ with a slowly decreasing horizontal peak force and hardly any additional damage. The first LVDTs at the bottom of the pier's North and South faces had to be removed at $\mu_\Delta = 6.0$ North 2^{nd}. Only one cycle was applied at the remaining ductility amplitudes, since a kind of residual force level seemed to have been reached, as the horizontal force only decreased slightly and not much additional damage occurred. The top displacement was gradually increased to $\mu_\Delta = 10.0$ which was also the maximum displacement applied to VK3 (see [Bim10]). Some more LVDTs were removed during these cycles. When $\mu_\Delta = 10.0$ South was applied, the normal force rose to 1344 kN before the increase was noticed and the pressure lowered, which resulted in a kink in the force-displacement relationship at 40 mm displacement. After completing the $\mu_\Delta = 10.0$ cycles the test was concluded. The remaining horizontal force capacity was $F = 201\,\text{kN} = 0.22\,F_{max,pos}$ and $F = \text{-}101\,\text{kN} = 0.12\,F_{max,neg}$, respectively. A picture of the test unit after

the test was completed is presented in Figure 4.4 along with one at $\mu_\Delta = 3.0$, when the crack pattern was already fully developed.

4.2.2 Hard-Wired Measurements

In the following graphs, some of the hard-wired measurement data is presented. In Figures 4.5 through 4.7, the horizontal force measured with the actuator's internal load-cell is plotted against the top displacement, corrected according to Equation (4.2). During this test, disturbances of the load-cell signal occurred twice but were not recognized as such during the test. In contrast to the disturbances observed during the other tests, the signal did not just jump to an obviously wrong value in between but was irregularly fluctuating by 7 kN before it eventually went back to a stable signal. The force-signal of the two half-cycles in which the disturbances occurred is therefore replaced with the force determined from the pressure transducers corrected for the offset between the two.

The curvatures presented in Figure 4.8 were determined from the measurements of the LVDT chains along the side faces of the pier. A horizontal distance of 1544 mm between the devices was used to calculate the curvatures, because the center lines of the LVDTs were mounted 22 mm away from the surface. In general, all curvatures are displayed until the devices had to be removed to protect them from damage.

The strains plotted in Figure 4.10 were also determined from the LVDTs using the measured deformation and the base lengths which can be seen in Figure 3.5. Those strains, which represent the strains 22 mm away from the surface, were projected to the pier's surface with linear interpolation, i.e. with a plane sections assumption. The strains are presented for the first cycles of some selected load steps. In general, the peak values of the cycles have not been used, but those at the end of the time frame in which the top displacement was maintained constant, because they correspond best to the manual and optical measurements, which were usually also taken towards the end of that time interval. At $\mu_\Delta = 3.0$ North, the splice was already starting to degrade and large cracks opened up. The strain value determined from the measurement of LVDT VertDef_N02 is therefore very large. As the same scale as for the other plots was chosen to better visualize the smaller strains, the value is outside the plot region in this case.

No strain gauge measurements are presented for this test unit, because the measurements were wrong due to an incorrect assembly in the connecting box, see also Section 4.2.1. This means the plots showing the reinforcement strain distribution and the strain-slip relation are missing. However,

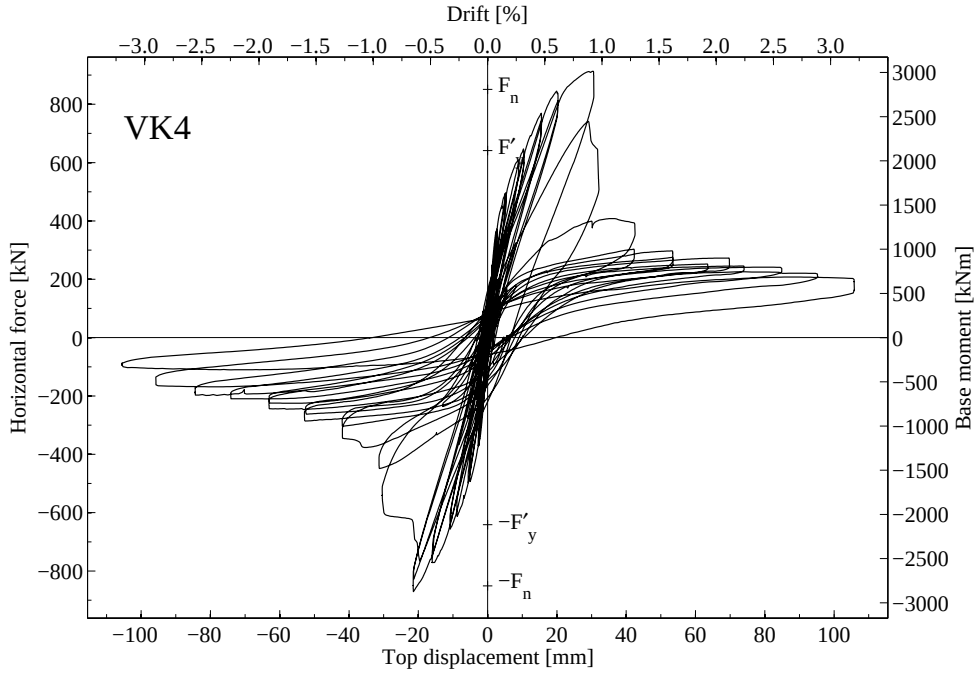

Figure 4.5: Measured force - deformation response of test unit VK4.

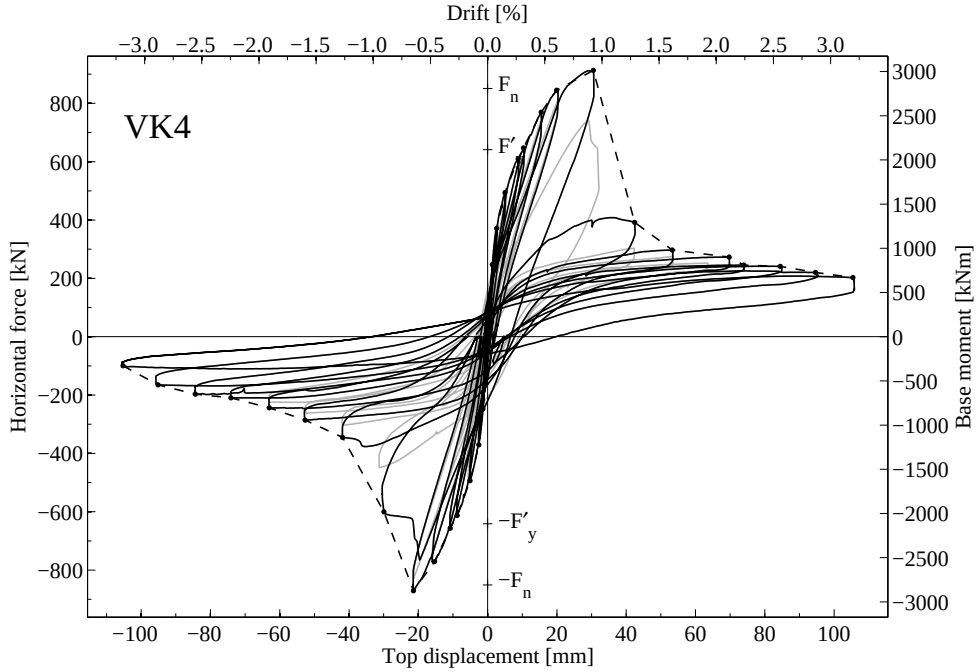

Figure 4.6: Measured force - deformation response of test unit VK4 with emphasized first cycles and envelope of first cycles.

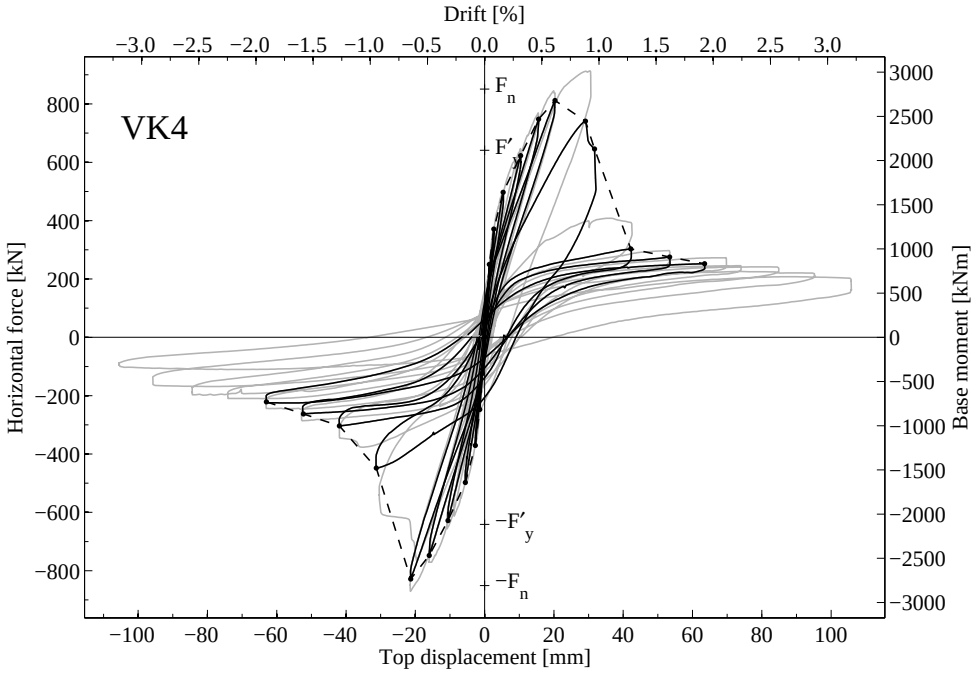

Figure 4.7: Measured force - deformation response of test unit VK4 with emphasized second cycles and envelope of second cycles.

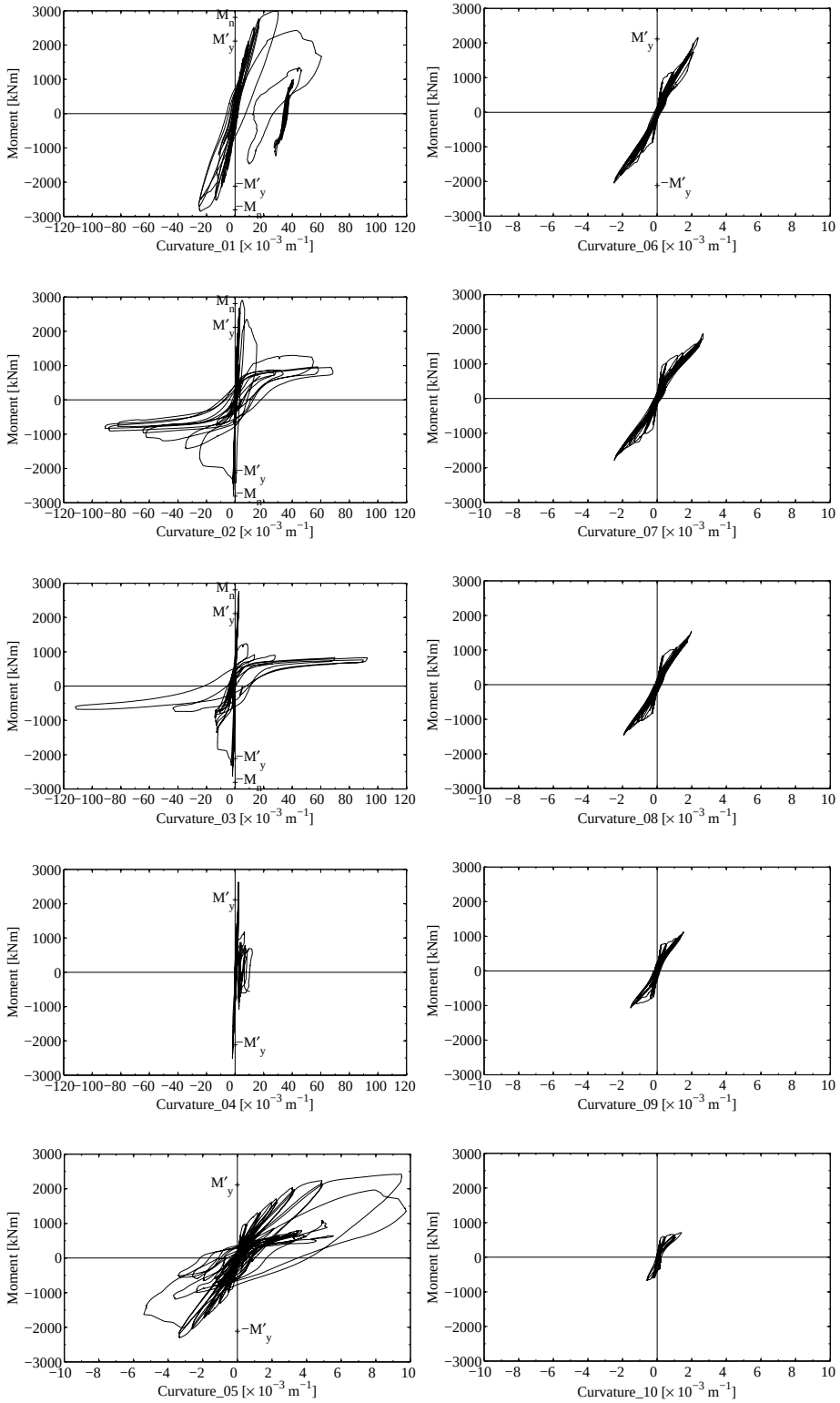

Figure 4.8: Measured moment-curvature relationships 01 to 10 of test unit VK4.

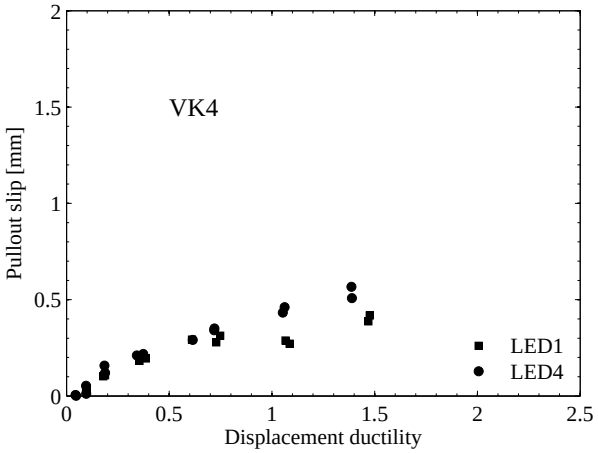

Figure 4.9: Pullout slip of reinforcement bars measured right above foundation (LED) against displacement ductility.

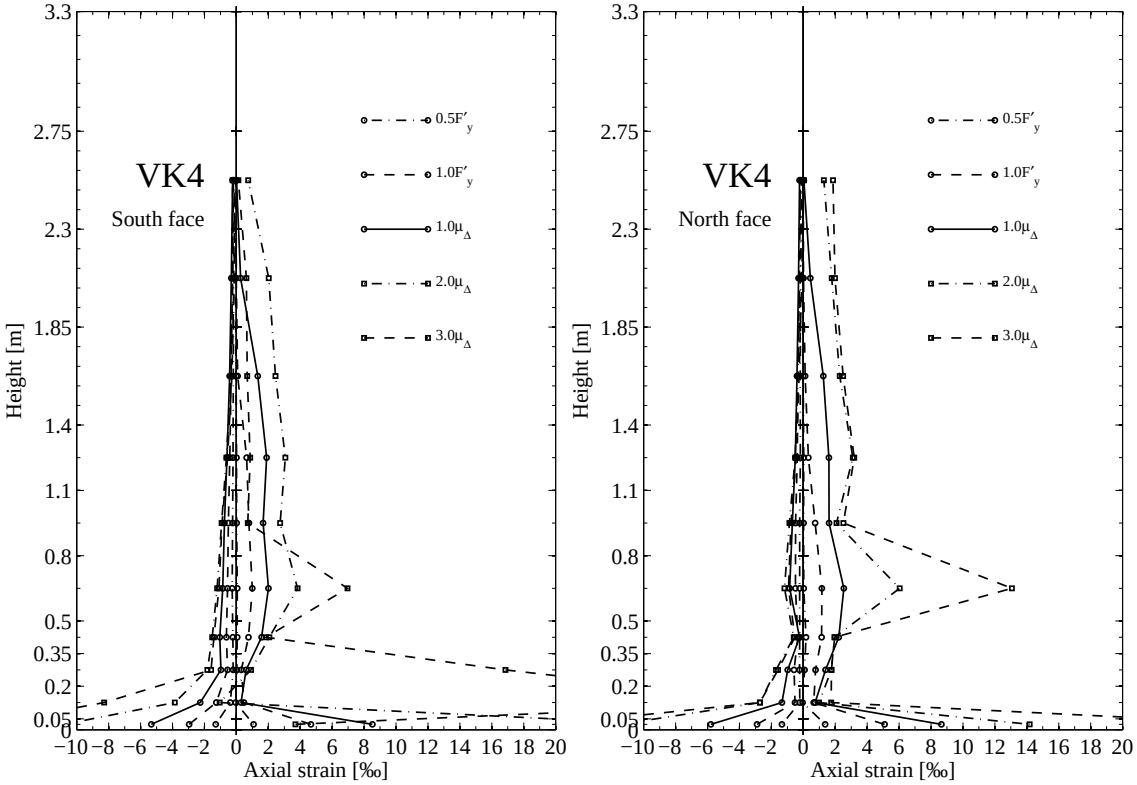

Figure 4.10: Strains along the South and North face of test unit VK4 calculated from deformations measured by means of the LVDTs and projected to the test unit's surface, at selected load steps. The value at +0.125m, which is determined from measurements in the damaged splice region and outside the plot range, is 34.5 ‰.

4.2.3 Optical Measurement Results

In Figures 4.11 and 4.12, plots with the principal strains calculated from the optical measurements are presented. The strains are computed from the measurements taken during two minutes long time intervals at the peaks of the cycles while the top displacement was kept constant according to the procedure described in Section 3.2.2. The largest strains are obtained for the bottom row, since its vertical base length is small but the deformations large due to the base crack. Because these strains exceed the strains along the pier by far, they have not been included in the plots since it would be difficult to read the plots if they were included and drawn to the same scale. The piers are always drawn to a scale of 1:50 and the largest strain has the same length in each plot. This constant strain length was chosen to visualize both the load steps with small as well as those with large strains equally well. For the calculation of the strains according to Section 4.1.2 the mean values of the transformed coordinates were used, no further corrections were made. However, as marker rows 10 and 12 seemed obviously false, these rows have not been considered. The mean values of the strains ε_x in the rows above and below were assumed as horizontal strains for these marker rows, the same values ε_y and γ_{xy}, calculated from the markers in rows 9 and 11, as well as 11 and 13, were assumed for both rows of elements. It should be kept in mind that the plots assigned to load step $1.0F'_y$ (Figures 4.11a and 4.11a) present the strains corresponding to $1.0/1.297 = 0.77F'_y$ horizontal force, since load step $1.0F'_y$ did not exist due to the error in the horizontal force signal (see Section 4.2.1). Sometimes, more than one measurement with a two minute time frame was made while the top displacement was maintained constant. In these cases, a "before Def" or "after Def" in the plots indicates whether the measurement has been taken before or after the manual measurements ("Deformeter" measurements) were taken.

In Figure 4.13 the deformation components determined at each load step up to $\mu_\Delta = 3.0$ are presented and compared to top displacement measured by the LVDTs and corrected according to Equation (4.2). Components are only presented up to the first cycles to $\mu_\Delta = 3.0$, because the lap-splice was severely damaged afterwards and determination of meaningful components therefore difficult.

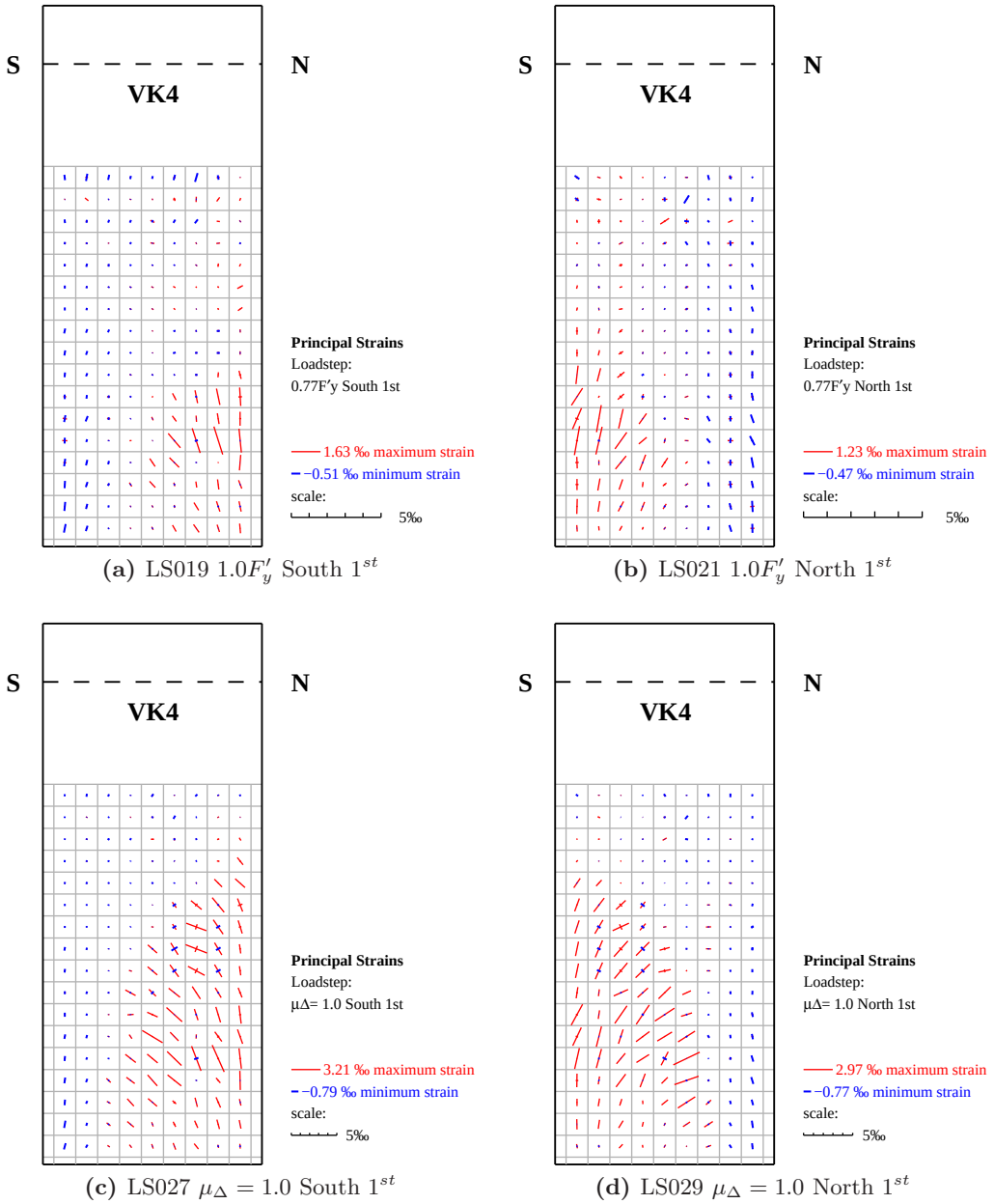

(a) LS019 $1.0F'_y$ South 1^{st} **(b)** LS021 $1.0F'_y$ North 1^{st}

(c) LS027 $\mu_\Delta = 1.0$ South 1^{st} **(d)** LS029 $\mu_\Delta = 1.0$ North 1^{st}

Figure 4.11: Principal strains of VK4 at $1.0/1.297 = 0.77F'_y$ (a), (b) and at $\mu_\Delta = 1.0$ (c), (d).

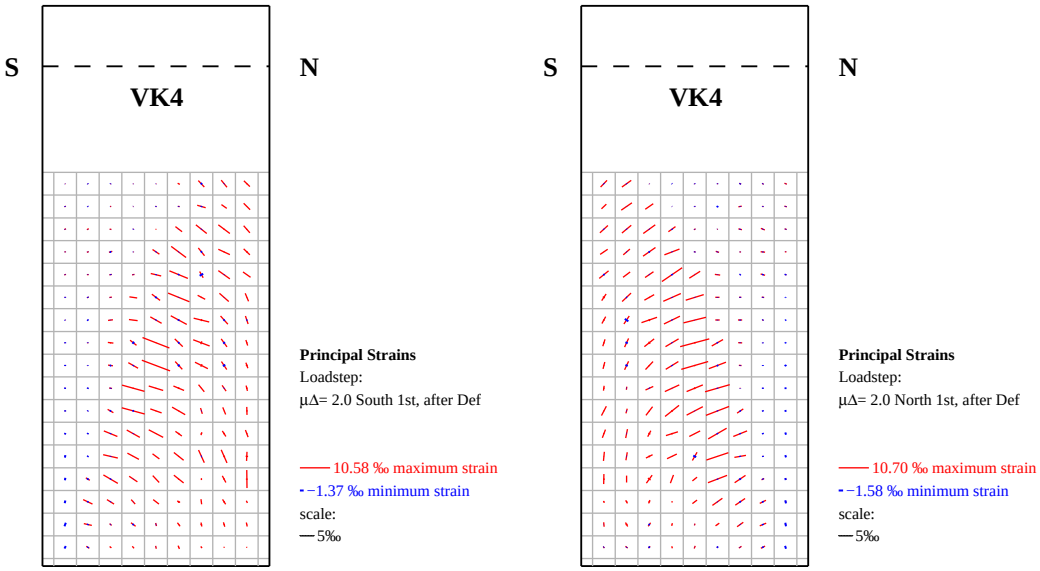

(a) LS051 $\mu_\Delta = 2.0$ South 1^{st} **(b)** LS053 $\mu_\Delta = 2.0$ North 1^{st}

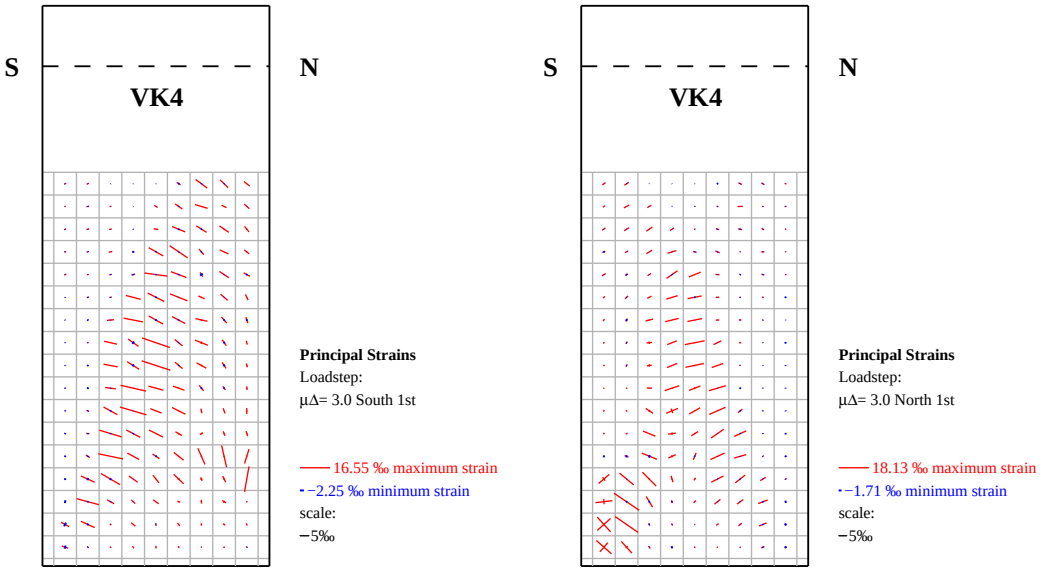

(c) LS067 $\mu_\Delta = 3.0$ South 1^{st} **(d)** LS069 $\mu_\Delta = 3.0$ North 1^{st}

Figure 4.12: Principal strains of VK4 at $\mu_\Delta = 2.0$ (a), (b) and at $\mu_\Delta = 3.0$ (c), (d).

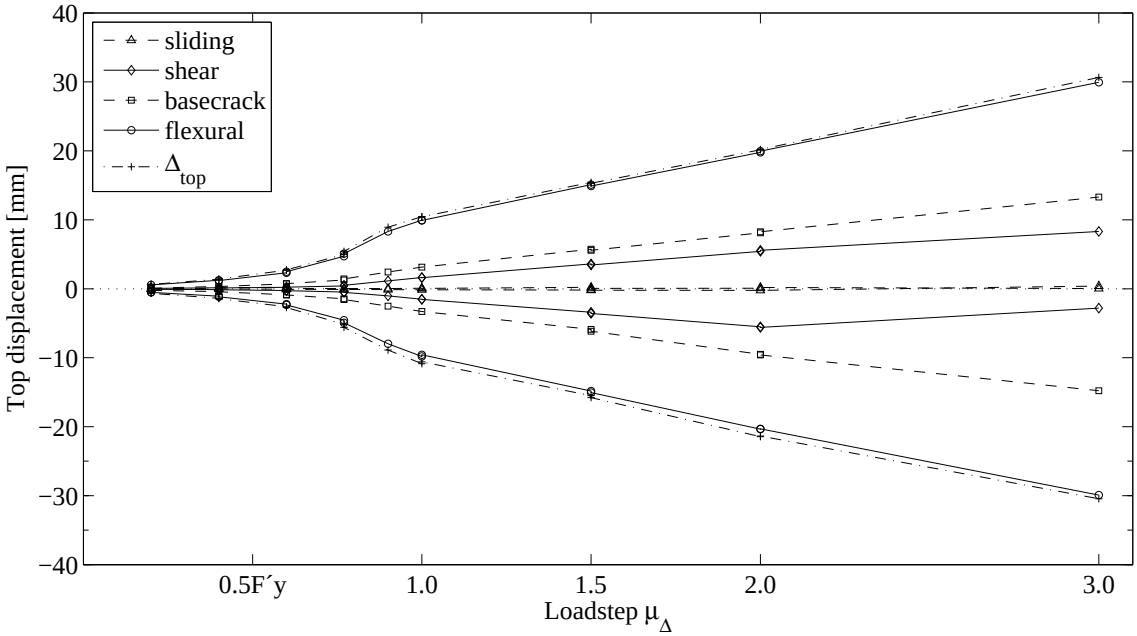

Figure 4.13: Sum of deformation components of VK4 at the 1^{st} and 2^{nd} cycles at the end of the shear span compared to the top displacement measured by the LVDTs.

4.2.4 Cracks

The monitored cracks as well as the complete crack pattern are presented in Figure 4.14. Table 4.1 summarizes the widths of some of the cracks at certain load steps. Cracks that were already visible but too narrow to determine their widths are indicated with < 0.05. Figure 4.14 also shows how cracks were numbered and along which pattern their widths were determined.

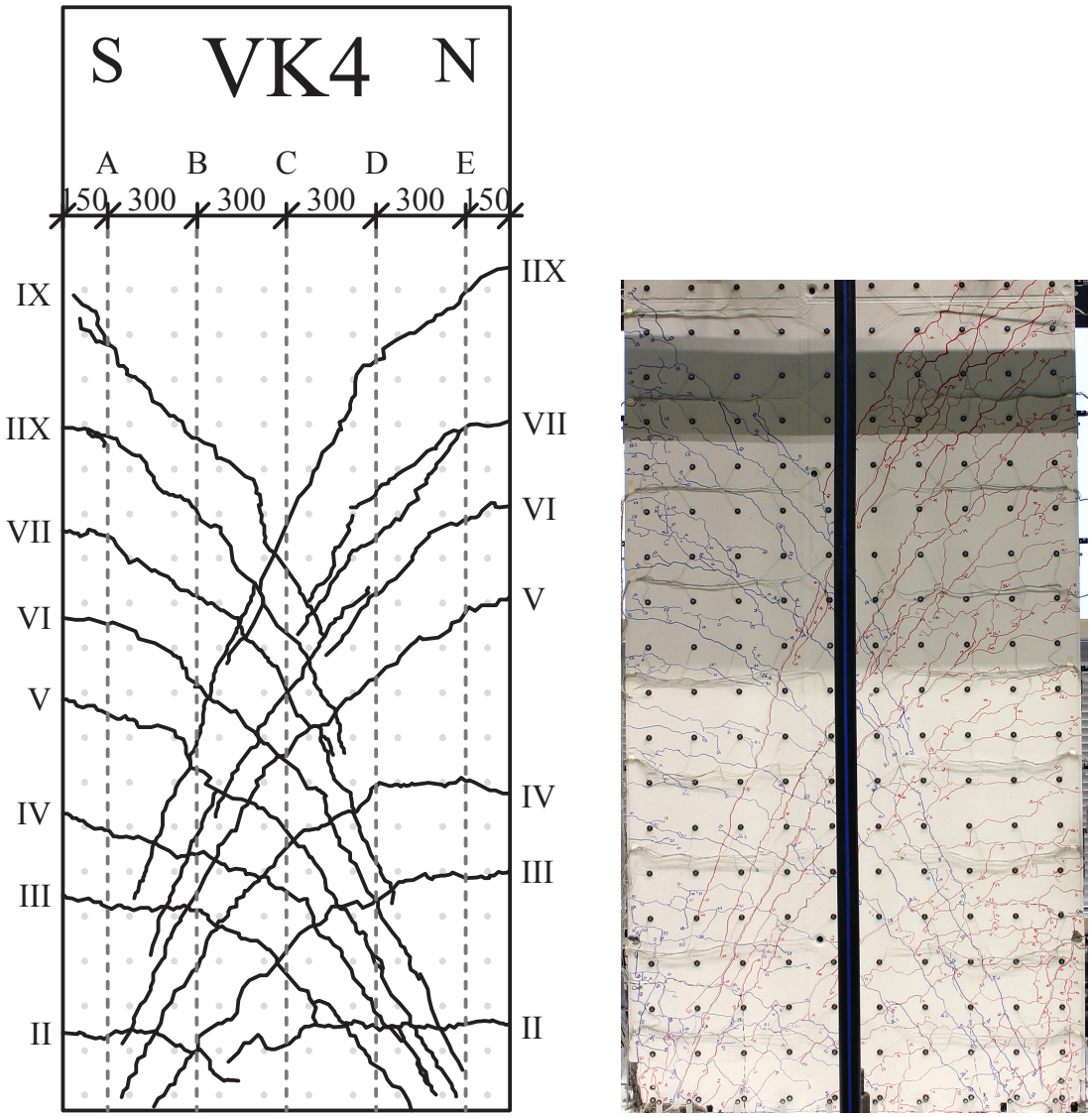

Figure 4.14: Drawing of monitored cracks (left) and picture of complete crack pattern (right) of test unit VK4.

		Crack widths [mm]									
		1^{st} cycles South						1^{st} cycles North			
		A	B	C	D	E		A	B	C	D	E
$1.5\mu_\Delta$	IV			0.2	0.05	0.1	IV	0.15	0.05	0.2		
$2.0\mu_\Delta$				0.35	0.1	0.1		0.25	0.1	0.4	0.15	
$3.0\mu_\Delta$			0.45	0.85	0.15	0.15		0.05	0	0.65	0.1	
$4.0\mu_\Delta$			2×0.2	0.4	0	0.05		0.05	0	0.25		
$1.5\mu_\Delta$	VI			0.25	0.2	0.1	VI	0.05	0.1	0.2		
$2.0\mu_\Delta$				0.4	0.5	0.1		0.05	0.15	0.5	0.25	
$3.0\mu_\Delta$			0.4	0.8	0.4	0.1		<0.05	0.05	0.65	0.7	
$4.0\mu_\Delta$			0.2	1.0	0.3	0.05		0	0	0.45	0.4	

Table 4.1: Widths of cracks of test unit VK4 at selected load steps and locations.

4.3 Test Unit VK5

4.3.1 Test Observations

Test unit VK5 had the same reinforcement layout as VK4 but a larger shear-span-to-depth-ratio. Testing began on March 18^{th}, 2010, by applying the vertical force and ended on March 29^{th}, 2010. Before the vertical load was applied, all the reference measurements, including optical and two manual measurements, were taken and the hard-wired devices were set to zero. Only parts of the pier could be measured with the optical system in this test, since only one sensor was available. Therefore, the optical measurements merely served as supplementary measurements in the lower part of the pier. After the vertical load of 1300 kN was applied, a new set of manual measurements was taken (LS002) and the actuator was connected to the test unit the next day. No horizontal force signal was transmitted from the internal load-cell when the first horizontal loading was applied. Hence, the test unit was unloaded, the actuator disconnected and the force signal checked.

After the problem with the signal had been solved, the actuator was reconnected and the two cycles to $0.25F'_y = 119$ kN were conducted. Only fine cracks were visible in the construction joint between foundation and pier at the South and North face of the pier. At LS007 and LS009, $0.5F'_y = 238$ kN South and North 1^{st}, manual measurements were taken and cracks began to develop along the sides of the pier were the stirrups were located. Most of them were short and almost only visible along the South and North face, but not on the front face of the pier. During the first cycle with $0.75\,F'_y = 356$ kN peak horizontal force, flexural cracks had developed mainly up to 1.55 m. Some of the cracks reached from the edges to the center line of the pier and then turned towards the pier base. In the area with the lap splice, cracks were rather short and fine, but the base crack and two cracks right above the splice were 0.1 - 0.15 mm wide at load step $0.75\,F'_y$ South. At $0.75\,F'_y$ North 1^{st} the base crack was 0.15 to 0.2 mm wide and the crack above the splice 0.2 to 0.25 mm. A decrease in stiffness was noticeable in the force displacement curve in both loading directions, when about 250 kN horizontal force were exceeded. After completing the second cycle with $0.75\,F'_y$ target force, testing was ended for the day.

The next day testing continued with load steps LS019 and LS021, $1.0\,F'_y = 475$ kN South and North, in which manual measurements were taken again, which lasted about 1 1/2 hours per load step. From these load steps on, crack widths were determined along a certain pattern at the peak displacements of all first cycles in each ductility level. While loading to LS019, the actuator suddenly shut down at 187 kN force, but was immediately turned back on. Hence, there is a small extra loop in each plot of the hard-wired data. Existing cracks became steeper and new ones developed up to 2.40 m height as well as between previous cracks, with a spacing meanwhile corresponding to about half the spacing between the hoops, i.e. 10 cm.

After the night break, testing continued with the cycle at ductility level $\mu_\Delta = 1.0 = \pm 19.5$ mm, where the next manual measurements were taken. Cracks grew slightly longer and the cracks that opened the most in the base region of the pier were the ones above the splice and at the construction joint. The crack widths within the lap-splice area were comparably small and a few fine vertical cracks developed in this region. At $\mu_\Delta = 1.5 = \pm 29.3$ mm top displacement, cracks had developed up to 3.15 m, spanned over 3/4 of the pier's width and became steeper. The first cracks in the foundation, which seemed to start at the location of the reinforcement

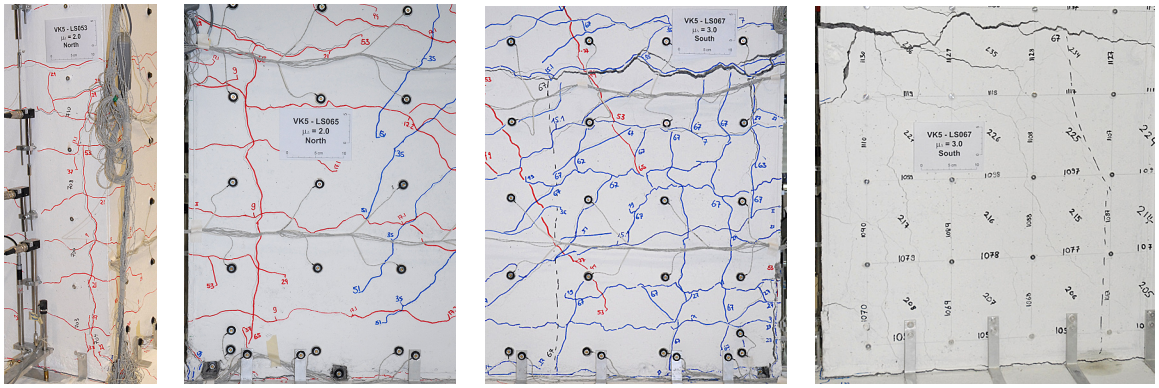

(a) LS053 **(b)** LS065 **(c)** LS067 **(d)** LS067

Figure 4.15: Pictures of the vertical cracks at the Southern edge of the pier at LS053, μ_Δ = 2.0 North 1^{st} (a) and LS065, μ_Δ = 2.0 North 2^{nd} (b), as well as front view (c) and back view (d) of the crack above the splice at the Northern edge at LS067, μ_Δ = 3.0 South. The dashed line indicates the area with internal cracks in the splice region, which sounded hollow.

bars in the corner, formed as well in these load steps. Between $\mu_\Delta = 1.5$ South and $\mu_\Delta = 1.5$ North, there was a testing break for the night.

At $\mu_\Delta = 2.0$ the crack pattern generally looked the same as at $\mu_\Delta = 1.5$. Since the cracks on the back of the test unit crossed the horizontal and vertical pencil lines drawn to define the manual measurement grid, the slip along some of the cracks could clearly be seen. The crack crossing the line marking measurement no. 1139 (see Figure 3.10) had about 1 mm slip. In the South-East corner of the pier, one vertical crack opened along the entire splice length at $\mu_\Delta = 2.0$ North, see Figure 4.15a. The peak horizontal forces in this cycle were F = 632 kN at $\mu_\Delta = 2.0$ South 1^{st} and F = -639 kN at $\mu_\Delta = 2.0$ North 1^{st}. After this load step, the testing was stopped for the day.

During the second load application to $\mu_\Delta = 2.0$ North one could hear a clicking noise and when the target displacement was reached, a vertical crack on the front face was visible 10 cm from the South edge spanning over the entire splice length (Figure 4.15b). When loading was reversed, the displacement accidentally increased about 1 mm before the load was actually reversed, hence a small kink is visible in the load-deformation curve. While the top displacement was increased to $\mu_\Delta = 3.0$ South for the first time, apparently two of the lap splices at the North side of the pier failed and the horizontal force began to decrease at around 44 mm top displacement. When the target displacement was reached, the load had dropped by almost 40 kN and there were many vertical cracks in the splice region under tension as well as a horizontal crack, right above the splice, opening up about 7 mm (see Figures 4.15c and 4.15d). At the front and the back of the test unit, the concrete cover was apparently loose up to the sixth splice from the edge, corresponding to a 45 cm wide region, which could be detected from the sound by knocking on the surface. The maximum horizontal force was applied to this test unit in the cycles at the theoretical ductility level $\mu_\Delta = 2.0$. By comparing the responses of test units VK5 and VK6 (see Section 4.4), one can see that VK5 could not reach its full moment capacity. While the reversed loading towards target displacement $\mu_\Delta = 3.0 = 31.5$ mm North was applied, the horizontal load decreased due to failing splices after the previously applied deformation was exceeded. At first, these seemed to be primarily the four splices at the South end, however, at approximately

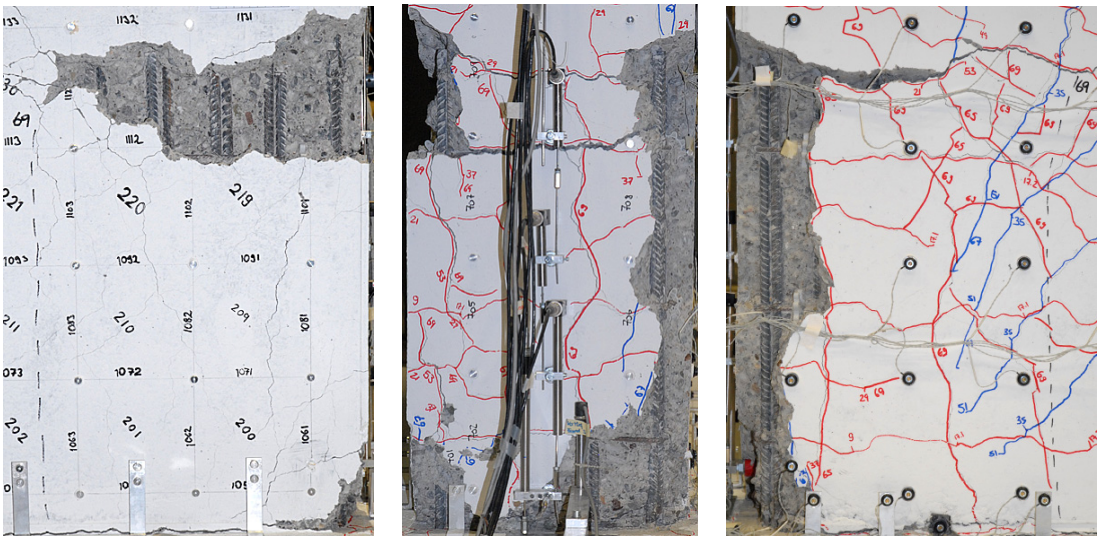

(a) West face **(b)** South face **(c)** East face

Figure 4.16: Views of the Southern bottom part of the pier at load step LS069, $\mu_\Delta = 3.0$ North 1^{st}. The dashed line indicates the area with internal cracks in the splice region, which sounded hollow.

50 mm top displacement more vertical cracks developed and eventually about five to six splices seemed to be covered by merely loose concrete once the target displacement was reached, see Figure 4.16. A crack right above the splice opened up to about 7 mm at the Southern edge of the pier, and the relative displacement between the two spliced bars in the S-W corner measured approximately 1 cm. Afterwards, the pier was unloaded horizontally, the vertical force locked in and the hydraulics were turned off for the night.

After the small cycles as well as the second cycle to $\mu_\Delta = 3.0$ were completed at the beginning of the next testing day, the horizontal force capacity had further decreased a bit. This time there were no sudden drops during the cycles but a steady, slow decrease. Parts of the concrete cover were loose enough to be removed at the peak positions of the cycles. There was a short pause during the loading to $\mu_\Delta = 3.0$ South 2^{nd} because of a force signal disturbance. While cycling to LS083 $\mu_\Delta = 4.0$ South 1^{st}, the test had to be halted at 38 mm to remove some concrete chunks that would otherwise have pushed against LVDT Support S01. Before the target displacement was reached, the horizontal force began to decrease again. On the front face, the cover concrete seemed to be loose up to the seventh splice and 2.3 cm relative displacement between the spliced bars could be measured at the North edge. While loading to $\mu_\Delta = 4.0$ North 1^{st}, loading had to be stopped again to remove cover concrete. At this load step, the concrete covering the splice sounded hollow along the entire length of the pier at the East and West faces. The horizontal forces were F = 300 kN = $0.48F_{max,pos}$ at $\mu_\Delta = 4.0$ South and F = -236 kN = $0.37F_{max,neg}$ at $\mu_\Delta = 4.0$ North. At these load steps, the last manual measurements were taken. During the second cycle, the load further decreased a bit. In the center position, i.e. at about zero top displacement, between $\mu_\Delta = 4.0$ South 2^{nd} and $\mu_\Delta = 4.0$ North 2^{nd} the LVDTs HorDisp_5 and _6, measuring the top displacement, were rearranged. Opposite offsets were introduced to the LVDTs to cover more than ±100 mm top displacement in total. After completing all load steps at the theoretical ductility level $\mu_\Delta = 4.0$, the first and second cycle to $\mu_\Delta = 5.0 = 97.5$ mm, with the small cycles in between, were applied. As all splices were already damaged by then,

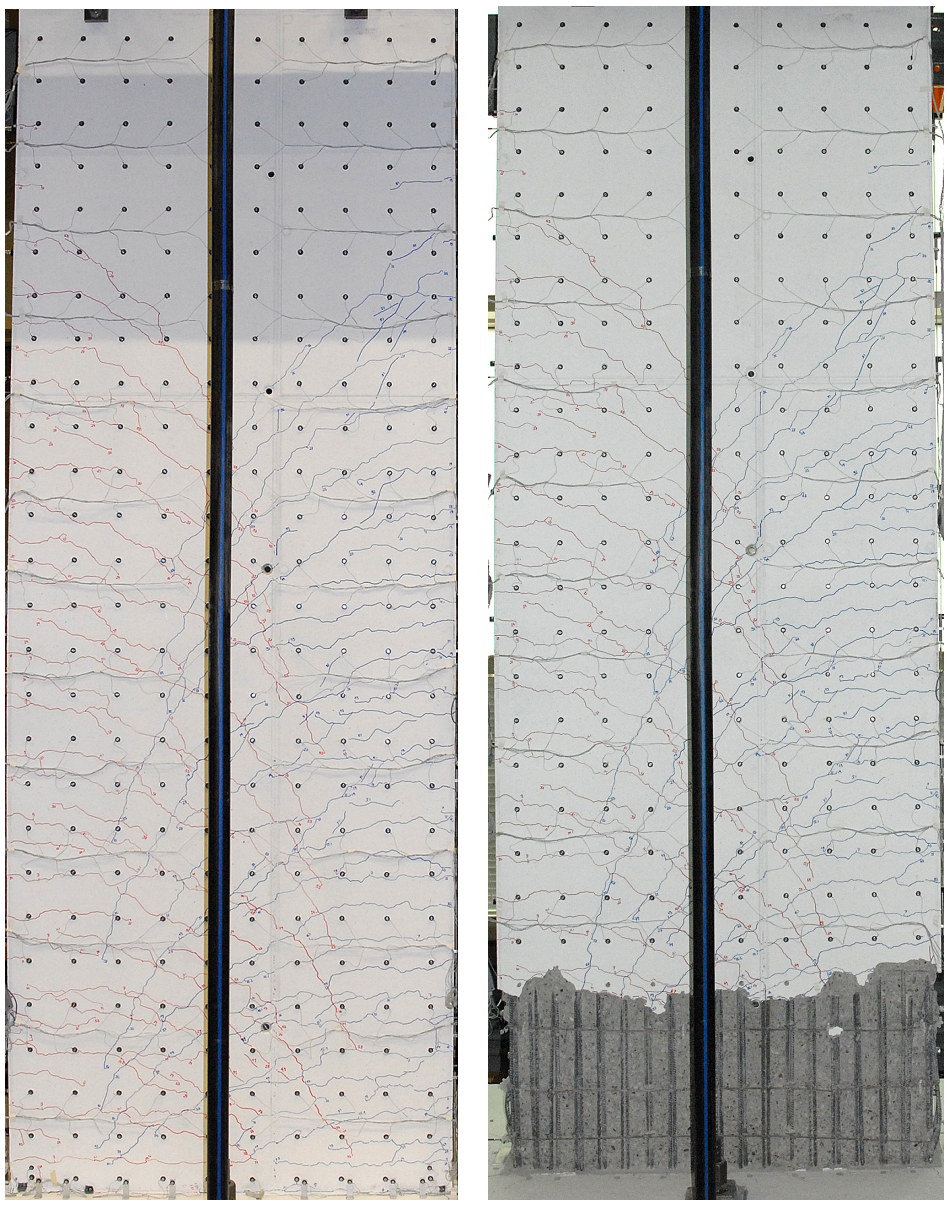

(a) $\mu_\Delta = 2.0$ South 1^{st} **(b)** after end of test

Figure 4.17: Test unit VK5: view at $\mu_\Delta = 2.0$ South 1^{st} (a) and after testing was completed (b).

the horizontal load decreased only slightly since not much additional damage occurred. Because of the degraded splice, the deformation primarily resulted from rocking movement in the splice region. The cover concrete around the splice could be completely removed and at $\mu_\Delta = 5.0$ North 2^{nd}, LVDTs 01 to 04 located near the base of the pier were dismounted. As the splice region was severely damaged by this time, only one cycle without intermediate small cycles was applied at each target displacement level subsequently. When the cycles to $\mu_\Delta = 7.0$, corresponding to 3 % drift (i.e. the same drift reached at $\mu_\Delta = 10.0$ in the tests of the shorter specimen), were completed, the test was ended. The remaining horizontal force capacity was $F = 170$ kN $= 0.27\, F_{max,neg}$ and $F =$ -147 kN $= 0.23\, F_{max,neg}$, respectively. Pictures of the test unit taken

after the end of the test and after the crack pattern had been fully developed are presented in Figure 4.17.

4.3.2 Hard-Wired Measurements

In the following graphs, some of the hard-wired measurement data is presented. In Figures 4.18 through 4.20, the horizontal force measured with the actuator's internal load-cell is plotted against the top displacement, corrected according to Equation (4.2). The first half-cycle, which had to be interrupted due to the missing actuator force-signal is included in the plots, with the force determined from the pressure transducers.

The curvatures presented in Figures 4.21 and 4.22 were determined from the measurements of the LVDT chains along the side faces of the pier. A horizontal distance of 1544 mm between the devices was used to calculate the curvatures, because the center lines of the LVDTs were mounted 22 mm from the surface (see Figure 3.6). In general, all curvatures are displayed until the devices had to be removed to protect them from damage.

The strains plotted in Figure 4.24 were also determined from the LVDTs using the measured deformation and the base lengths which can be seen in Figure 3.6. Those strains, which represent the strains 22 mm away from the surface, were projected to the pier's surface with linear interpolation, i.e. it was assumed that plane sections remain plane. At $\mu_\Delta = 3.0$ the strains at the top of the splice were very large since the crack had opened up widely. Because the same scale as for the other plots was chosen in order to better visualize the smaller strains, these values are outside the plot region.

In Figure 4.23 the strains of the reinforcement measured by means of the strain gauges are presented at selected load steps while the gauges yielded proper readings. At each position, the mean value of the measurements at the back and the front of the test unit are presented. Strain gauge DMS1 was damaged from the beginning, so at the South face only the measurement of strain gauge DMS2 is presented. The strains calculated from the LVDT and strain gauge measurements are presented for the first cycles of some selected load steps. In general, the peak values of the cycles have not been used, but those at the end of the time frame in which the top displacement was maintained constant, because they correspond best to the manual and optical measurements, which were usually also taken towards the end of that time interval.

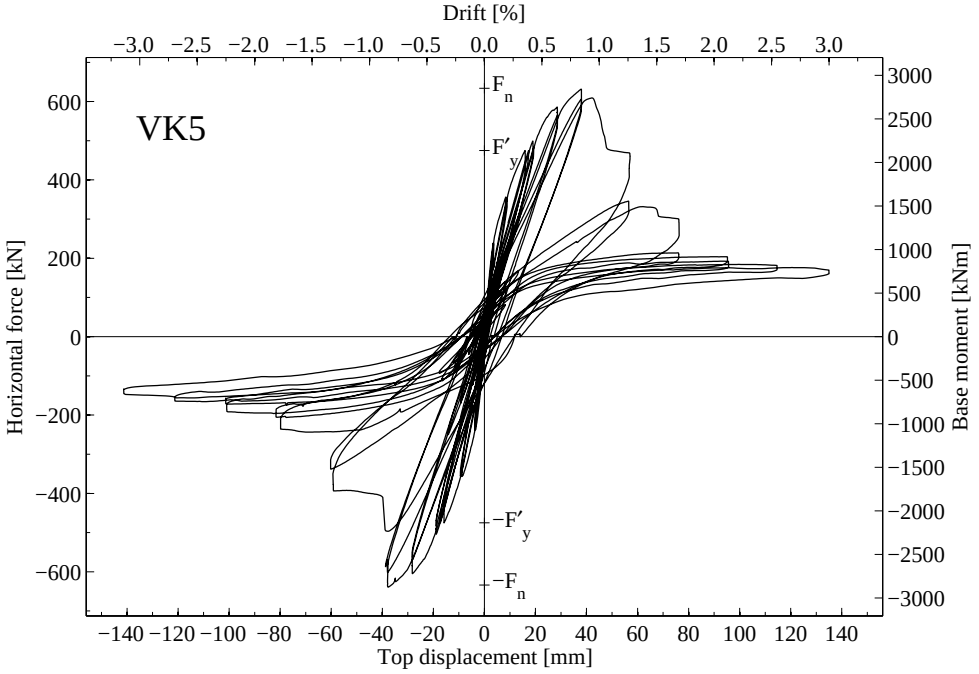

Figure 4.18: Measured force - deformation response of test unit VK5.

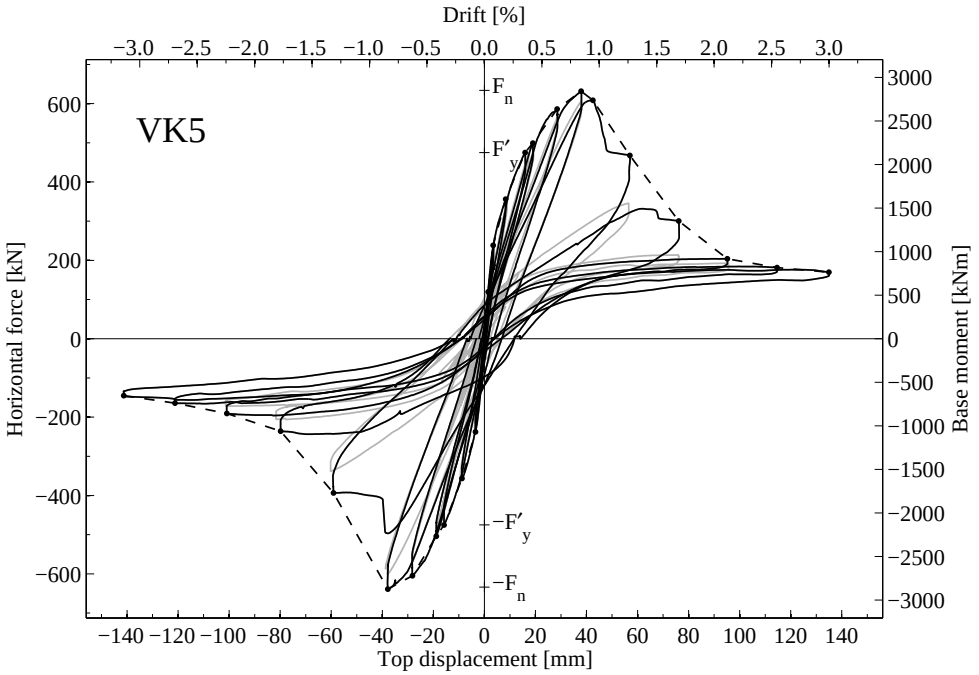

Figure 4.19: Measured force - deformation response of test unit VK5 with emphasized first cycles and envelope of first cycles.

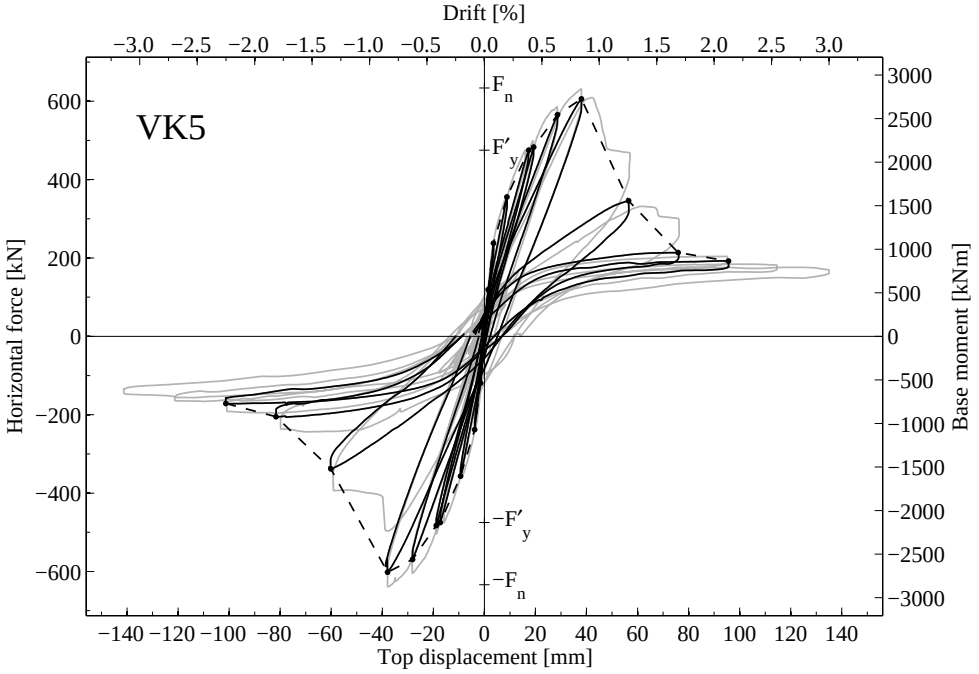

Figure 4.20: Measured force - deformation response of test unit VK5 with emphasized second cycles and envelope of second cycles.

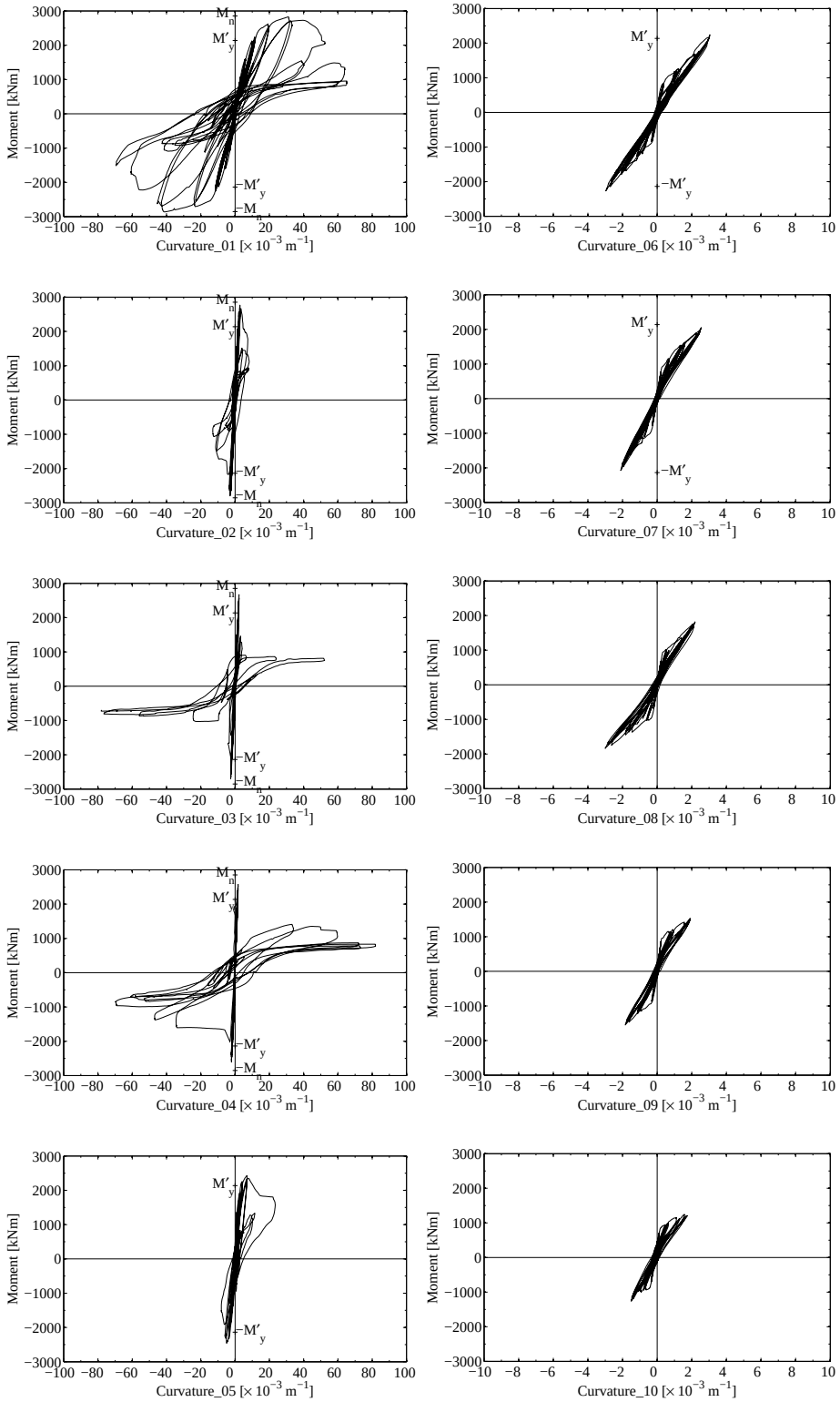

Figure 4.21: Measured moment-curvature relationships 01 to 10 of test unit VK5. Curvatures 01 to 04 are shown up to $\mu_\Delta = 5.0$ 2^{nd}, when the corresponding LVDTs were removed. All other curvatures are displayed to the end.

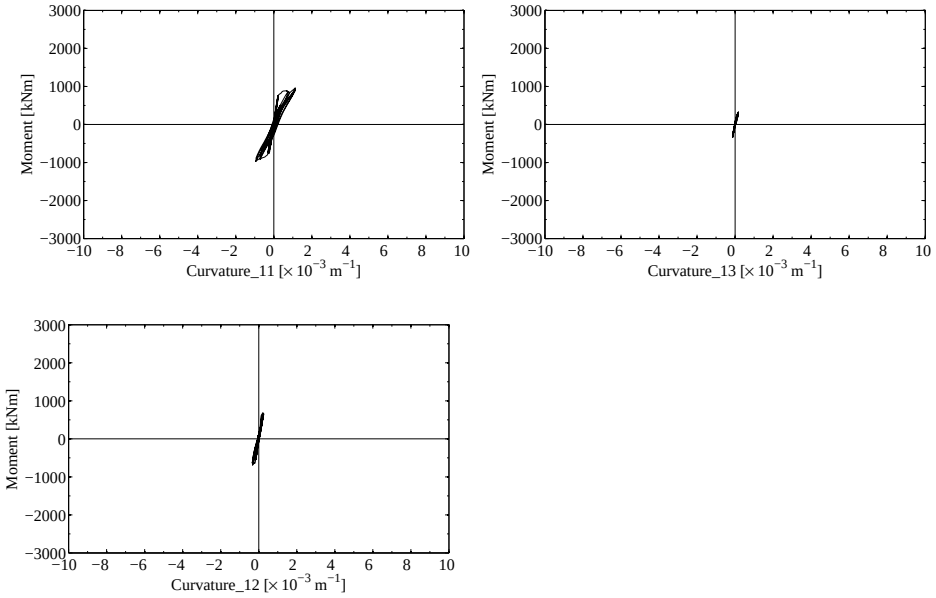

Figure 4.22: Measured moment-curvature relationships 11 to 13 of test unit VK5.

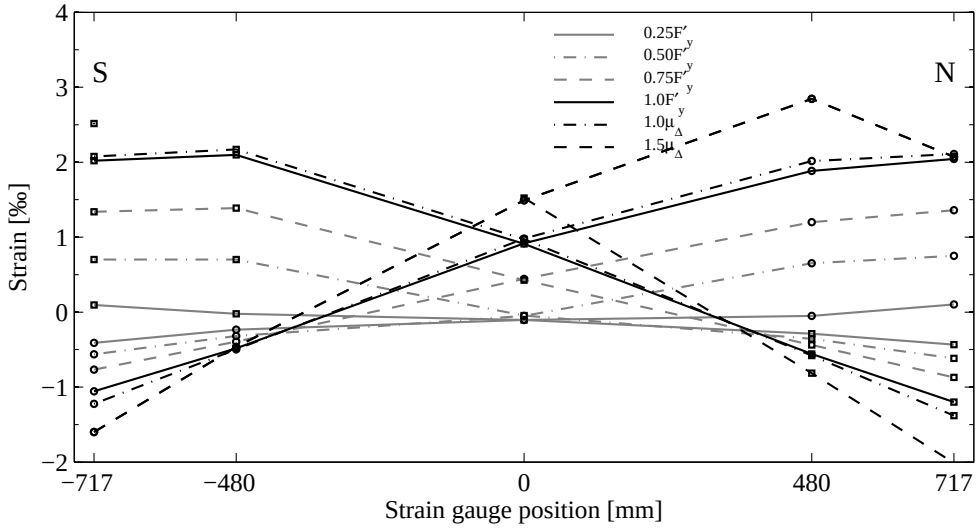

Figure 4.23: Mean longitudinal reinforcement strains of VK5 measured by the strain gauges, at selected first cycle load steps.

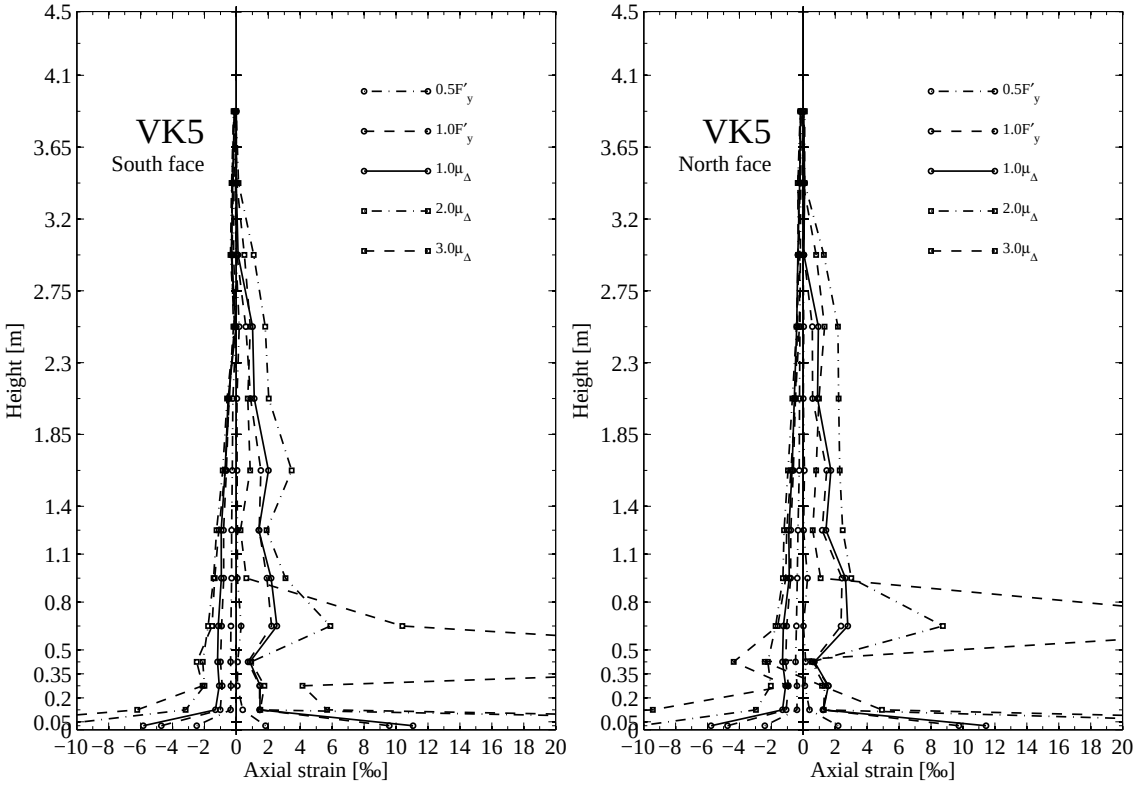

Figure 4.24: Strains along the South and North face of test unit VK5 calculated from deformations measured by means of the LVDTs and projected to the test unit's surface, at selected first cycle load steps. The values outside the plot range, measured over the large crack at the top of the splice, are 47.1 ‰ at the South face and 33.6 ‰ at the North face.

4.3.3 Manual Measurement Results

In Figures 4.25 to 4.26, plots with the principal strains calculated from the manual measurements are presented. The strains are calculated in the same way as those from the optical measurements, according to Section 4.1.2 The largest strains are obtained for the bottom row, since its vertical base length is small but the deformations large due to the base crack. Because these strains exceed the strains along the pier by far, they have not been included in the plots since it would be difficult the read the plots if they were included and drawn to the same scale. The piers are always drawn to a scale of 1:50 and the largest strain has the same length in each plot. This constant strain length was chosen to visualize both the load steps with small as well as those with large strains equally well. Missing bolts are indicated with a gray dot in the grid. If a bolt was missing, its deformation data was interpolated, i.e. the displacement in horizontal direction was assumed to be the mean of the horizontal displacements of the bolt to the left and the right, the displacement in vertical direction was assumed to be the mean of the vertical displacements of the bolts above and below. Apart from this and the error compensation described in Section 4.1.3, no further corrections were made.

Deformation components were determined for all load steps in which manual measurements were made, that means only for the first cycles of this test unit, and are presented in Figure 4.27. Components are only presented up to the first cycles to $\mu_\Delta = 3.0$, because the lap-splice was severely damaged afterwards and determination of meaningful components therefore difficult.

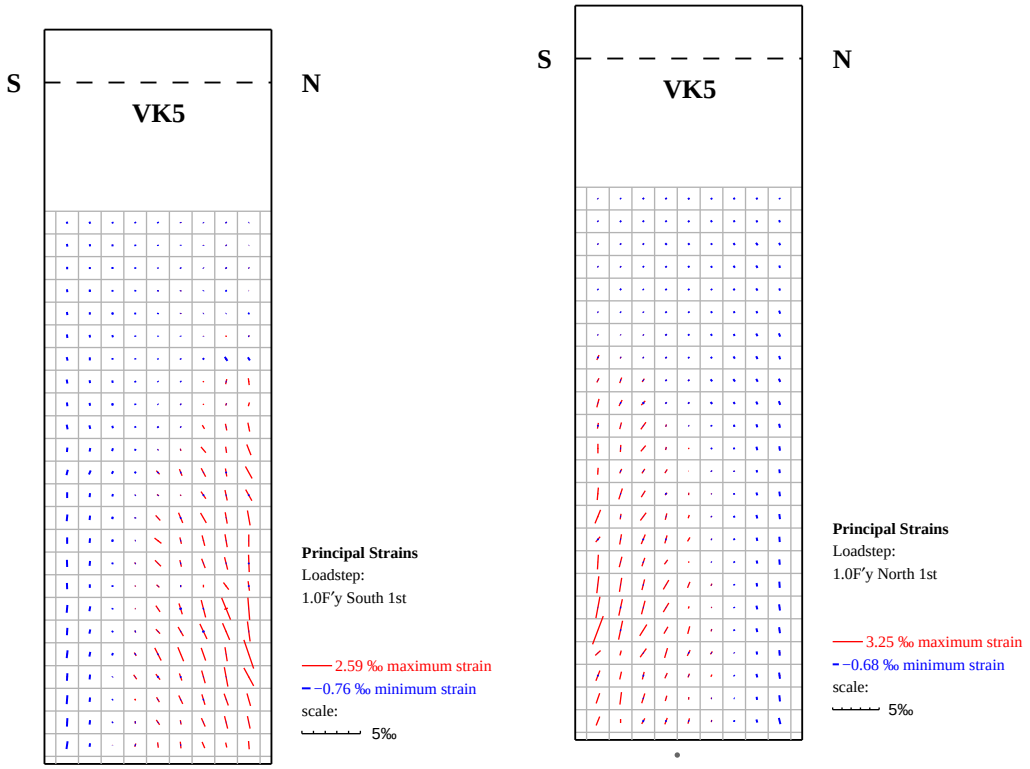

(a) LS019 $1.0F_y'$ South 1^{st} **(b)** LS021 $1.0F_y'$ South 1^{st}

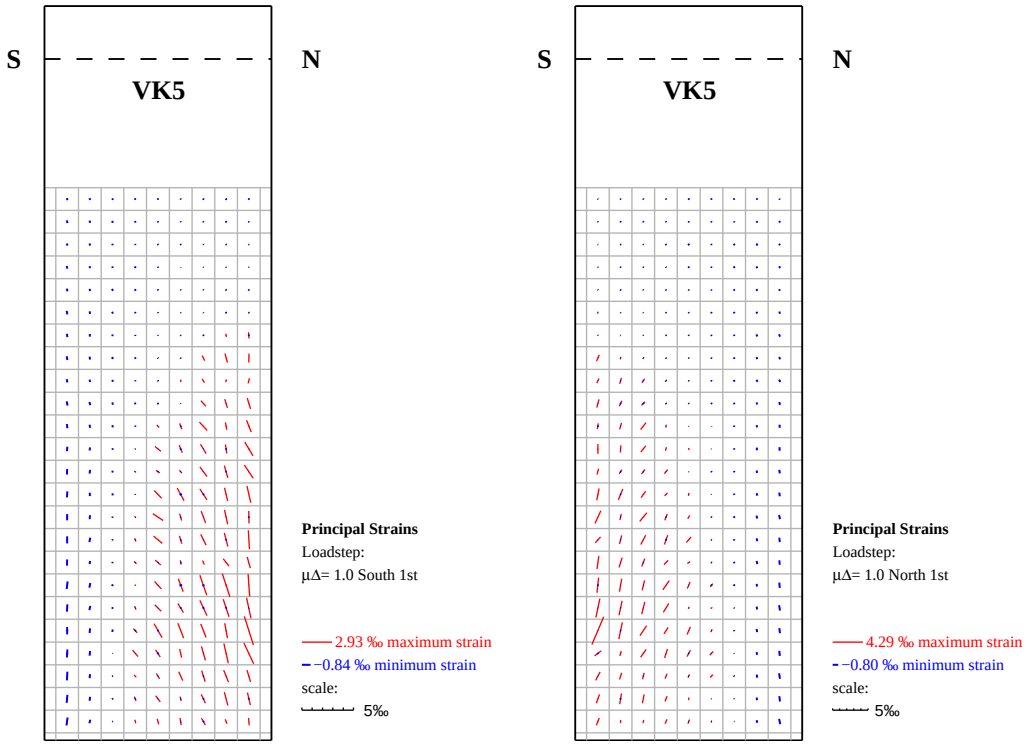

(c) LS027 $\mu_\Delta = 1.0$ South 1^{st} **(d)** LS029 $\mu_\Delta = 1.0$ North 1^{st}

Figure 4.25: Principal strains of VK5 at $1.0F_y'$ (a), (b) and at $\mu_\Delta = 1.0$ (c), (d).

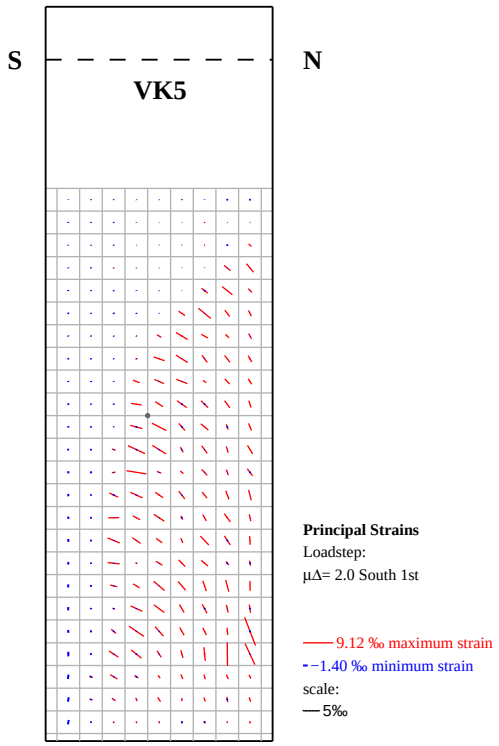

(a) LS051 $\mu_\Delta = 2.0$ South 1^{st}

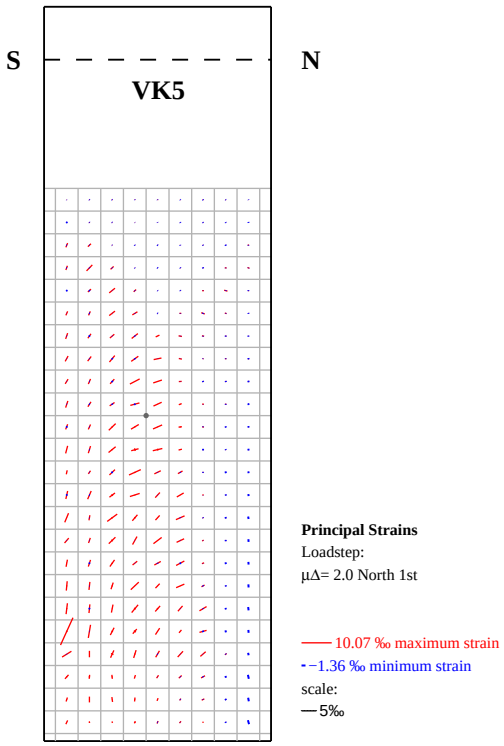

(b) LS053 $\mu_\Delta = 2.0$ North 1^{st}

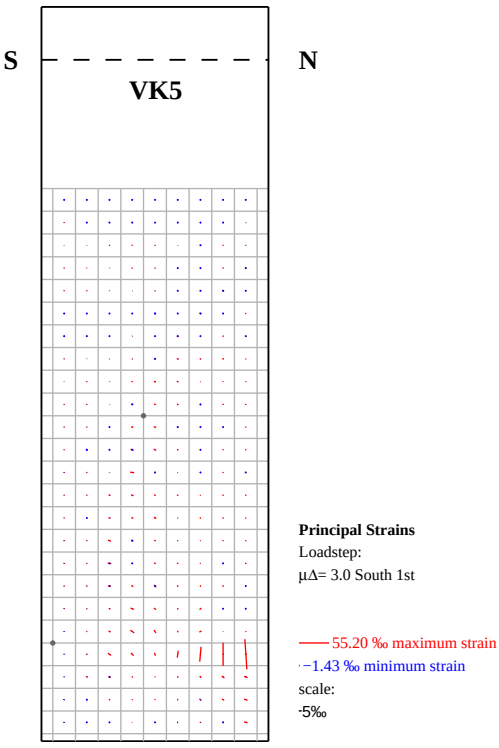

(c) LS067 $\mu_\Delta = 3.0$ South 1^{st}

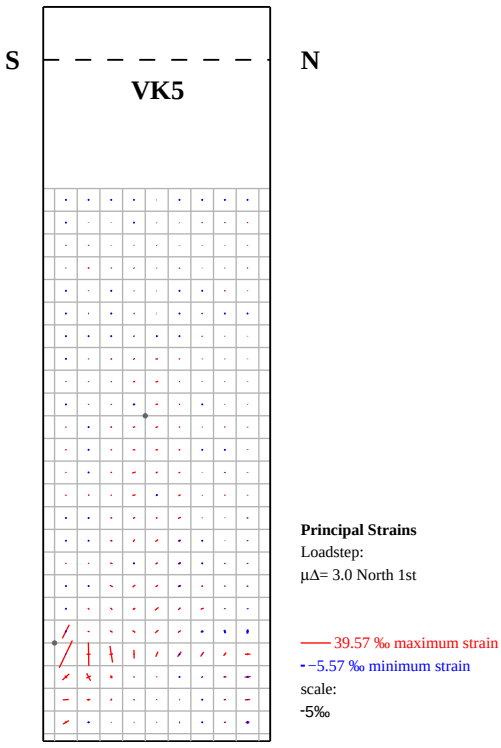

(d) LS069 $\mu_\Delta = 3.0$ North 1^{st}

Figure 4.26: Principal strains of VK5 at $\mu_\Delta = 2.0$ (a), (b) and at at $\mu_\Delta = 3.0$ (c),(d).

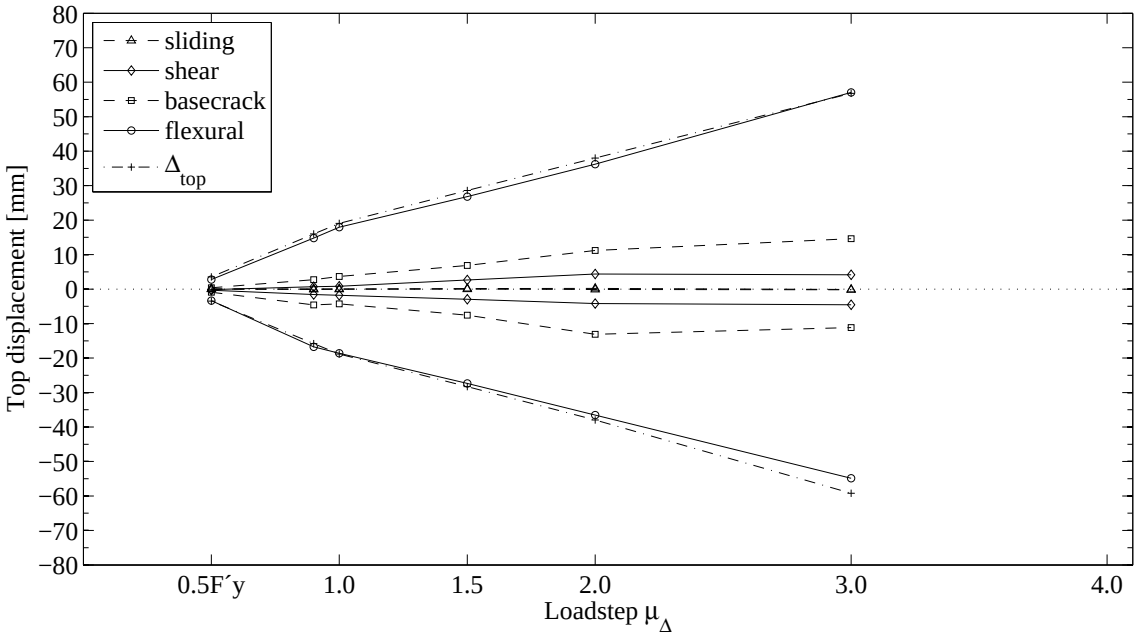

Figure 4.27: Sum of deformation components of VK5 at the 1^{st} cycles at the end of the shear span compared to the top displacement measured by the LVDTs.

4.3.4 Cracks

The monitored cracks as well as the complete crack pattern are presented in Figure 4.28. Table 4.2 summarizes the widths of some of the cracks at certain load steps. Cracks that were already visible but too narrow to determine their widths are indicated with < 0.05. Figure 4.28 also shows how cracks were numbered and along which pattern their widths were determined.

		Crack widths [mm]									
		1^{st} cycles South						1^{st} cycles North			
		A	B	C	D	E		A	B	C	D	E
$1.0F'_y$	III			0.05	0.1	0.15	III	0.25	0.05			
$1.5\mu_\Delta$				0.15	0.1	0.4		0.25	0.15+0.05	0.15		
$2.0\mu_\Delta$			0.15	0.3	0.2	1.2		0.35	0.1+0.15	0.15		
$3.0\mu_\Delta$			0.25	1.0	0.1	0.4		0	1.0	0.25		
$1.0F'_y$	V						V	0.15	0.1	<0.05		
$1.5\mu_\Delta$				0.3	0.1	0.25		0.25	0.4	0.15		
$2.0\mu_\Delta$			0.4	0.55	0.15	0.3		0.3	0.5	0.35		
$3.0\mu_\Delta$				0.55	0.05	0.1		0.05	0.3	0.55	0.2	
$1.0F'_y$	VII						VII					
$1.5\mu_\Delta$			0.1	0.15	0.2	0.1		0.2	0.2	0.1		
$2.0\mu_\Delta$			0.3	0.4	0.45	0.15		0.15	0.2	0.3		
$3.0\mu_\Delta$			0.45	0.25	0.15	0.05		0.05	0.1	0.15		

Table 4.2: Monitored cracks of test unit VK5 and widths of some of them.

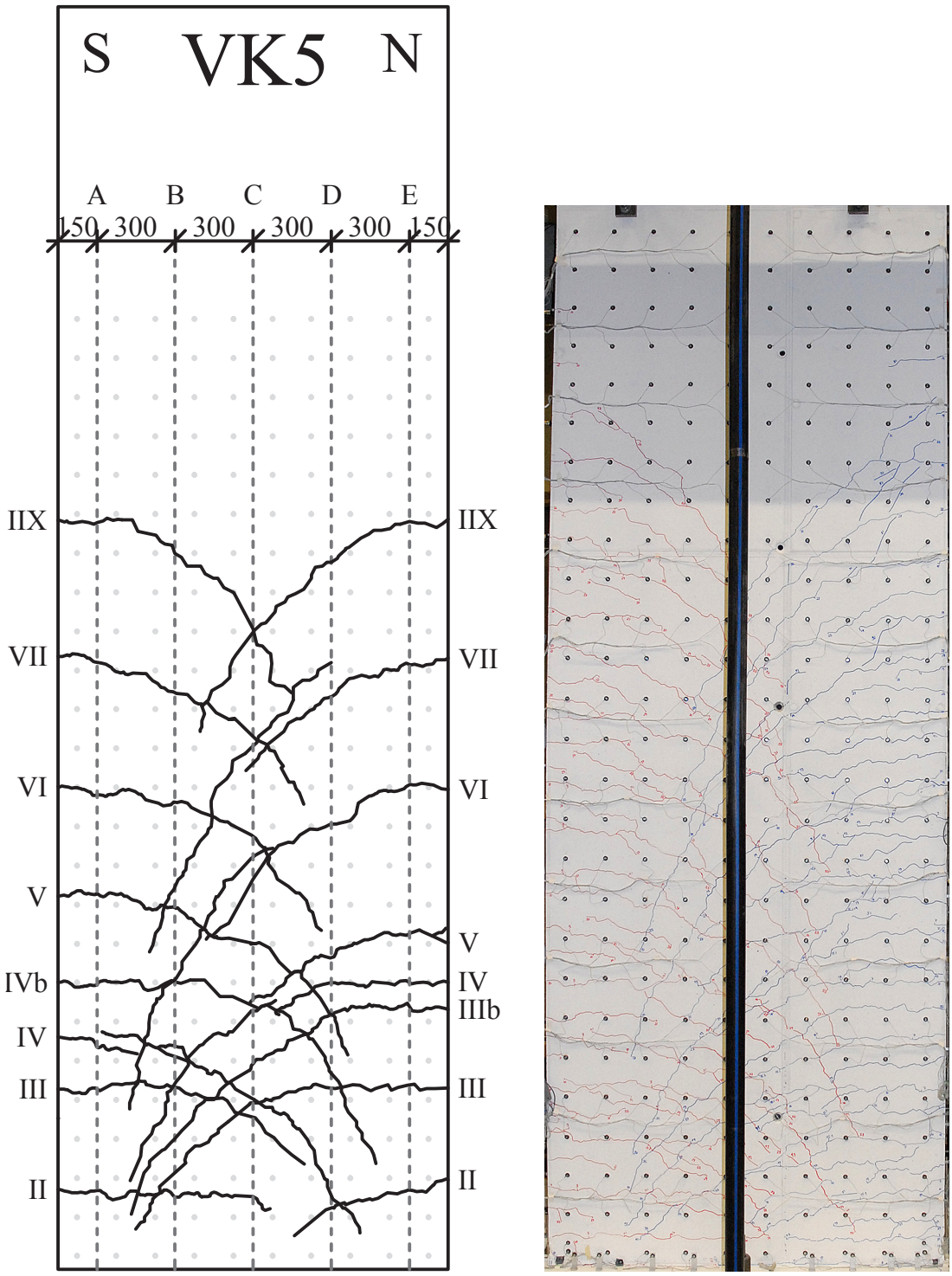

Figure 4.28: Drawing of monitored cracks (left) and picture of complete crack pattern (right) of test unit VK5.

4.4 Test Unit VK6

4.4.1 Test Observations

Test unit VK6 was equal to test unit VK5 except for the longitudinal reinforcement, which was not spliced. Testing began on May 12^{th}, 2010, by applying the vertical load and ended with failure of the specimen on June 1^{st}, 2010. Before the vertical load was applied, all the reference measurements, including optical and two manual measurements, were taken and the hard-wired devices were set to zero. Then the vertical load of 1300 kN was slowly applied and new optical and manual measurements were taken. The next day, when testing was not possible due to a public holiday, the vertical load was kept constant. Some disturbances were found in the signal of HorDisp_4 the following day and the connecting cable was exchanged. Afterwards, all signals seemed reasonable and after the weekend first the normal force was readjusted to the target value and then the horizontal actuator connected.

At $0.25\,F_y'$ (± 119 kN) South and North, respectively, very fine cracks formed at the base of the pier and grew larger during the cycle with horizontal target loads of $0.5\,F_y' = \pm 238$ kN. By then, fine cracks were visible up to the height of the fifth stirrup, i.e. about 90 cm on the North side and fourth stirrup i.e. about 70 cm on the South side. At these load steps, manual measurements were taken, which lasted about 1 1/2 hours each time. While those were performed, there were some disturbances in the hydraulic circuit controlling the vertical force causing it to fluctuate more than usual. Throughout the whole test, some problems with keeping the desired pressure occurred, hence the vertical force could only be kept in a range of about 1300 ± 20 kN. This fluctuation of the vertical load could also be observed between load steps $0.5\,F_y'$ South 2^{nd} to $0.75\,F_y'$ North 1^{st}. While loading towards $0.75\,F_y' = 326$ kN target force for the first time, the load-deformation curve flattened a bit after about F = 250 kN horizontal force was exceeded. This decrease in stiffness could also be observed in the reversed loading direction at approximately the same load value. At $0.75\,F_y'$ South, almost perfectly horizontal flexural cracks were visible, mainly up to approximately 1.0 m height. Only a few shorter ones were visible above that. One crack at 65 cm height reached almost to the center of the pier. At $0.75\,F_y'$ North a similar crack pattern had formed on the Southern side of the pier up to 1.20 m height. When the second cycle to $0.75\,F_y'$ were completed, testing was ended for the day.

The next day, testing resumed with the first application of $1.0\,F_y' = 475$ kN horizontal target force. At this load step, manual measurements were taken and crack widths determined for the first time. The crack widths were still small at that load step, hence many of the measured cracks were only 0.05 mm wide. Cracks formed up to 2.30 m and their widths were determined up to 1.50 m. A few of the cracks reached from the edges beyond the center of the pier and turned towards the base of the pier at their tips. In the foundation, cracks formed at the edges of the pier, starting at the reinforcement bars in the corners. The same set of measurements as at $1.0\,F_y'$ South and similar observations regarding the cracks, except for the ones in the foundation, were made at $1.0\,F_y' = 475$ kN North. Crack widths were slightly larger with up to 0.15 mm width, though. After completing the second cycle, the top displacement was increased to $\mu_\Delta = 1.0 = 19.5$ mm South, which required $F = 522$ kN horizontal force. Cracks grew slightly longer while their widths did not increase much. At the Northern side, some very fine vertical cracks were visible at the edges between the horizontal cracks. Once the manual as well as the

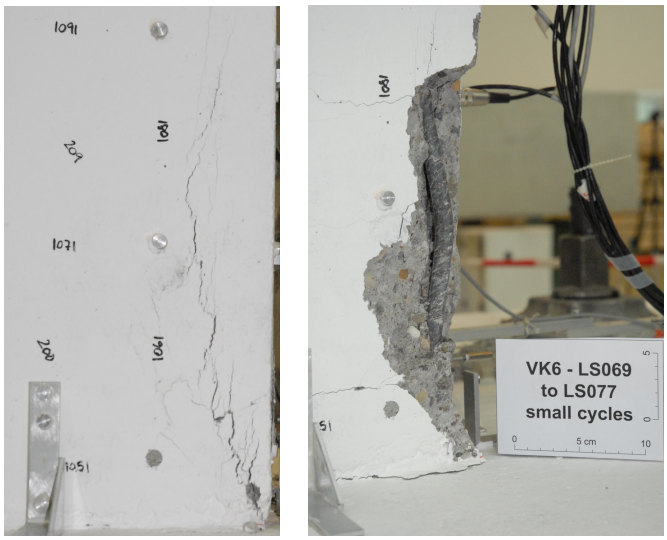

(a) LS067 **(b)** LS077

Figure 4.29: South-West bottom corner of the pier a) at LS067, $\mu_\Delta = 3.0$ S 1^{st} and b) at LS077, after the small cycles between the first and second cycle to $\mu_\Delta = 3.0$.

crack width measurements were completed, the pier was unloaded horizontally and all hydraulic devices turned off for the night.

At $\mu_\Delta = 1.0$ North 1^{st}, cracks were slightly longer than before, new ones formed in between the existing ones and their widths increased slightly compared to load step $1.0F'_y$ North. The value of the horizontal force, $F = 523\,\text{kN}$, was similar to that at $\mu_\Delta = 1.0$ South 1^{st}. At the South-East corner a crack formed in the foundation, which seemed to start where the longitudinal reinforcement bar was located. During the cycle, the pressure in the hydraulic circuit and therefore the normal force fluctuated again. When the top displacement was increased to $\mu_\Delta = 1.5 = \pm 29.3\,\text{mm}$ new cracks formed up to about 2.80 m. In the lower part of the pier, they spanned over about 3/4 of the length and had inclinations of up to 45° especially in the center part of the pier. At the Northern edge of the pier, a new, rather wide, crack developed at approximately 45 cm height between two previously monitored ones, which was subsequently monitored as well. In both loading directions, crack widths were mainly in the range of 0.05 - 0.2 mm on the pier's surface whereas the base crack was up to 0.9 mm wide. During the following small cycles, the vertical load was slightly lower than the target load and the first strain gauge (DMS1) stopped working. Shortly afterwards, before cycling from $\mu_\Delta = 1.5$ South 2^{nd} to $\mu_\Delta = 1.5$ North 2^{nd}, strain gauge DMS8 stopped working, as well. After this load step was completed, testing ended for the day.

The next day, testing started with applying the top displacement $\mu_\Delta = 2.0 = 39\,\text{mm}$ South for the first time. During loading, a force threshold value, which was still active in the control, caused the actuator to turn off at 130 kN, but the force dropped only about 10 kN before loading was resumed. Hence, there is a very small extra loop in all hard-wired measurements. In the center part of the pier, crack widths of up to 0.4 mm were determined and one crack, located 45 cm above the base, was even 1.4 mm wide near the Northern edge of the pier, see Figure 4.30a. The cracks reached far into the Southern part of the pier and the first fine vertical cracks were visible at the corners of the compression zone. Before loading was reversed, two more strain

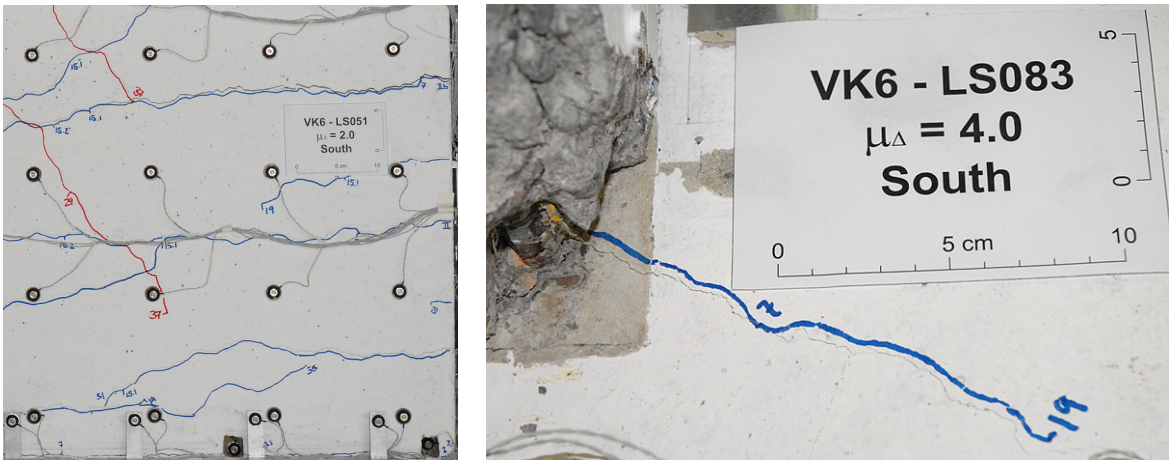

(a) LS051 **(b)** LS083

Figure 4.30: Front face view of the Northern bottom part of the pier at LS051, $\mu_\Delta = 2.0$ South 1^{st} (a) and picture of the crack in the foundation at the North-East corner of the pier, taken at LS085, when the cover concrete had spalled off (b).

gauges, DMS7 & 10, stopped working and HorDisp_4 was replaced by another LVDT because the signal was noisy again. At the reversed load step, $\mu_\Delta = 2.0$ North 1^{st}, similar observations regarding the crack pattern could be made and the largest crack width of 0.8 mm was measured at a crack located 65 cm above the base. The only vertical cracks within the compression zone formed next to the recess provided to fix the LED marker on the reinforcement bar. In both loading directions, the applied horizontal forces were similar with $F = 649$ kN and $F =$ -647 kN. The normal force fluctuated slightly more than usual again during the small cycles and the second cycle to $\mu_\Delta = 2.0$ South. During unloading from $\mu_\Delta = 2.0$ South 2^{nd} the horizontal force signal was again disturbed and the test had to be halted for about 20 minutes.

After the night break, the second loading towards $\mu_\Delta = 2.0$ North 2^{nd} was applied, followed by the first one to $\mu_\Delta = 3.0$ South. At this load step, the maximum horizontal force $F = 675$ kN was reached. The crack pattern did not change much compared to $\mu_\Delta = 2.0$ South except for additional cracks in the compression zone and a few steeper cracks forming in between the existing ones. Crack widths increased up to 0.65 mm in the center part of the pier. The crack located 45 cm above the base, which was already rather wide in previous cycles, was 1.6 mm wide near the Northern edge of the pier. Cracks in the compression zone were mainly visible in the outer 10 cm of the pier up to 35 cm height. At $\mu_\Delta = 3.0$ North, the peak horizontal force in the negative loading direction, $F =$ -658 kN, was reached. At this stage, some cracks grew longer and cracking extended up to 40 cm higher than previously. New vertical cracks formed in the compression zone. While loading to $0.75\,\mu_\Delta$, corresponding to 6 - 11 mm top displacement, the concrete cover fell off in the S-W corner of the pier, showing for the first time that the reinforcement bar in the corner had buckled. The point with the largest lateral deflection was located about 20 cm above the foundation, see Figure 4.29. Considering that a long vertical crack in that corner had already formed at $\mu_\Delta = 3.0$ South, it is conceivable that buckling started at that stage. Loading to $\mu_\Delta = 3.0$ South 2^{nd} could not be applied that same day, because the sunlight became too strong, making optical measurements impossible. Hence, furher testing was postponed to the next day.

At $\mu_\Delta = 3.0$ South 2^{nd} another bar located at the South face of the pier buckled right above the first stirrup. Upon reaching the reversed load step $\mu_\Delta = 3.0$ North 2^{nd}, the Northern bottom part of the pier was therefore checked for buckling bars. No buckled bar could be detected because the cover concrete had not yet spalled off. However, the concrete cover sounded hollow around the existing vertical crack, indicating that buckling of the bars had already started on the North side as well. While the top displacement was increased towards $\mu_\Delta = 4.0$ South 1^{st}, the loading had to be stopped briefly at +16 mm displacement, because some spalling concrete was pushing against the LVDTs and therefore had to be removed. All four reinforcement bars on the South face had buckled when the target top displacement was reached. On the North side, a new crack in the foundation developed and, since some cover concrete was already missing, one could see that the previously developed crack in the North-East corner started where the corner longitudinal reinforcement bar was located, see Figure 4.30b. In the compression zone, one vertical crack was almost 65 cm long and the concrete cover had begun to spall off on the South face. At LS085, $\mu_\Delta = 4.0$ North 1^{st}, the bar in the North-East corner bent outwards about 3 cm and the concrete cover had spalled off. At the North-West corner, the cover concrete was also missing, but the bar did not buckle equally much. At LS095, $\mu_\Delta = 4.0$ South 2^{nd}, the widths of the cracks which had developed in the foundation at the edges of the pier were measured. The one in the N-W corner was 0.1 mm wide and the one in the N-E corner 0.15 mm (see Figure 4.30b for a picture of the crack at a previous load step). After cycling to $\mu_\Delta = 4.0$ North 2^{nd}, further testing had to be postponed to the next day because of the sun.

When LS097, $\mu_\Delta = 4.0$ North 2^{nd}, was reached, the concrete cover at the bottom of the South side could be completely removed and the cracks in the foundation which had developed around the reinforcement bars were visible. After unloading to the center position, the LVDTs HorDisp_5 and _6 were rearranged. Opposite offsets were introduced to the LVDTs so that the peak displacements in Southern direction were only measured by HorDisp_5 from then on, and those in the opposite direction by HorDisp_6. When loading to $\mu_\Delta = 5.0$ South, the vertical reinforcement bars began bending outwards towards LVDTs VertDef_S01 and _S02, hence the measurements of these devices were influenced once the bars touched them. The cover concrete had spalled off in the outer 20 cm of the compression zone up to 45 cm height and the core concrete was also crushed a few centimeters inwards. Above the area with the crushed core concrete some vertical cracks formed. When loading was reversed to $\mu_\Delta = 5.0$ North, the test was stopped twice, once at 27 mm top displacement to cut and remove the short leg of a stirrup before it would have pushed against a LVDT and once at 3 mm top displacement to change the support of VertDef_N01 and _S01 and increase the clear distance of the LVDTs to the buckling reinforcement bars. Damage in the compression zone at $\mu_\Delta = 5.0$ North was comparable to the damage of the compression zone at $\mu_\Delta = 5.0$ South. Some more concrete loosened during the small cycles as well as during the second cycle. During the latter, the test had to be interrupted again, first to protect and eventually to temporarily remove some LVDTs (VertDef_S02 and _S03), because they could no longer be mounted securely. During the second cycle at $\mu_\Delta = 5.0$ testing was paused for the night.

Damage of the compression zones increased further during the second cycle and the applied horizontal force dropped considerably compared to the first cycle. During $\mu_\Delta = 6.0$ the damage of the concrete in the compression zone increased further and mainly some of the steep cracks, ending in the compression zone, opened significantly. About 40 cm from the side edges of the pier, all cracks turned downwards almost vertically and the compression zones were severely

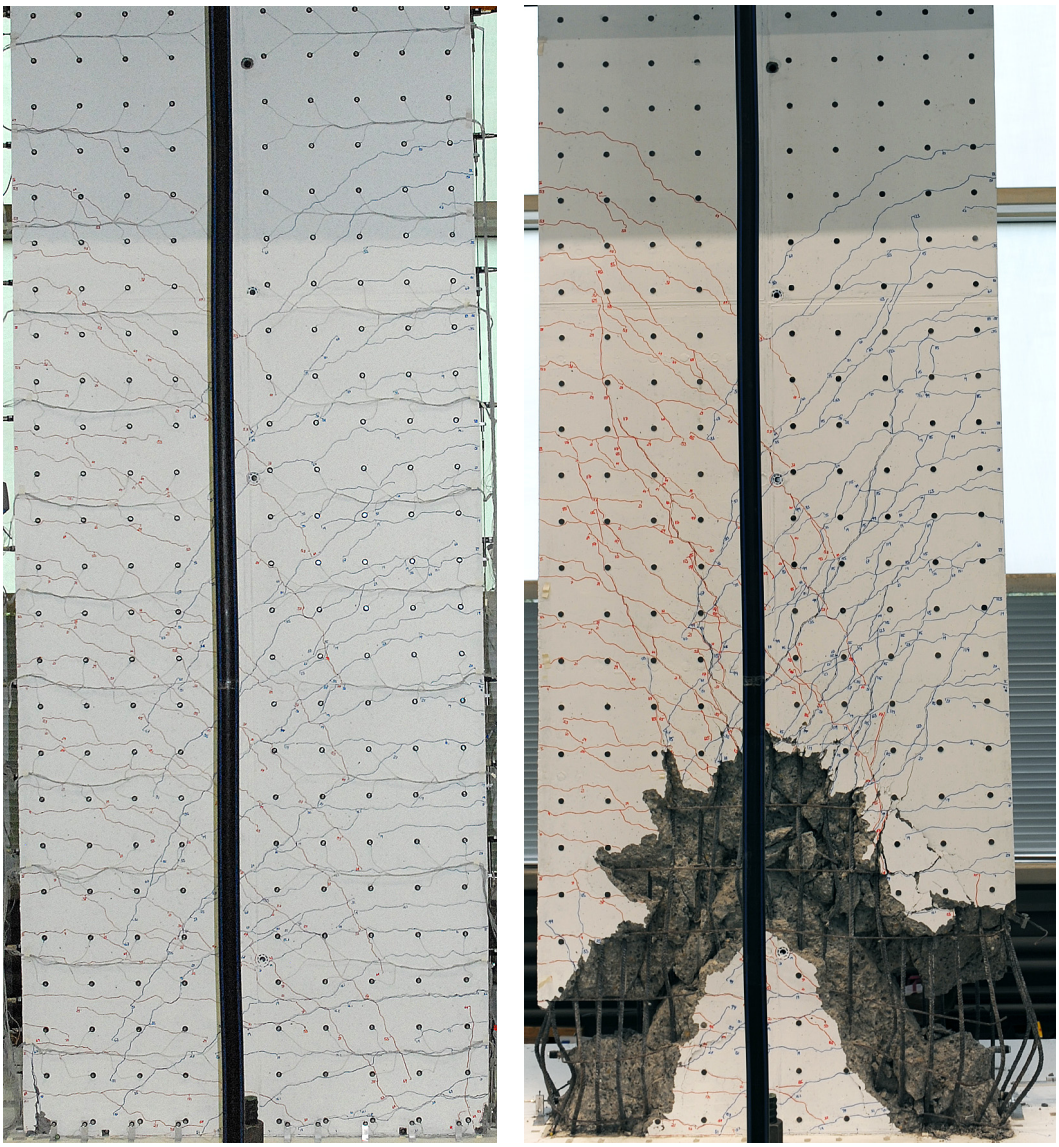

(a) $\mu_\Delta = 3.0$ South 2^{nd} **(b)** after failure

Figure 4.31: Test unit VK6 at $\mu_\Delta = 3.0$ South 2^{nd} (a) and after failure (b).

damaged within the outer 20 cm. In both loading directions, the horizontal forces had dropped significantly to F = 345 kN = 51 %$F_{max,pos}$ and F = -244 kN = 37 %$F_{max,neg}$. No small cycles were applied between the first and second cycle from this target displacement level onwards. During the second cycle at $\mu_\Delta = 6.0$ the cover concrete along some shear cracks in the lower part of the pier, which had opened significantly, was loose and could be removed. In the center part of the pier, there was a concrete wedge shaped by the shear cracks which was considerably less damaged than the surrounding concrete, see Figure 4.31. The main deformation at that time seemed to be due to rocking around that concrete wedge. When the top displacement was increased to $\mu_\Delta = 7.0$ South 1^{st}, damage at the bottom part of the pier slightly increased. Right before the target displacement at $\mu_\Delta = 7.0$ North was reached, the reinforcement bar in the South-West corner of the pier, which had previously buckled, ruptured. When the second

loading to $\mu_\Delta = 7.0$ South was applied, horizontal and vertical forces started to decrease at about +83 mm and the test unit could eventually not carry both loads anymore, hence the test was ended.

4.4.2 Hard-Wired Measurements

In the following graphs, some of the hard-wired measurement data is presented. In Figures 4.32 through 4.34, the horizontal force measured with the actuator's internal load-cell is plotted against the top displacement, corrected according to Equation (4.2).

The curvatures presented in Figures 4.35 and 4.36 were determined from the measurements of the LVDT chains along the side faces of the pier. A horizontal distance of 1544 mm between the devices was used to calculate the curvatures, because the center lines of the LVDTs were mounted 22 mm from the surface. In general, all curvatures are displayed until the devices had to be removed to protect them from damage.

The strains plotted in Figure 4.39 were also determined from the LVDTs using the measured deformation and the base lengths which can be seen in Figure 3.6. Those strains, which represent the strains 22 mm away from the surface, were projected to the pier's surface with linear interpolation, i.e. it was assumed that plane sections remain plane.

In Figure 4.37 the strains of the reinforcement measured by means of the strain gauges are presented at selected load steps. At each position, the mean value of the measurements at the back and the front of the test unit are presented. The strain gauges readings are only presented up to μ_Δ =1.0 because they did not appear reliable afterwards and completely stopped working soon after μ_Δ =1.0. The strains calculated from the LVDT and strain gauge measurements are presented for the first cycles of some selected load steps. In general, the peak values of the cycles have not been used, but those at the end of the time frame in which the top displacement was maintained constant, because they correspond best to the manual and optical measurements, which were usually also taken towards the end of that time interval.

The diagram in Figure 4.38a displays the pullout slip of reinforcement bars measured right above foundation against the readings of strain gauges glued to the same bars. The four considered bars were all located along the East face of the wall (see Figure 3.4), i.e.: i) LED 1 was glued on the South-East corner bar, ii) LED 2 was glued on a bar located 270 mm far away from the South-East corner, iii) LED 3 was glued on a bar located 270 mm far away from the North-East corner, and iv) LED 4 was glued on the North-East corner bar. For the reasons outlined in the previous paragraph, the results pertain to the elastic deformation range of the reinforcement. Furthermore, as strain gauge number 9 of this test unit was not working, strain gauge no. 10 is used instead in this plot. Figure 4.38b shows the pullout of the outer reinforcement bars, i.e. LED1 and LED4, against the displacement ductility, over the range over which measurements were available.

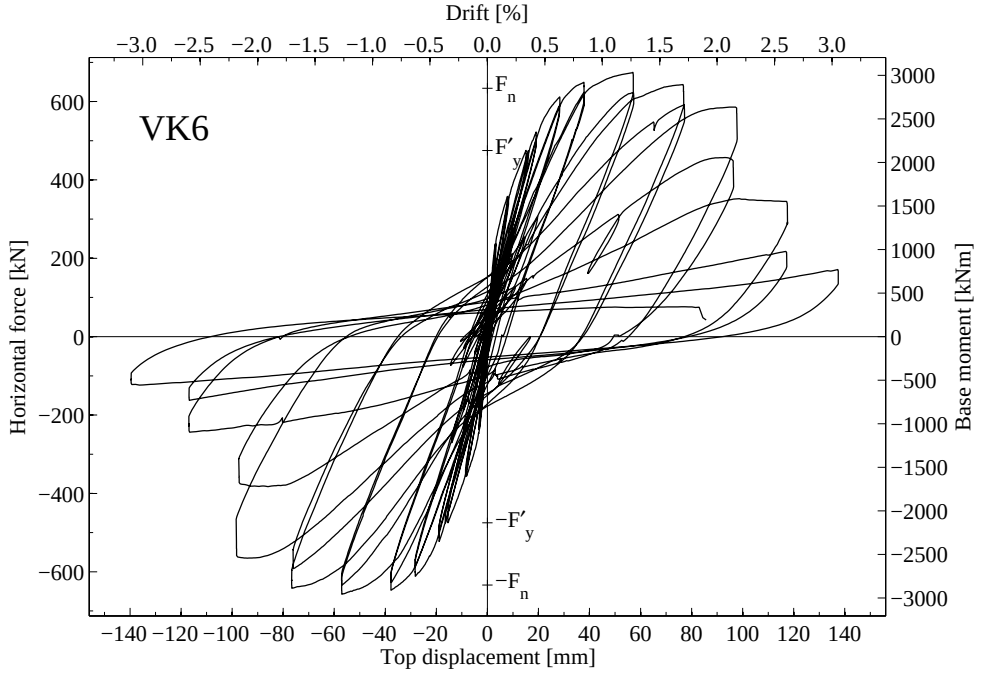

Figure 4.32: Measured force - deformation response of test unit VK6.

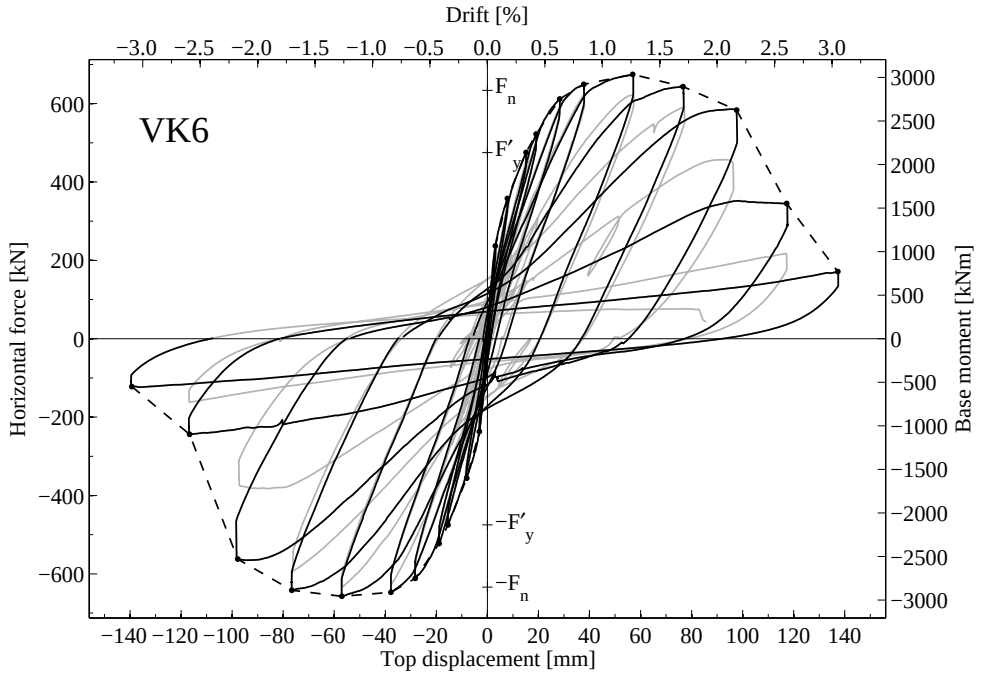

Figure 4.33: Measured force - deformation response of test unit VK6 with emphasized first cycles and envelope of first cycles.

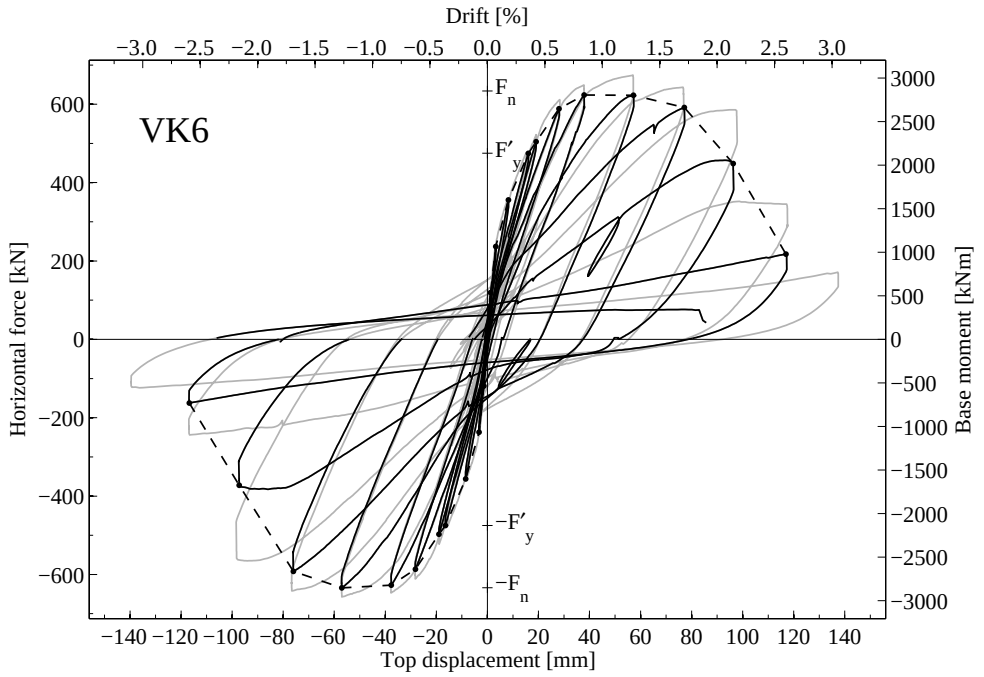

Figure 4.34: Measured force - deformation response of test unit VK6 with emphasized second cycles and envelope of second cycles.

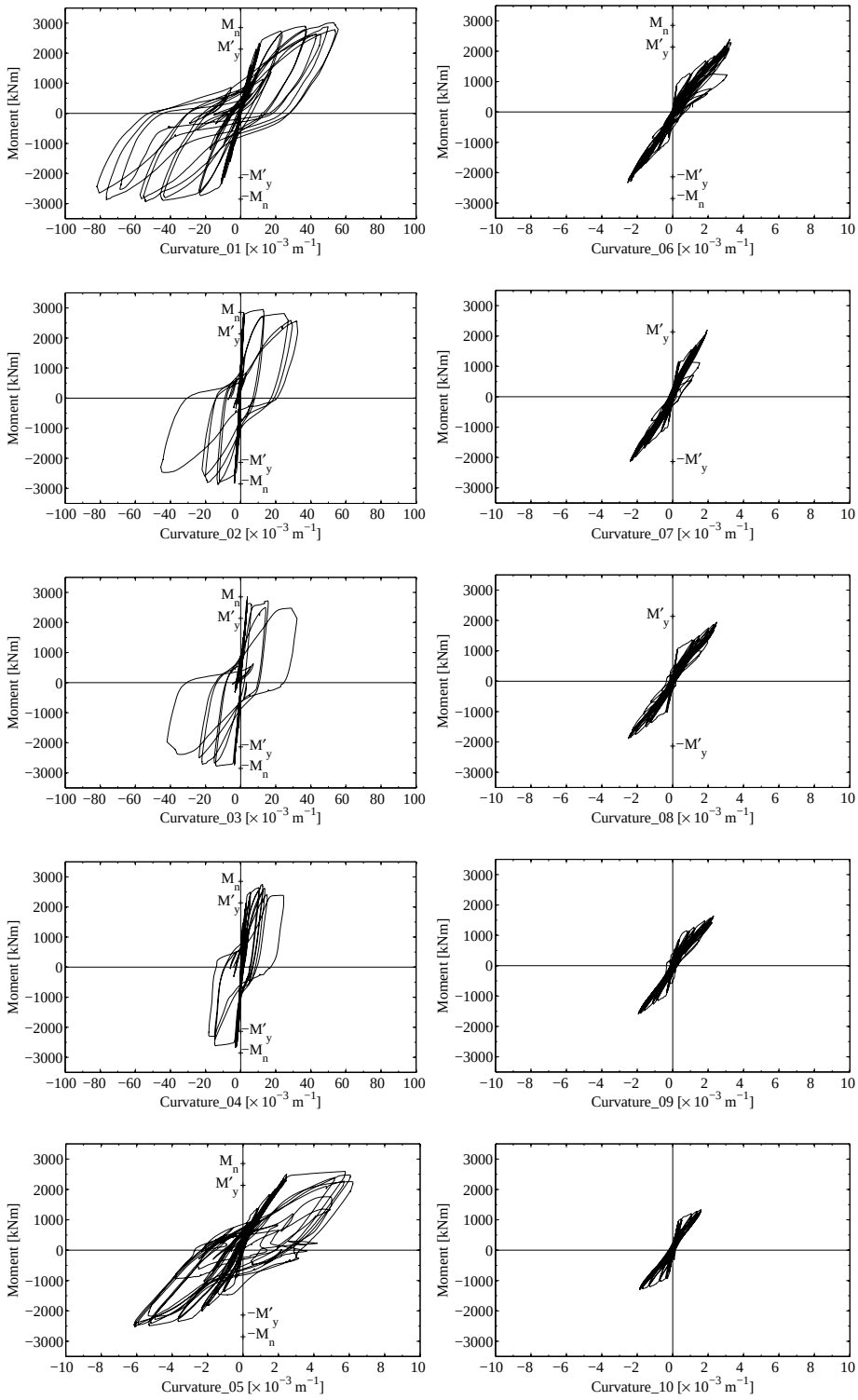

Figure 4.35: Measured moment-curvature relationships 01 to 10 of test unit VK6. Curvatures 01 to 04 are only shown up to the small cycles between $\mu_\Delta = 5.0$ 1^{st} and 2^{nd}, as some of these LVDTs had to be temporarily removed after that. All other curvatures are displayed to the end.

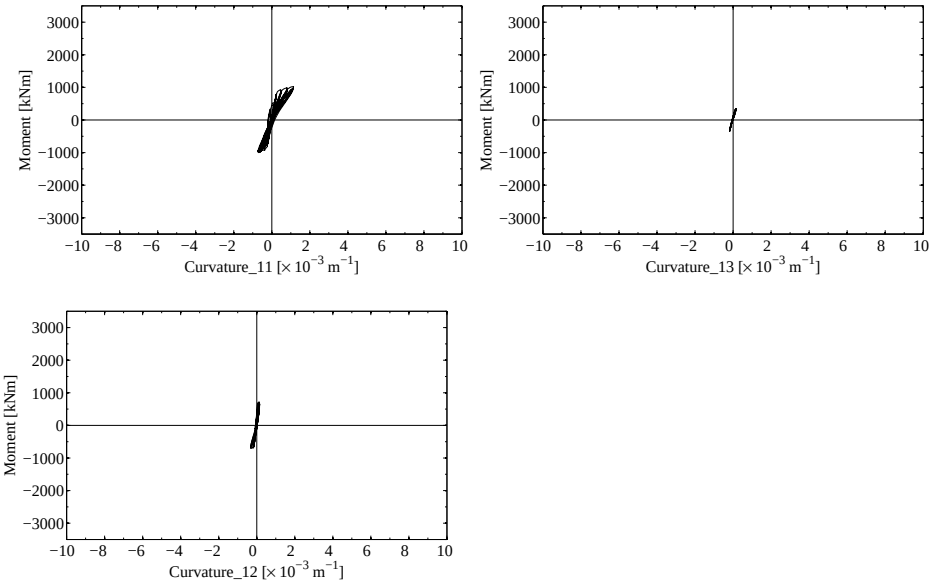

Figure 4.36: Measured moment-curvature relationships 11 to 13 of test unit VK6.

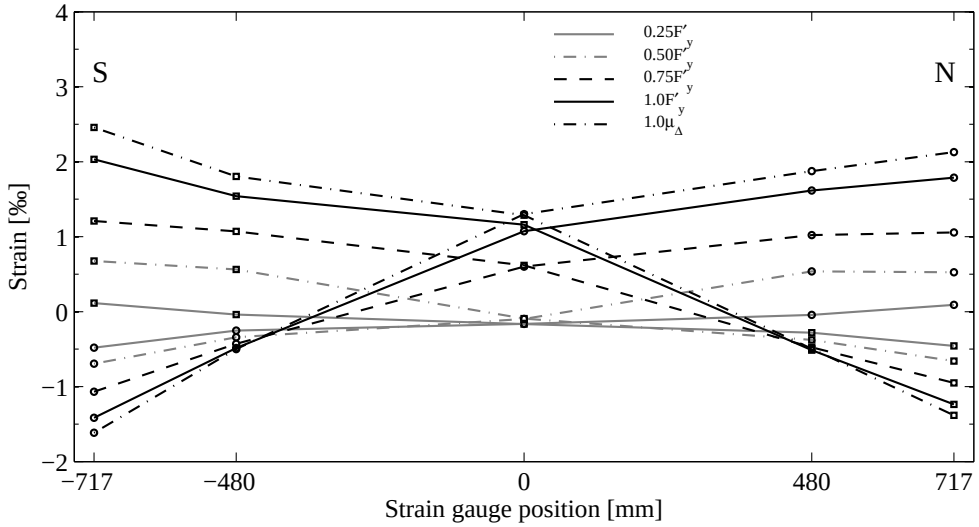

Figure 4.37: Mean longitudinal reinforcement strains of VK6 measured by the strain gauges, at selected load steps.

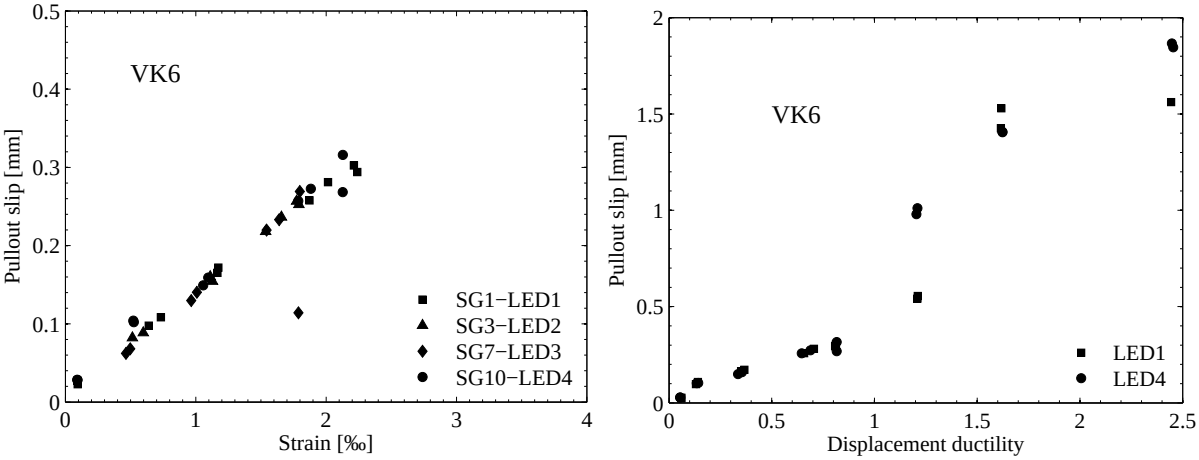

(a) Pullout slip of reinforcement bars measured right above foundation (LED) against readings of strain gauges (SG).

(b) Pullout slip of reinforcement bars measured right above foundation (LED) against displacement ductility.

Figure 4.38: Pullout slip of reinforcement bars of VK6.

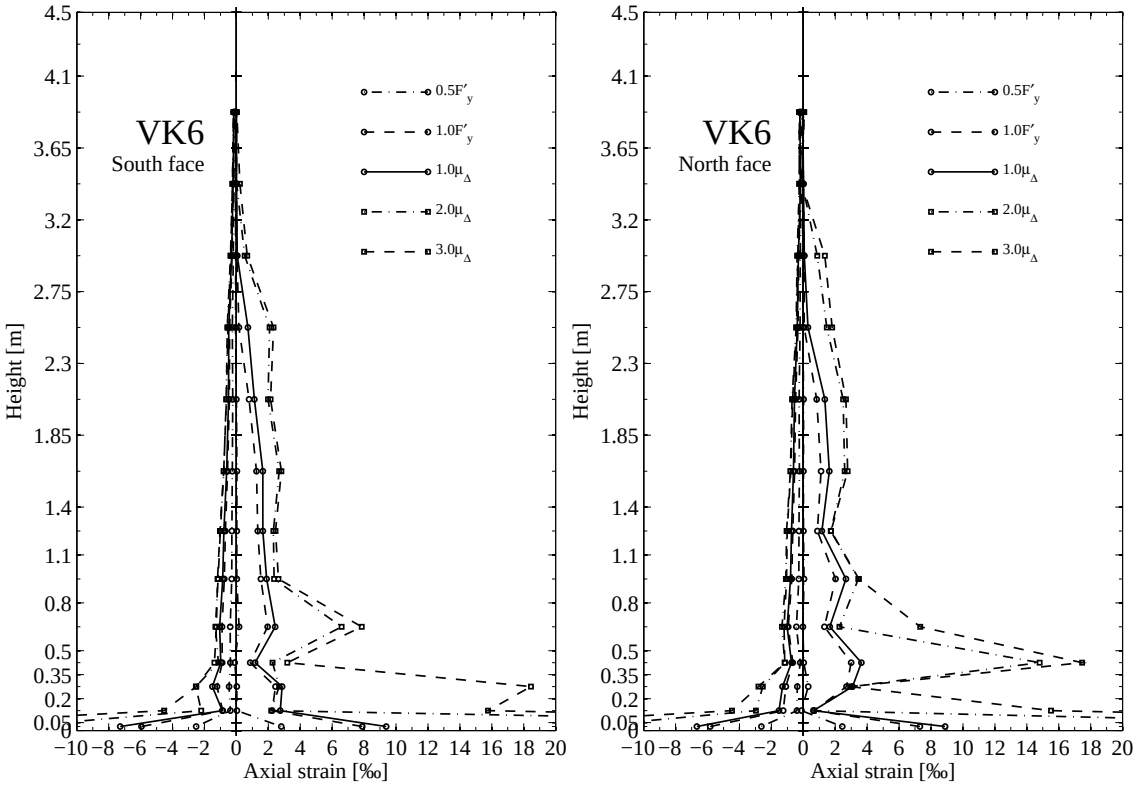

Figure 4.39: Strains along the South and North face of test unit VK6 calculated from deformations measured by means of the LVDTs and projected to the test unit's surface, at selected load steps.

4.4.3 Optical Measurement Results

In Figures 4.40 to 4.42, plots with the strains calculated from the optical measurements are presented. The strains are computed from the measurements taken during two minutes long time intervals at the peaks of the cycles while the top displacement was kept constant according to the procedure described in Section 3.2.2. The largest strains are obtained for the bottom row, since the base length is small there but the deformations large due to the base crack. Because these strains exceed the strains along the pier by far, they have not been included in the plots since it would be difficult the read the plots if they were included and drawn to the same scale. The piers are always drawn to a scale of 1:50 and the largest strain has the same length in each plot. This constant strain length was chosen to visualize both the load steps with small as well as those with large strains equally well. For the calculation of the strains according to Section 4.1.2 the mean values of the transformed coordinates were used, no further corrections were made.

However, as marker number 102, i.e. the second marker from the left in row 11, obviously yielded false results, its horizontal displacement values were replaced by the mean displacements of markers 101 and 103, and its vertical displacements by the mean values of markers 92 and 112. In the plots, the comments after the load steps indicate when the optical measurement data was collected, i.e. whether it was before or after the manual ("Deformeter") measurements were taken.

The deformation components are presented up to load step $\mu_\Delta = 4.0$, after which too many markers were missing at the bottom of the pier. Components are only presented up to the second cycle to $\mu_\Delta = 4.0$ in Figure 4.43, because the concrete in the bottom part of the pier was severely crushed afterwards and determination of meaningful components therefore difficult.

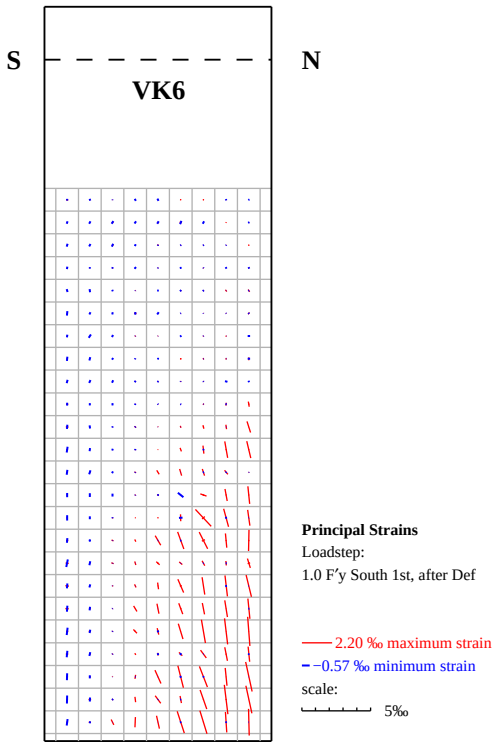

(a) LS019 $1.0F_y'$ South 1^{st}

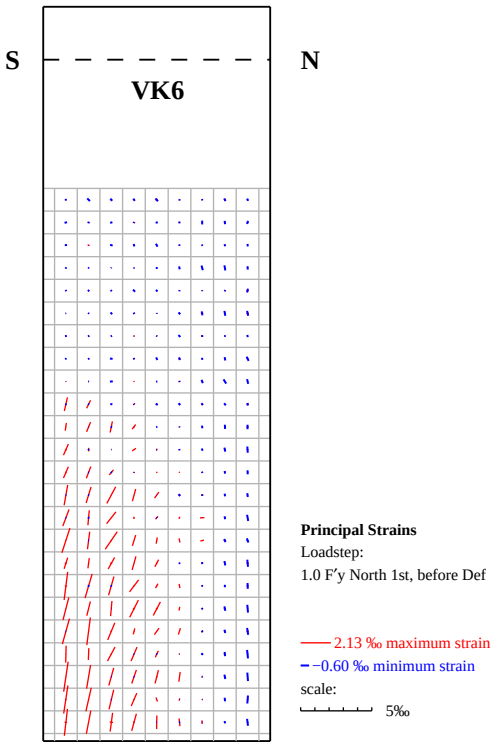

(b) LS021 $1.0F_y'$ North 1^{st}

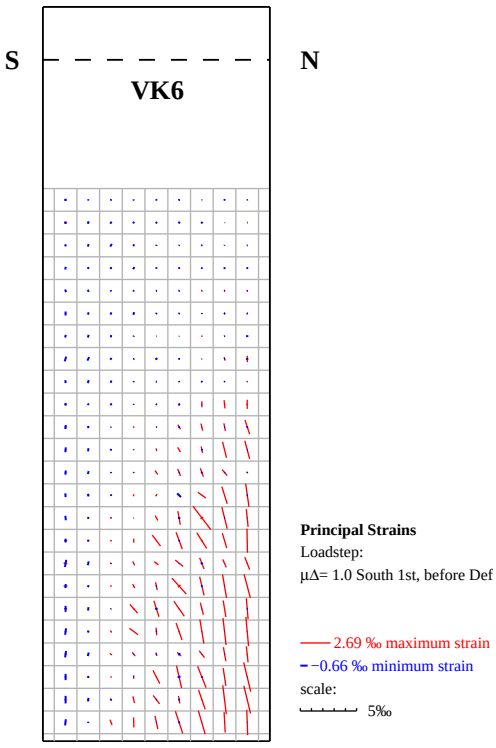

(c) LS027 $\mu_\Delta = 1.0$ South 1^{st}

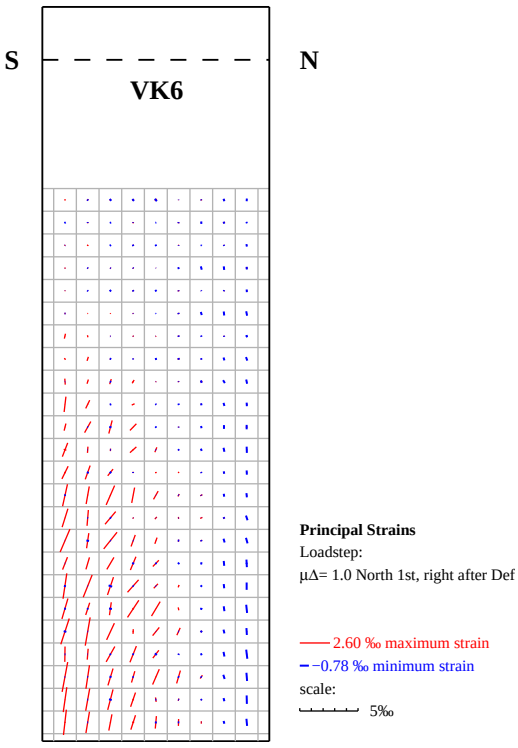

(d) LS029 $\mu_\Delta = 1.0$ North 1^{st}

Figure 4.40: Principal strains of VK6 at $1.0F_y'$ (a), (b) and at $\mu_\Delta = 1.0$ (c), (d).

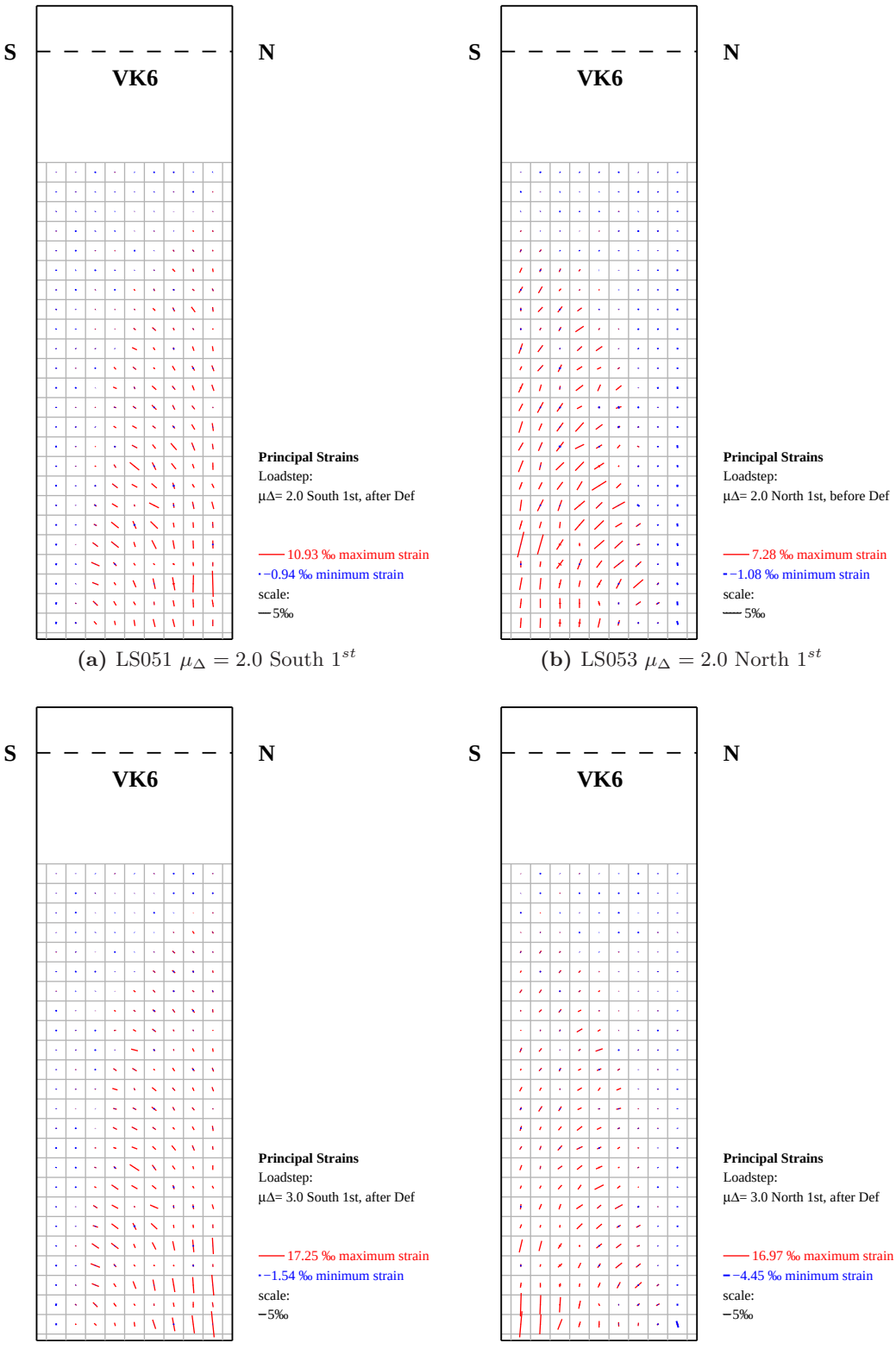

(a) LS051 $\mu_\Delta = 2.0$ South 1^{st}

(b) LS053 $\mu_\Delta = 2.0$ North 1^{st}

(c) LS067 $\mu_\Delta = 3.0$ South 1^{st}

(d) LS069 $\mu_\Delta = 3.0$ North 1^{st}

Figure 4.41: Principal strains of VK6 at $\mu_\Delta = 2.0$ (a), (b) and at $\mu_\Delta = 3.0$ (c), (d).

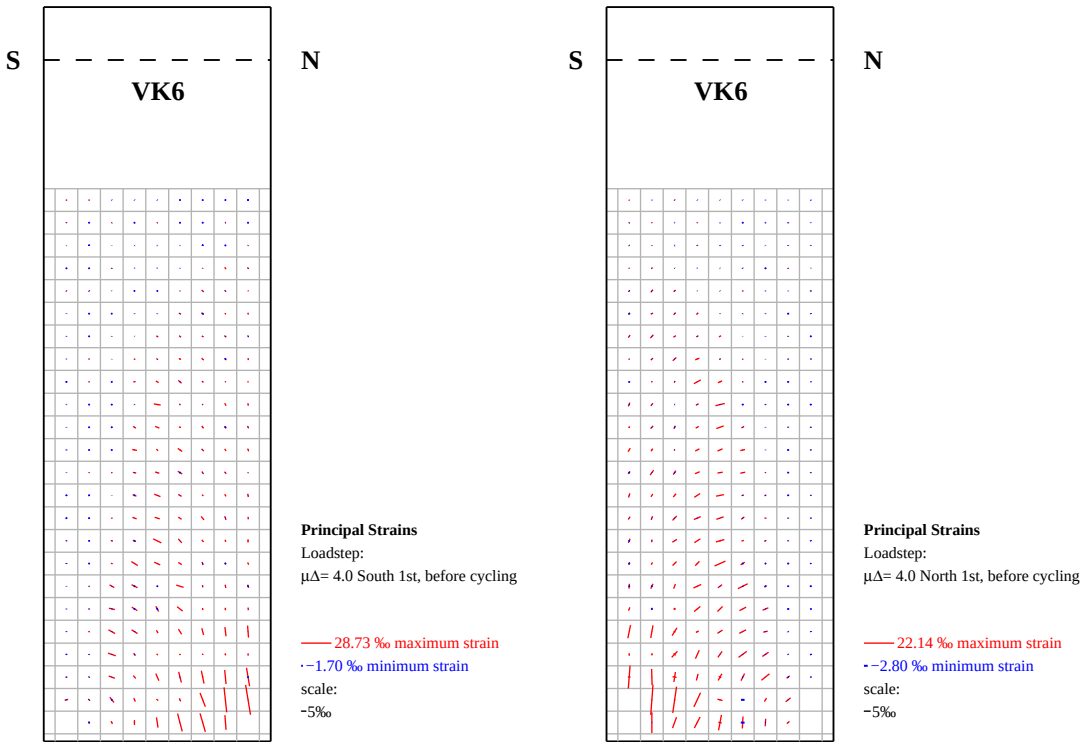

(a) LS083 $\mu_\Delta = 4.0$ South 1^{st} **(b)** LS085 $\mu_\Delta = 4.0$ North 1^{st}

Figure 4.42: Principal strains of VK6 at $\mu_\Delta = 4.0$.

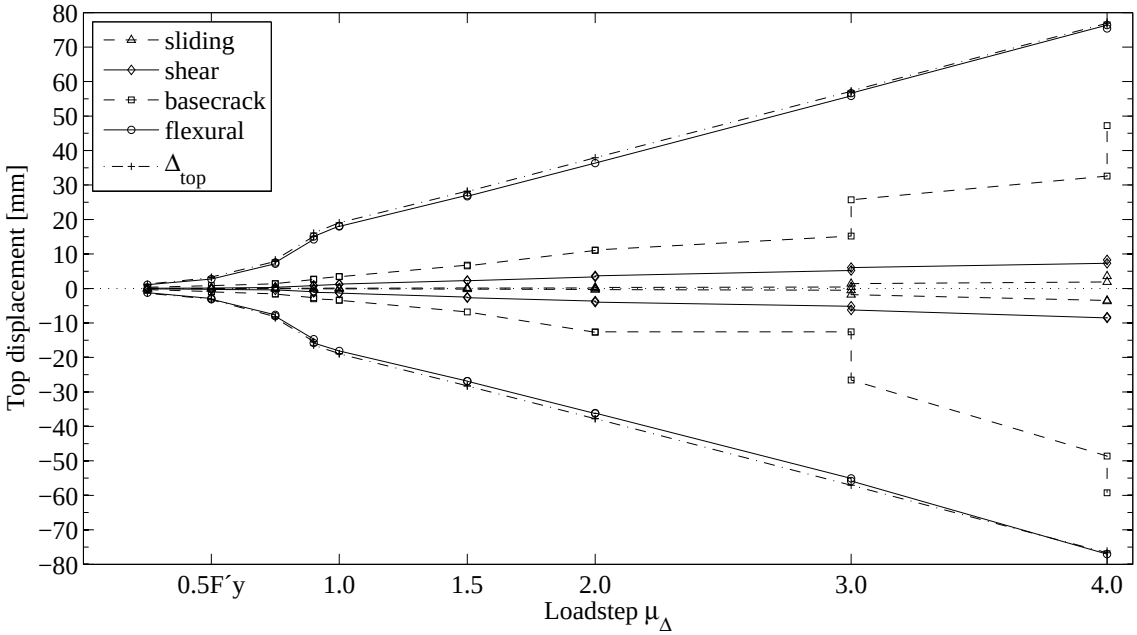

Figure 4.43: Sum of deformation components of VK6 at the 1^{st} and 2^{nd} cycles at the end of the shear span compared to the top displacement measured by the LVDTs. Between the 1^{st} and 2^{nd} cycle to $\mu_\Delta = 3.0$ one LED at the bottom corner fell off, therefore the increase in the base crack and sliding components, which were then determined with the second row markers.

4.4.4 Cracks

The monitored cracks as well as the complete crack pattern are presented in Figure 4.44. Table 4.3 summarizes the widths of some of the cracks at certain load steps. Cracks that were already visible but too narrow to determine their widths are indicated with < 0.05. Figure 4.44 also shows how cracks were numbered and along which pattern their widths were determined.

		Crack widths [mm]									
		1^{st} cycles South						1^{st} cycles North			
		A	B	C	D	E		A	B	C	D	E
$1.0F'_y$	III				0.05	0.05	III	0.1	2× <0.05	<0.05		
$1.5\mu_\Delta$				0.05	0.1	0.05 + 0.1		0.35	0.1	0.15	<0.05	
$3.0\mu_\Delta$				<0.05	0.45	1.2		1.1	0.15	0.2	0.15	
$5.0\mu_\Delta$					0.4	1.2		0.9	0.5	0.1		
$1.0F'_y$	V			<0.05	<0.05	0.05	V	0.1	0.05			
$1.5\mu_\Delta$				0.1	0.05	0.05 + 0.1		0.1	0.15	0.1		
$3.0\mu_\Delta$			0.2	0.55	0.1	0.05 + 0.15		0.1	0.1	0.35	0.15	
$5.0\mu_\Delta$			0.9	0.8	0.1	0.1		0.05	0.1	0.7	0.7	
$1.0F'_y$	IIX						IIX					
$1.5\mu_\Delta$					0.05	0.05		0.05	<0.05	<0.05		
$3.0\mu_\Delta$				0.3	0.2	0.05		0.1	0.05	0.3		
$5.0\mu_\Delta$				0.5	0.3	0		0.05	0.05	0.7		

Table 4.3: Monitored cracks of test unit VK6 and widths of some of them.

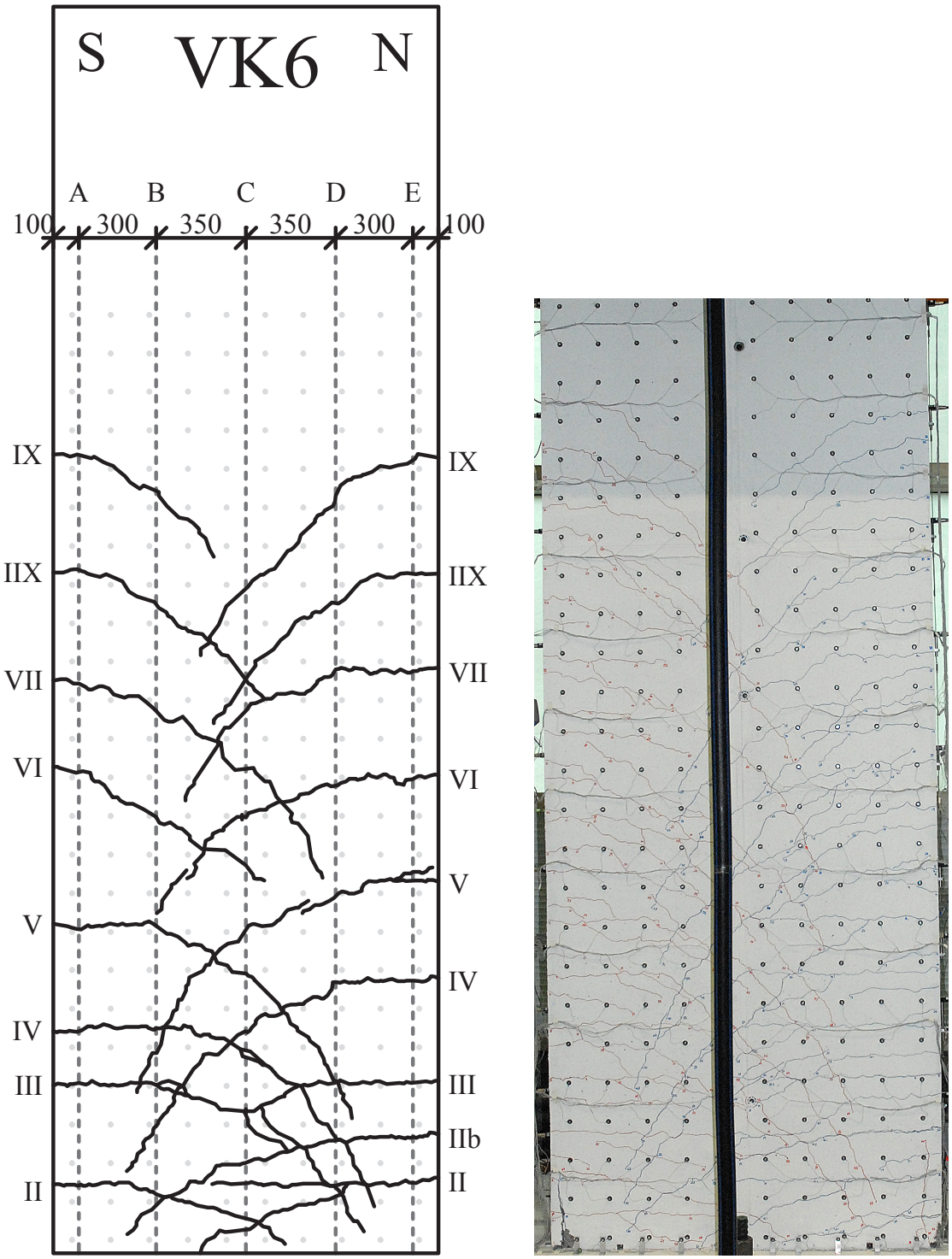

Figure 4.44: Drawing of monitored cracks (left) and picture of complete crack pattern (right) of test unit VK6.

4.5 Test Unit VK7

4.5.1 Test Observations

Test unit VK7 had, except for the higher transverse reinforcement ratio, the same layout as test unit VK3, see [Bim10]. Testing began on August 18^{th}, 2010 by applying the vertical load and ended with failure of the test unit on September, 1^{st}, 2010. Before the load was applied, all the reference measurements were taken and the hard-wired devices were set to zero. The vertical load was applied slowly until 1300 kN were reached and a new set of optical measurements was taken. No manual measurements were taken during this test. Over night, the vertical load was kept constant. The following day, due to an unsatisfactory quality of the optical measurements, the load was released to 200 kN and then reapplied to take new measurements with and without axial load. The load could not be lowered further without completely releasing the pressure from the circuit, which could possibly have meant that also the anchors of the tendons had to be readjusted before the new load application. Therefore, the new reference measurements were made with this load, which corresponds to an average compressive stress of only 0.4 MPa over the entire cross section. Since the new measurements appeared to be satisfactory, the actuator was connected and loading was started the next day.

During the first cycle to $0.25\,F_y' = 160$ kN target force only hairline cracks were detected at the edges of the pier's base, which were not marked at that stage. When $0.5\,F_y$ South 1^{st}, corresponding to $F = 321$ kN horizontal force, was reached, the base crack opened over a length of approximately 50 cm. Another crack opened 7.5 cm above the base, which corresponds to the location of the first stirrup. A small crack was visible in the foundation at the South-West corner of the pier at $0.5\,F_y'$ South 1^{st}. At $0.5\,F_y'$ South 2^{nd}, the base crack was 0.1 mm wide. While loading towards $0.75\,F_y' = 481$ kN target force in positive loading direction, a small drop of the horizontal force occurred when 400 kN were reached and the stiffness decreased slightly afterwards. Several almost perfectly horizontal flexural cracks were detected up to about 1.0 m height. Loading was then reversed towards $0.75\,F_y' = -481$ kN North 1^{st}. At -339 kN and -405 kN small drops of the horizontal force, which were followed by slight decreases in stiffness, occurred. Cracks were detected up to 1.10 m however they had a steeper angle at their ends than in the previous load step and were longer than those on the North side of the pier, spanning from the edge to the center line of the pier. After the second cycle with $0.75\,F_y$ horizontal target force was completed, the test unit was unloaded to zero horizontal force, the hydraulic circuit of the vertical force was locked in to keep the load constant and all hydraulic devices were turned off for the weekend.

Testing was resumed with load step $1.0\,F_y'$ South 1^{st} after the weekend. When 459 kN horizontal force were reached, the actuator suddenly turned off due to a connection failure of the controller and the force dropped slightly before it was turned back on. The test unit was less stiff than the other comparable units with $a/d = 2.2$ and the horizontal displacement at $1.0\,F_y'$ was larger than $\mu_\Delta = 1.0 = 10.5$ mm. Cracks became steeper and formed up to 2 m height, stretching over 2/3 of the pier's length near the bottom. Their spacing often corresponded to the stirrup spacing of 7.5 cm. The cracks on the pier were 0.05 to 0.1 mm wide and the base crack 0.1 to 0.2 mm. Foundation cracks were visible on both edges of the Northern side of the pier.

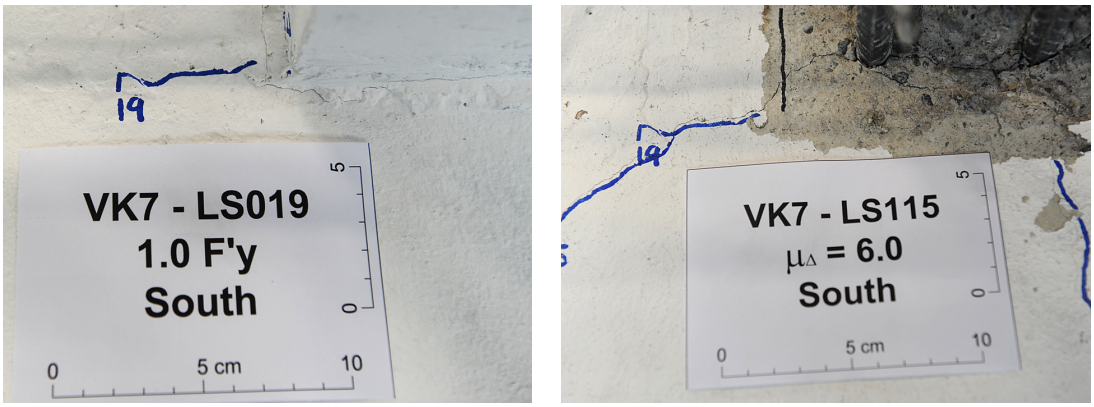

(a) LS107 **(b)** LS115

Figure 4.45: Crack in the foundation at the North-West edge of the pier at LS019, when it was first visible (a) and after the concrete cover had spalled off (b).

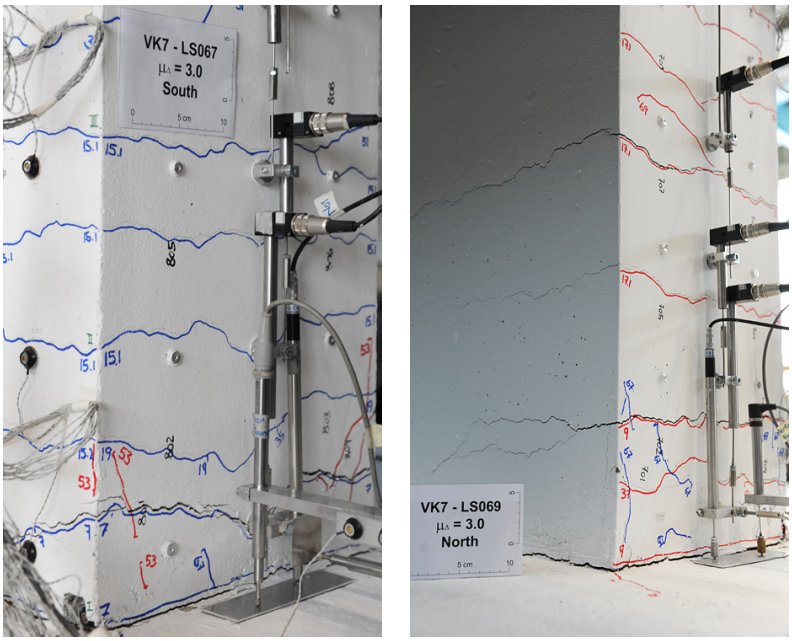

(a) $\mu_\Delta = 3.0$ South 1^{st} North face **(b)** $\mu_\Delta = 3.0$ North 1^{st} South face

Figure 4.46: South and North face at the bottom of the pier at load steps $\mu_\Delta = 3.0$ South, LS067, (a) and North, LS069 (b).

While the loading was reversed to $1.0\,F'_y$ North 1^{st} the development of the cracks was closely monitored, to identify when the steeper shear cracks would develop. Cracks seemed to become noticeably steeper when about 500 - 570 kN horizontal force were applied. Crack widths were similar to those in the previous load step, only the width of the base crack increased to 0.3 mm. Additionally to the previously detected crack in the foundation at the South-West corner of the pier, another one developed at the South-East corner. During the cycle to $1.0\,F'_y$ South 2^{nd} the actuator had to be stopped due to an error in the horizontal force signal again, but the source of the disturbances was finally found and the test could be resumed after a short break. Since the top displacements in the following cycles to $\mu_\Delta = 1.0$ were smaller than those in the previous

cycles to $1.0\,F'_y$ horizontal force, no new cracks developed. When LS032, the center position after excursion to $\mu_\Delta = 1.0$ South 2^{nd}, was reached, all hydraulic devices were turned off for the night.

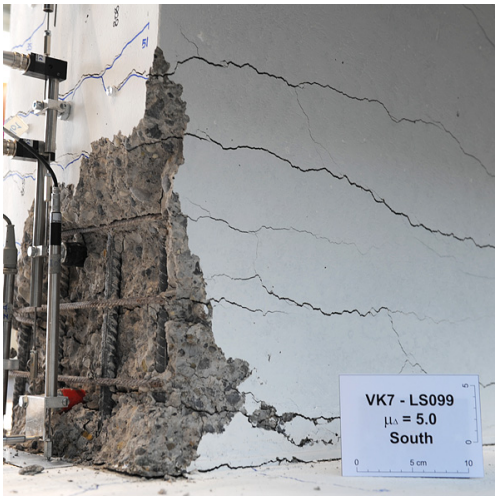

(a) $\mu_\Delta = 5.0$ South: North-West face

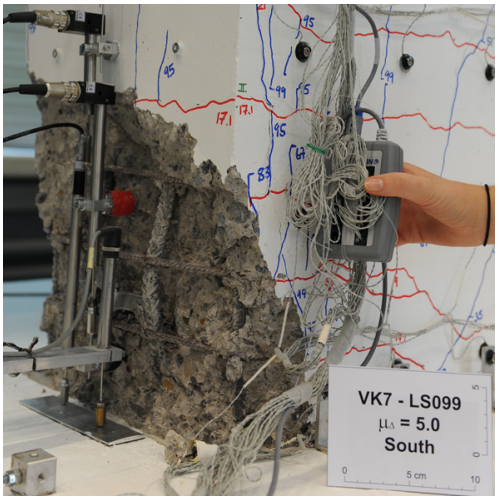

(b) $\mu_\Delta = 5.0$ South: South-East face

(c) $\mu_\Delta = 5.0$ North: North-West face

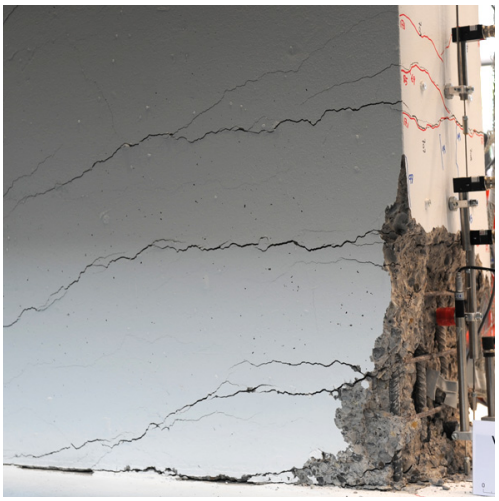

(d) $\mu_\Delta = 5.0$ North: South-West face

Figure 4.47: South and North face at the bottom of the pier at load steps $\mu_\Delta = 5.0$ South and North.

The next day, the second half-cycle to $\mu_\Delta = 1.0$ North was completed before the top displacement was increased to $\mu_\Delta = 1.5 = 15.75$ mm South for the first time. Some new cracks developed up to 40 cm above the previous ones, but in general the cracks mainly grew longer and wider with widths of 0.05 - 0.2 mm on the pier's surface. At the reversed load step, $\mu_\Delta = 1.5$ North, similar crack widths were measured. However, the horizontal force F = -710 kN was slightly lower than at the previous peak, where F = +737 kN was reached. Lower capacity in the negative loading direction was also noticed at previous load steps. In the following, the first set of small cycles and the second cycle to $\mu_\Delta = 1.5$ were applied before displacement was increased to

$\mu_\Delta = 2.0 = 21\,\text{mm}$ in positive loading direction. $F = 820\,\text{kN}$ horizontal force was reached at peak displacement and crack widths increased up to 0.25 mm. A new shear crack formed starting at about 2.45 m height on the North side of the pier, where previously only a short crack was visible, running down to about 1.55 m near the center of the pier. At $\mu_\Delta = 2.0$ North 1^{st}, observations were similar to those at $\mu_\Delta = 2.0$ South 1^{st}. An additional crack developed above the existing ones and the existing cracks mainly increased in length and width. After running the small cycles and second cycle to $\mu_\Delta = 2.0$, testing for this day was ended. Shortly after unloading from $\mu_\Delta = 2.0$ North 2^{nd} started, the actuator turned off due to some disturbance, but could be turned on again immediately.

During the following first cycle to $\mu_\Delta = 3.0 = \pm 31.5\,\text{mm}$ top displacement the pier's horizontal peak forces of $F = +903\,\text{kN}$ in positive and $F =$ -850 kN in negative loading direction were reached. New shear cracks formed above the existing cracks and the first vertical cracks in the compression zone were visible reaching up to about 20 - 25 cm height, see also Figure 4.46b. Once the small cycles were completed and load step $\mu_\Delta = 3.0$ South 2^{nd} was reached, some concrete in the corners at the North side of the pier spalled off. No new cracks developed and not much additional damage occurred up to $\mu_\Delta = 4.0$ North, when the reinforcement bar in the North-East corner, where the concrete cover previously spalled off, began to buckle. All hoops had their 90° hooks in that corner, hence the restraint of that bar was comparatively weak. At $\mu_\Delta = 4.0$ North 2^{nd}, three of the four bars on the North face of the pier had buckled, only the reinforcement bar in the North-West corner had not yet buckled. In general, there was less damage and spalling of cover concrete at the opposite side of the pier, where no hooks of the stirrups were placed. While the first loading to $\mu_\Delta = 5.0$ South was applied, the test had to be stopped shortly at approximately 4.7 mm top displacement and 245 kN horizontal force because the two middle reinforcement bars on the South face were buckling, pushing the concrete outwards towards the LVDTs. When loading in the opposite loading direction was applied, the stirrups on the North side were opened further and also the fourth reinforcement bar on the North face as well as the first one on the East face of the pier buckled. The bar in the North-West corner had a buckling length of about 15 cm, i.e. it was still held back by the second hoop. The other three bars were restrained only by the fourth hoop, meaning their buckling length was 30 cm, i.e. twice as long. During loading, the test had to be stopped two times, to prevent an open stirrup from pushing against a LVDT and to reposition another LVDT (VertDef_Foundation_North). After the first cycle to $\mu_\Delta = 5.0$ had been completed, the last set of small cycles was applied.

During the next cycles, degradation of the compression zones slowly increased with generally more damage in the Northern compression zone where the hooks of the stirrups were located, see Figure 4.47. While the first loading to $\mu_\Delta = 6.0 = 63\,\text{mm}$ South was applied, the short leg of one hoop located on the South face of the pier had to be cut open, because it was pushed outwards by the longitudinal bars and would have touched the LVDTs otherwise. As a consequence, the confinement of the longitudinal reinforcement on that side was weakened, however, the bars had already buckled by then anyways. When loading was reversed, the peak horizontal force in the negative loading direction $F =$ -632 kN occurred before the peak displacement was reached. In general, horizontal forces were still rather large at the first cycle at $\mu_\Delta = 6.0$, with 824 kN (91 % $F_{max,pos}$) at $\mu_\Delta = 6.0$ South, and -597 kN (70 % $F_{max,neg}$) at $\mu_\Delta = 6.0$ North. The absolute difference in the horizontal forces increased during the following cycles and the largest difference in the whole test was measured at the cycle at $\mu_\Delta = 7.0$. The peak forces in this cycle were

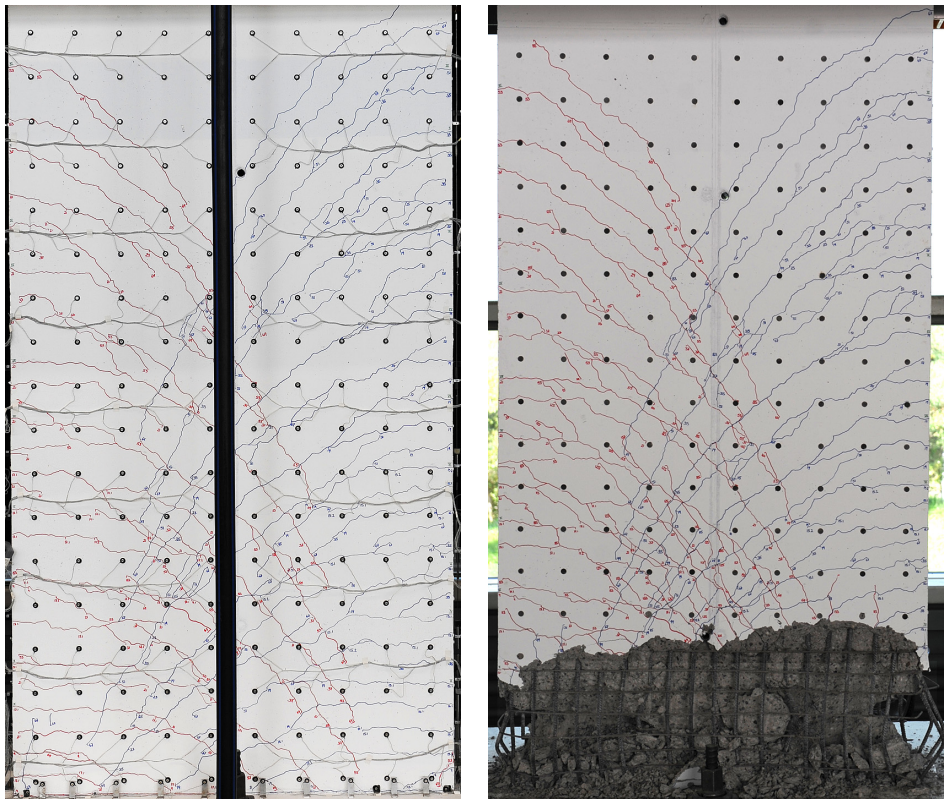

(a) $\mu_\Delta = 3.0$ North 1^{st} **(b)** after failure

Figure 4.48: View of VK7 at $\mu_\Delta = 3.0$ with completely developed crack pattern (a) and after failure (b).

$F = 748\,\text{kN}$ (83 % $F_{max,pos}$) in positive loading direction and $F = -427\,\text{kN}$ (50 % $F_{max,neg}$) in negative loading direction. When the second load step $\mu_\Delta = 7.0$ North was reached, only an about 25 cm wide strip of the concrete cover was left in the center of the pier, and the core concrete in the Northern bottom part of the pier was severely damaged, whereas there was still a large portion of core concrete left at the opposite edge of the pier. Already at $\mu_\Delta = 7.0$ North 1^{st} damage of the compression zone was so advanced that the second LVDT support on the North face was merely lying on loose concrete.

At LS131, $\mu_\Delta = 8.0$ South 1^{st}, LVDT VertDef_N03 went out of range because it bridged a crack which opened up significantly. Shortly before the target displacement was reached, the horizontal force slowly began decreasing to 491 kN (54 % $F_{max,pos}$), which was 40 kN lower than the peak load that occurred during the cycle. Before LS133, $\mu_\Delta = 8.0$ North 1^{st} was reached, the first three LVDTs on each side had to be removed to protect them from damage, because the pier was severely damaged and the reinforcement bars buckled significantly. Up to about 50 - 65 cm height, all the cover concrete had spalled off and in each direction, there was one flexural crack in the bottom part of the pier which opened up significantly. Right after the target displacement of LS133 was reached, the reinforcement bar in the S-W corner, which was sharply bent at LS131, fractured in tension. The horizontal force capacity dropped further during the second cycle. Afterwards, at zero top displacement, the LVDTs HorDisp_5 and _6 had to be rearranged. Opposite offsets were therefore introduced to the LVDTs, similar to what had been

done during the previous tests. Then, the top displacement was increased to $\mu_\Delta = 9.0$ South for the first time, where $236\,\text{kN} = 0.26F_{max,pos}$ horizontal force could still be applied. As the concrete at the bottom of the pier was severely damaged, almost all deformation resulted from the rotation in that area. After unloading, while the first loading to $\mu_\Delta = 9.0$ North was applied, the pier suddenly failed with an instantaneous loss of both normal and horizontal force carrying capacity.

4.5.2 Hard-Wired Measurements

In the following graphs, some of the hard-wired measurement data is presented. In Figures 4.49 to 4.51, the horizontal force measured with the actuator's internal load-cell is plotted against the top displacement, corrected according to Equation (4.2).

The curvatures presented in Figure 4.52 were determined from the measurements of the LVDT chains along the side faces of the pier. A horizontal distance of 1544 mm between the devices was used to calculate the curvatures, because the center lines of the LVDTs were mounted 22 mm from the surface. In general, all curvatures are displayed until the devices had to be removed to protect them from damage.

The strains plotted in Figure 4.55 were also determined from the LVDTs using the measured deformation and the base lengths which can be seen in Figure 3.7. Those strains, which represent the strains 22 mm away from the surface, were projected to the pier's surface with linear interpolation, i.e. with a plane sections assumption.

In Figure 4.53 the strains of the reinforcement measured with the strain gauges are presented at selected load steps. At each position, the mean value of the measurements at the back and the front of the test unit are presented. During this test, three gauges were damaged so the center value as well as the values at both edges were determined from one gauge only. Strains are presented up to load step μ_Δ =1.5, after which it was hard to tell whether the measurements were still reliable. The strains calculated from the LVDTs and strain gauge measurements are presented for the first cycles of some selected load steps. In general, the peak values of the cycles have not been used, but those at the end of the time frame in which the top displacement was maintained constant, because they correspond best to the manual and optical measurements, which were usually also taken towards the end of that time interval.

The diagram in Figure 4.54a displays the pullout slip of reinforcement bars measured right above foundation against the readings of strain gauges glued to the same bars. The three considered bars were all located along the East face of the wall (see Figure 3.4), i.e.: i) LED 1 was glued on the South-East corner bar, ii) LED 3 was glued on a bar located 270 mm far away from the North-East corner, and ii) LED 4 was glued on the North-East corner bar. LED2 could not be applied to this test unit as the styrofoam to create the hole in which the LED should have been placed moved during the casting. For the reasons outlined in the previous paragraph, the results pertain mostly to the elastic deformation range of the reinforcement. Furthermore, as strain gauge number 9 of this test unit was not working, strain gauge no. 10 is used instead in this plot. Figure 4.54b shows the pullout of the outer reinforcement bars, i.e. LED1 and LED4, against the displacement ductility, over the range over which measurements were available.

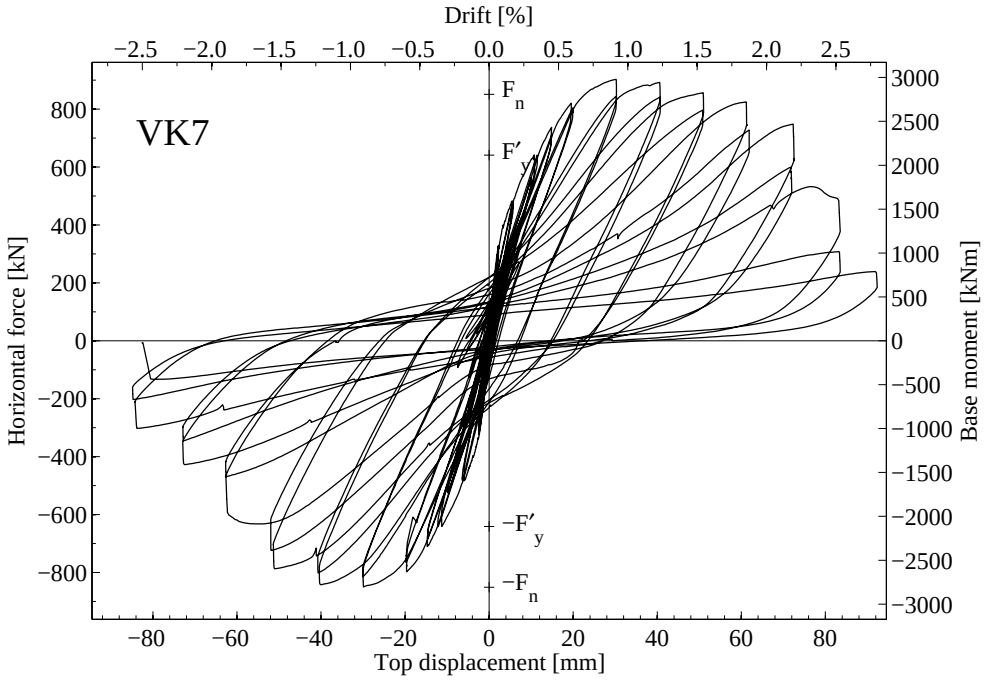

Figure 4.49: Measured force - deformation response of test unit VK7.

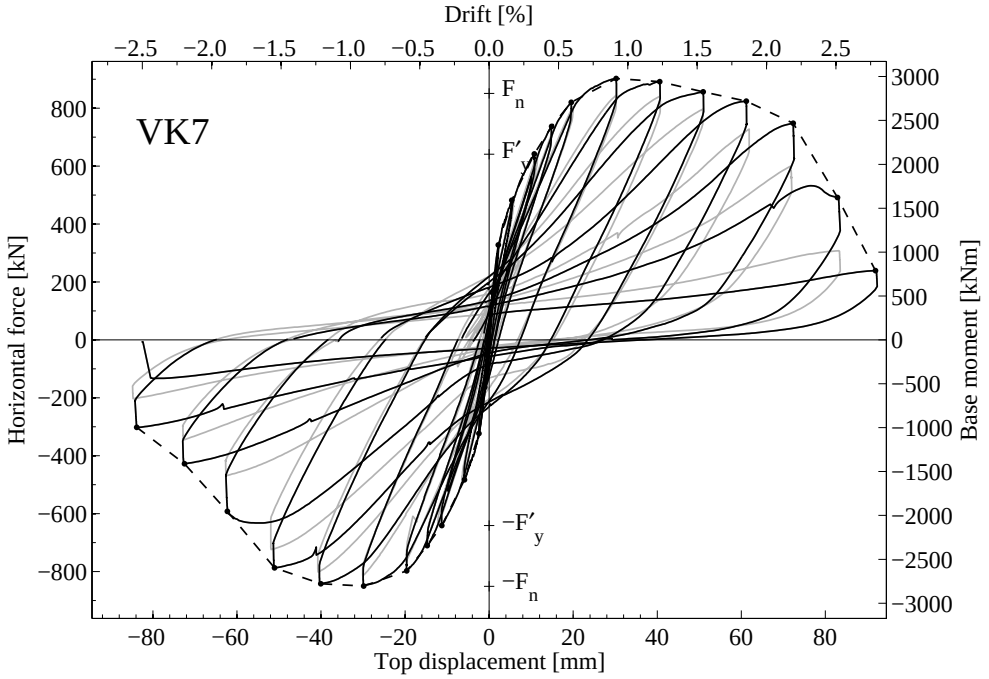

Figure 4.50: Measured force - deformation response of test unit VK7 with emphasized first cycles and envelope of first cycles.

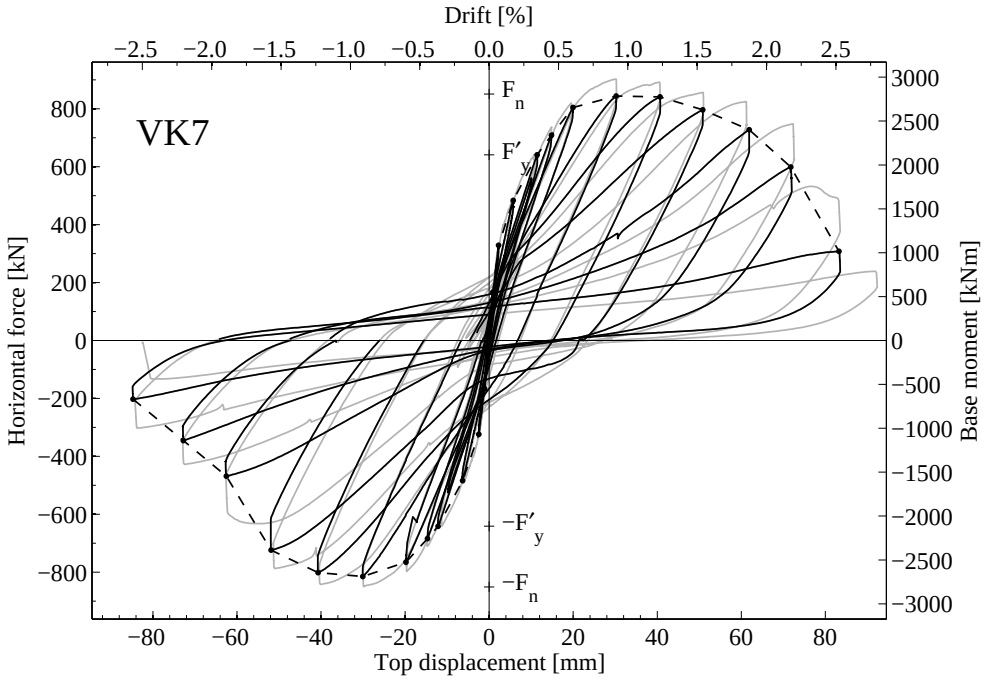

Figure 4.51: Measured force - deformation response of test unit VK7 with emphasized second cycles and envelope of second cycles.

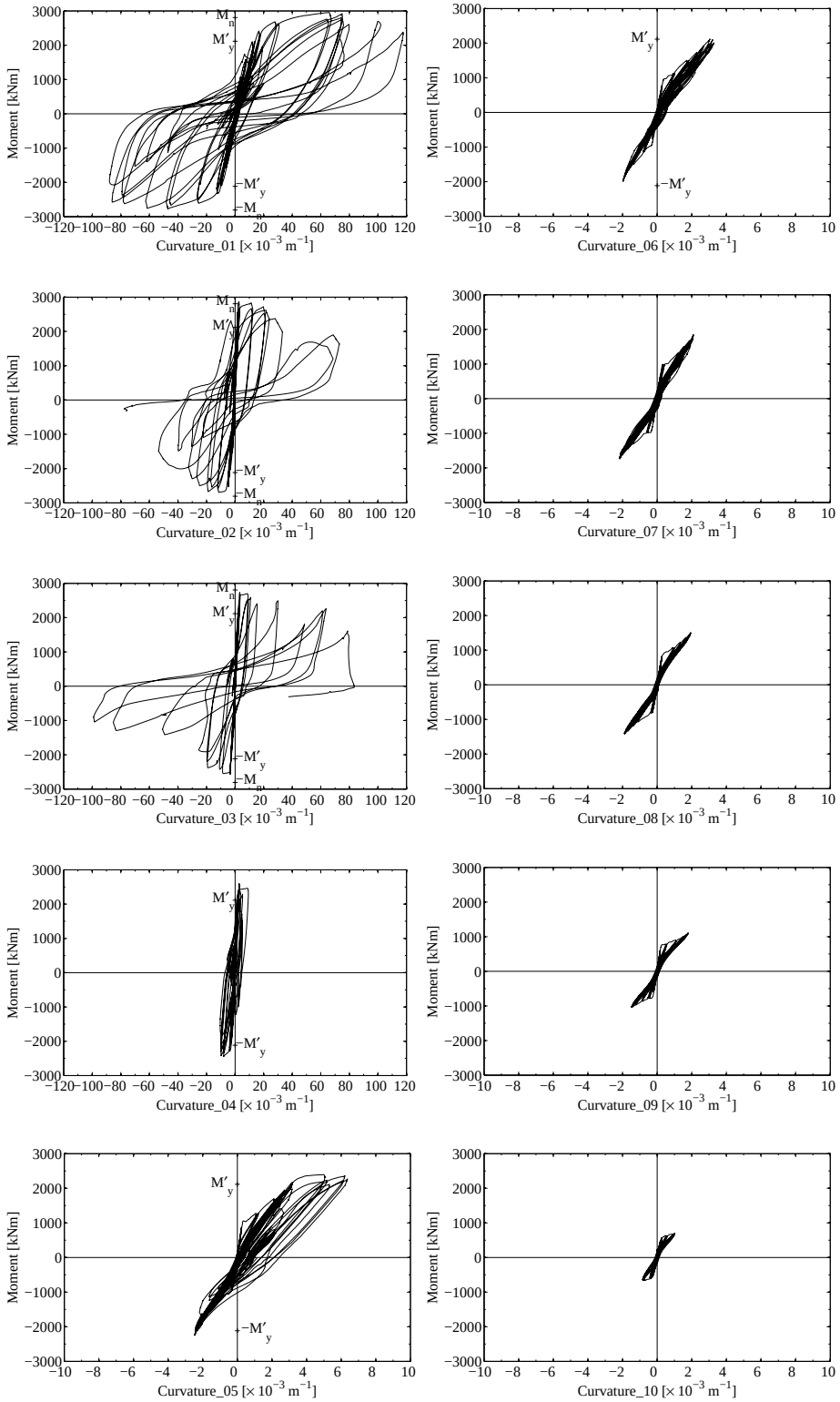

Figure 4.52: Measured moment-curvature relationships 01 to 10 of test unit VK7. Curvatures 01 to 03 are displayed up to load step $\mu_\Delta = 8.0$ South 1^{st}, after which the corresponding LVDTs were removed, all other curvatures are displayed to the end of the test.

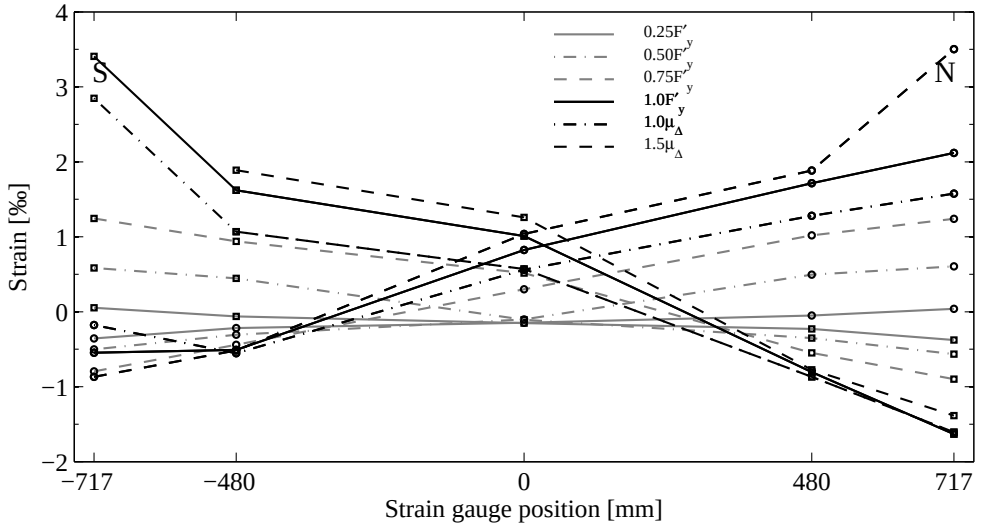

Figure 4.53: Mean longitudinal reinforcement strains of VK7 measured by the strain gauges, displayed at selected load steps. Usually the first cycle load steps are displayed, but all signals were very noisy between $0.75F_y'$ 2^{nd} and $1.0F_y'$ South 2^{nd}, therefore the second cycles of $1.0F_y'$ are shown.

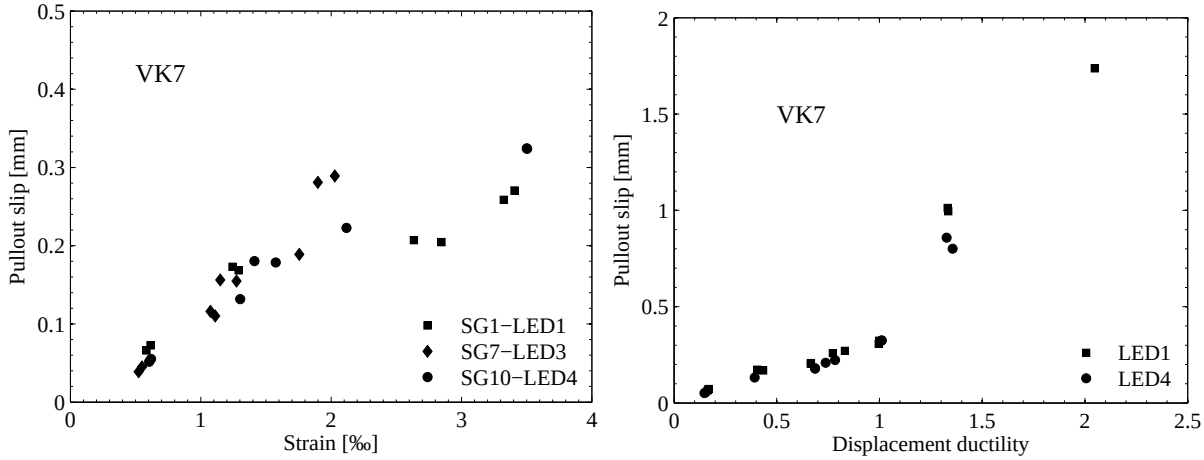

(a) Pullout slip of reinforcement bars measured right above foundation (LED) against readings of strain gauges (SG).

(b) Pullout slip of reinforcement bars measured right above foundation (LED) against displacement ductility.

Figure 4.54: Pullout slip of reinforcement bars of VK7.

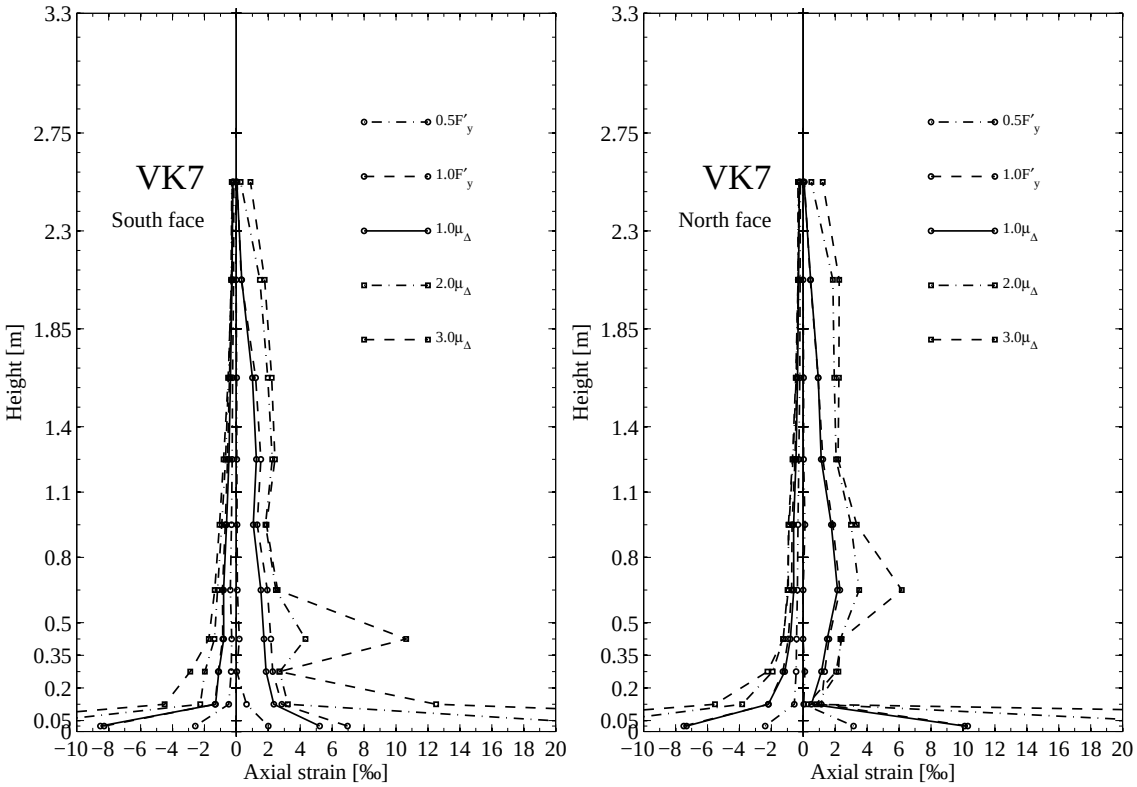

Figure 4.55: Strains along the South and North face of test unit VK7 calculated from deformations measured by means of the LVDTs and projected to the pier's surface, at selected load steps.

4.5.3 Optical Measurement Results

In Figures 4.56 to 4.59, plots with the strains calculated from the optical measurements are presented. The strains are computed from the measurements taken during two minutes long time intervals at the peaks of the cycles while the top displacement was kept constant according to the procedure described in Section 3.2.2. The largest strains are obtained for the bottom row, since the base length is small there but the deformations large due to the base crack. Because these strains exceed the strains along the pier by far, they have not been included in the plots since it would be difficult the read the plots if they were included and drawn to the same scale. The piers are always drawn to a scale of 1:50 and the largest strain has the same length in each plot. This constant strain length was chosen to visualize both the load steps with small as well as those with large strains equally well. For the calculation of the strains according to Section 4.1.2 the mean values of the transformed coordinates were used, no further corrections were made. However, as marker rows 10 and 12 seemed obviously false, these rows have not been considered. The mean values of the strains ε_x in the rows above and below were assumed as horizontal strains for these marker rows, the same values ε_y and γ_{xy}, calculated from the markers in rows 9 and 11, as well as 11 and 13, were assumed for both rows of elements.
The deformation components are presented up to load step $\mu_\Delta = 5.0$ in Figure 4.60. Afterwards, the concrete in the bottom part of the pier was severely crushed, which made determination of meaningful components difficult, because too many markers were missing at the bottom. Rows number 10 and 12 were not considered for the evaluation of the components as well.

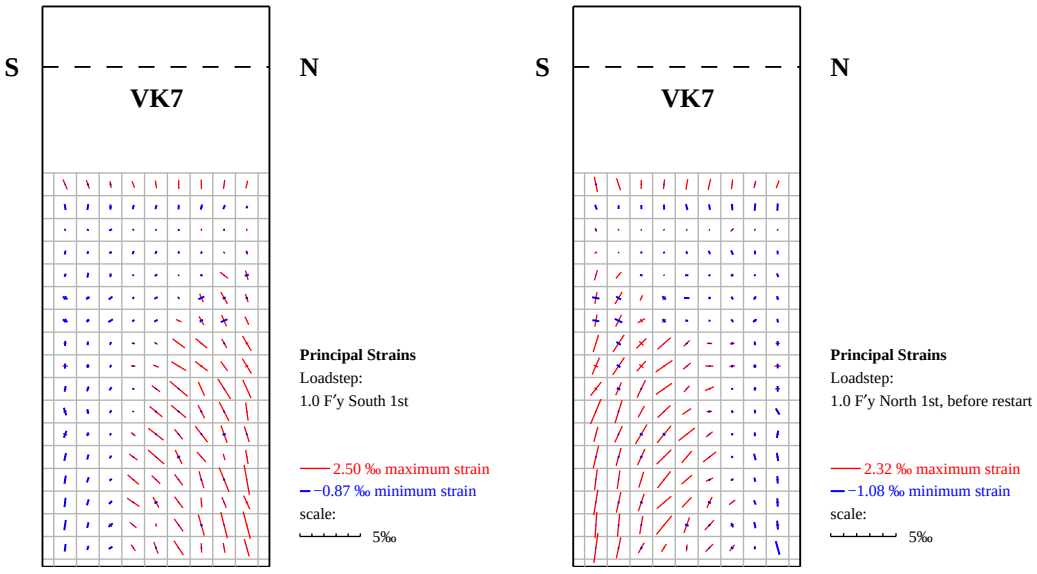

(a) LS019 $1.0F'_y$ South 1^{st} **(b)** LS021 $1.0F'_y$ South 1^{st}

Figure 4.56: Principal strains of VK7 at $1.0F'_y$.

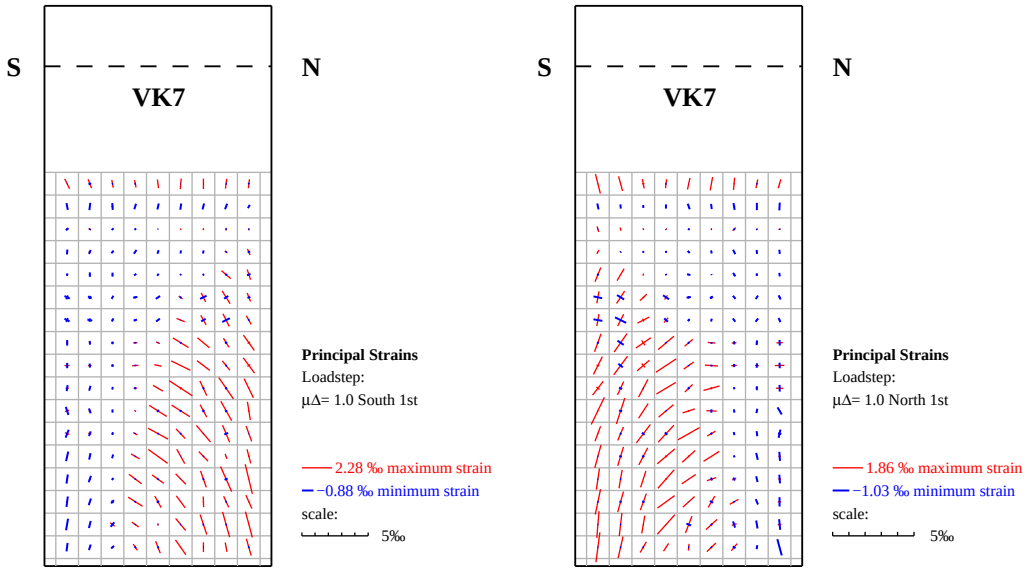

(a) LS027 $\mu_\Delta = 1.0$ South 1^{st} **(b)** LS029 $\mu_\Delta = 1.0$ North 1^{st}

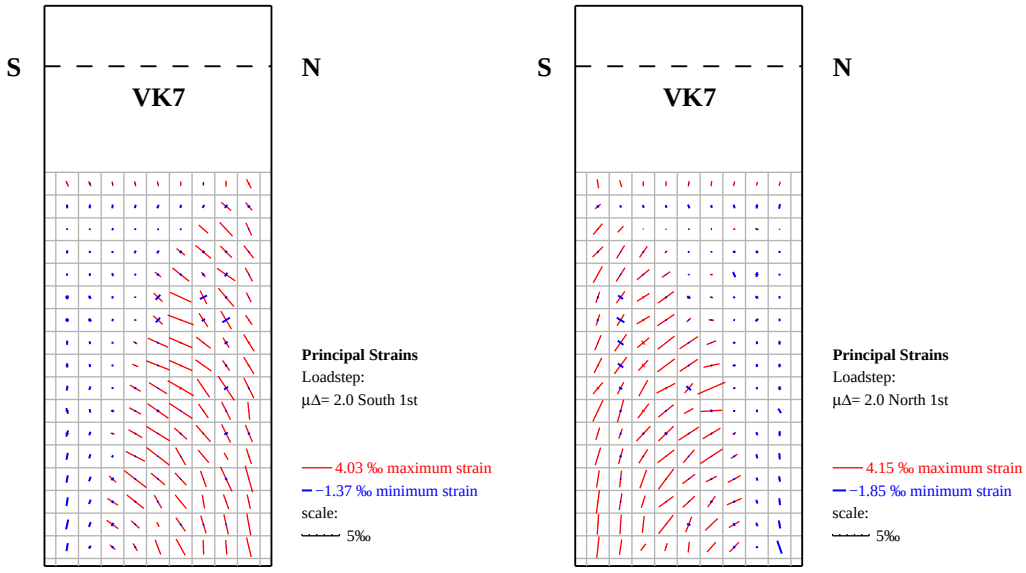

(c) LS035 $\mu_\Delta = 2.0$ South 1^{st} **(d)** LS037 $\mu_\Delta = 2.0$ North 1^{st}

Figure 4.57: Principal strains of VK7 at $\mu_\Delta = 1.0$ (a), (b) and $\mu_\Delta = 2.0$ (c), (d).

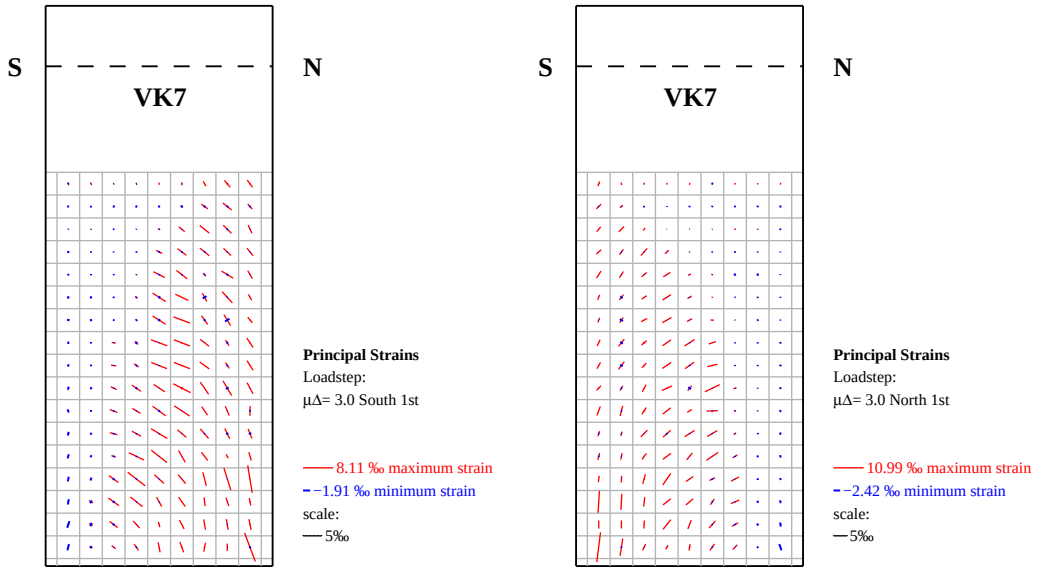

(a) LS067 $\mu_\Delta = 3.0$ South 1^{st} **(b)** LS069 $\mu_\Delta = 3.0$ North 1^{st}

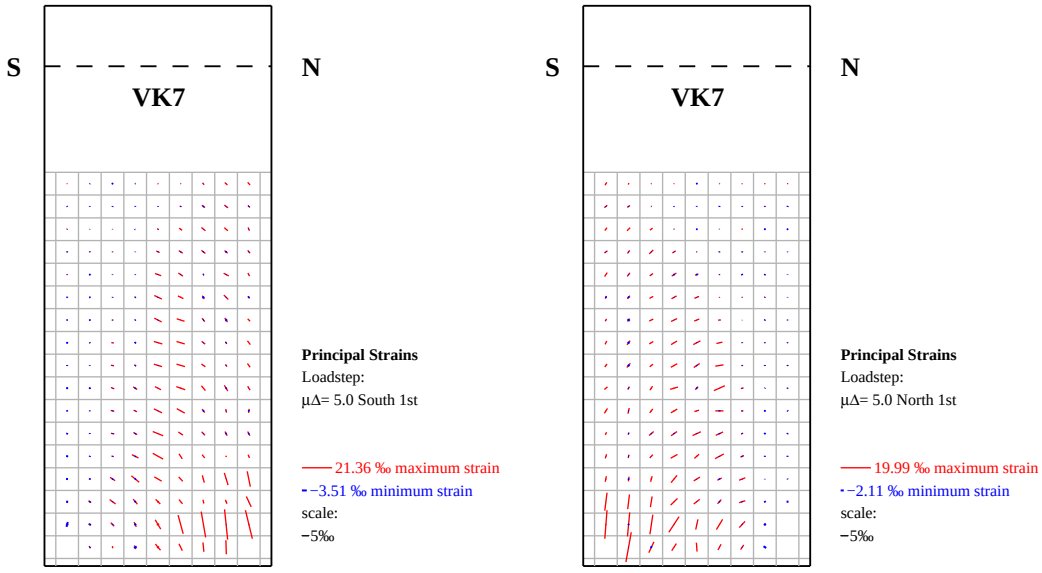

(c) LS099 $\mu_\Delta = 5.0$ South 1^{st} **(d)** LS0101 $\mu_\Delta = 5.0$ North 1^{st}

Figure 4.58: Principal strains of VK7 at $\mu_\Delta = 3.0$ (a), (b) and $\mu_\Delta = 5.0$ (c), (d).

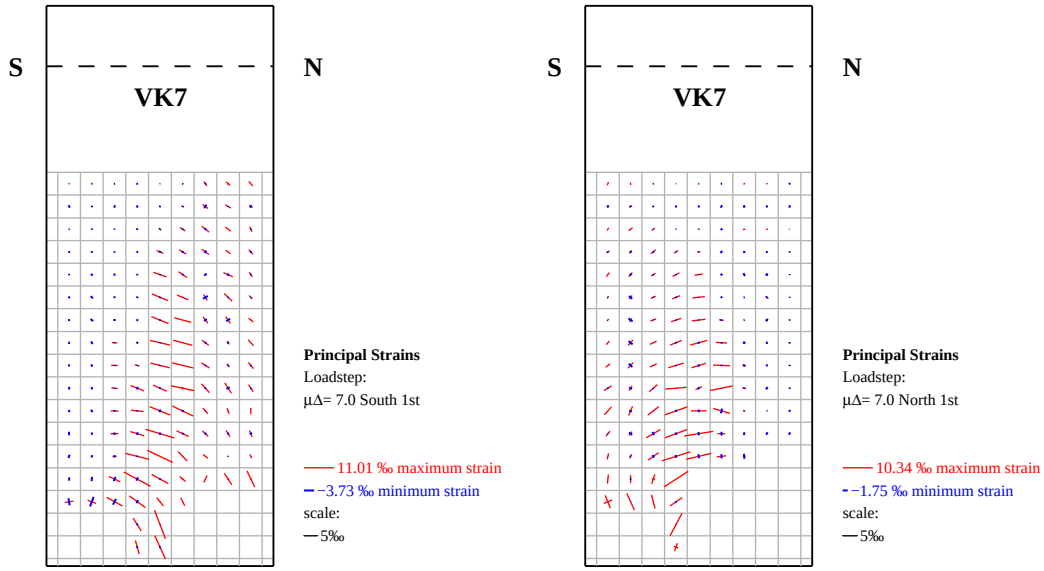

(a) LS0123 $\mu_\Delta = 7.0$ South 1^{st} **(b)** LS0125 $\mu_\Delta = 7.0$ North 1^{st}

Figure 4.59: Principal strains of VK7 at $\mu_\Delta = 7.0$.

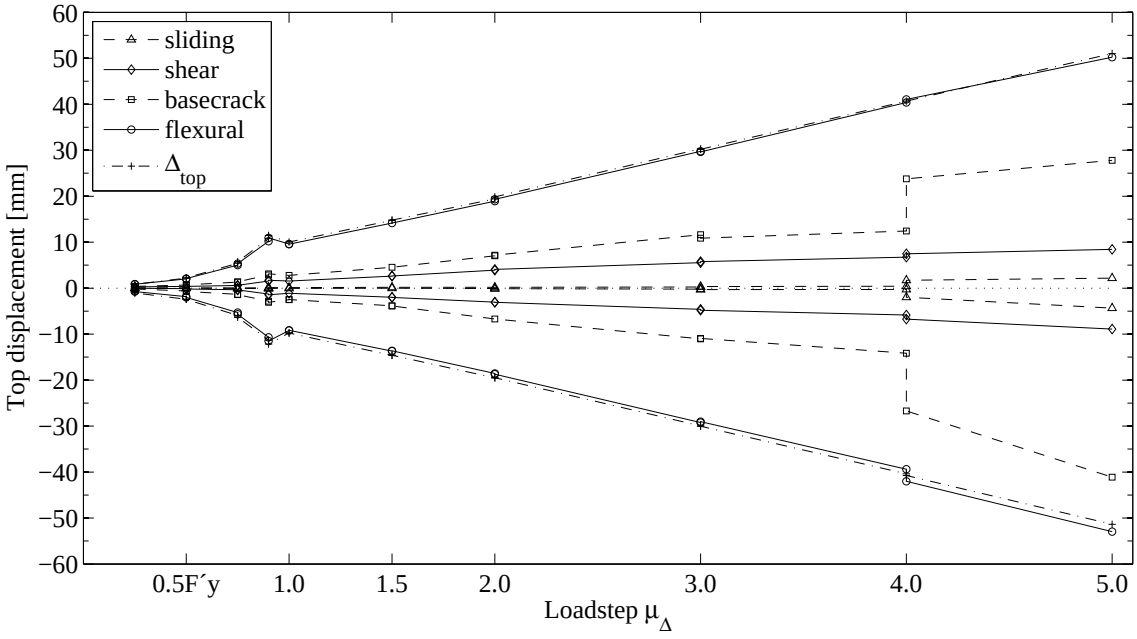

Figure 4.60: Sum of deformation components of VK7 at the 1^{st} and 2^{nd} cycles at the end of the shear span compared to the top displacement measured by the LVDTs. Between the 1^{st} and 2^{nd} cycle to $\mu_\Delta = 4.0$ one LED at the bottom corner fell off, therefore the increase in the base crack and sliding components, which were then determined from the second row markers. Note that the displacement at first yield was larger than at $\mu_\Delta = 1.0$, hence the kink in the graph.

4.5.4 Cracks

The monitored cracks as well as the complete crack pattern are presented in Figure 4.61. Table 4.4 summarizes the widths of some of the cracks at certain load steps. Cracks that were already visible but too narrow to determine their widths are indicated with < 0.05. Figure 4.61 also shows how cracks were numbered and along which pattern their widths were determined.

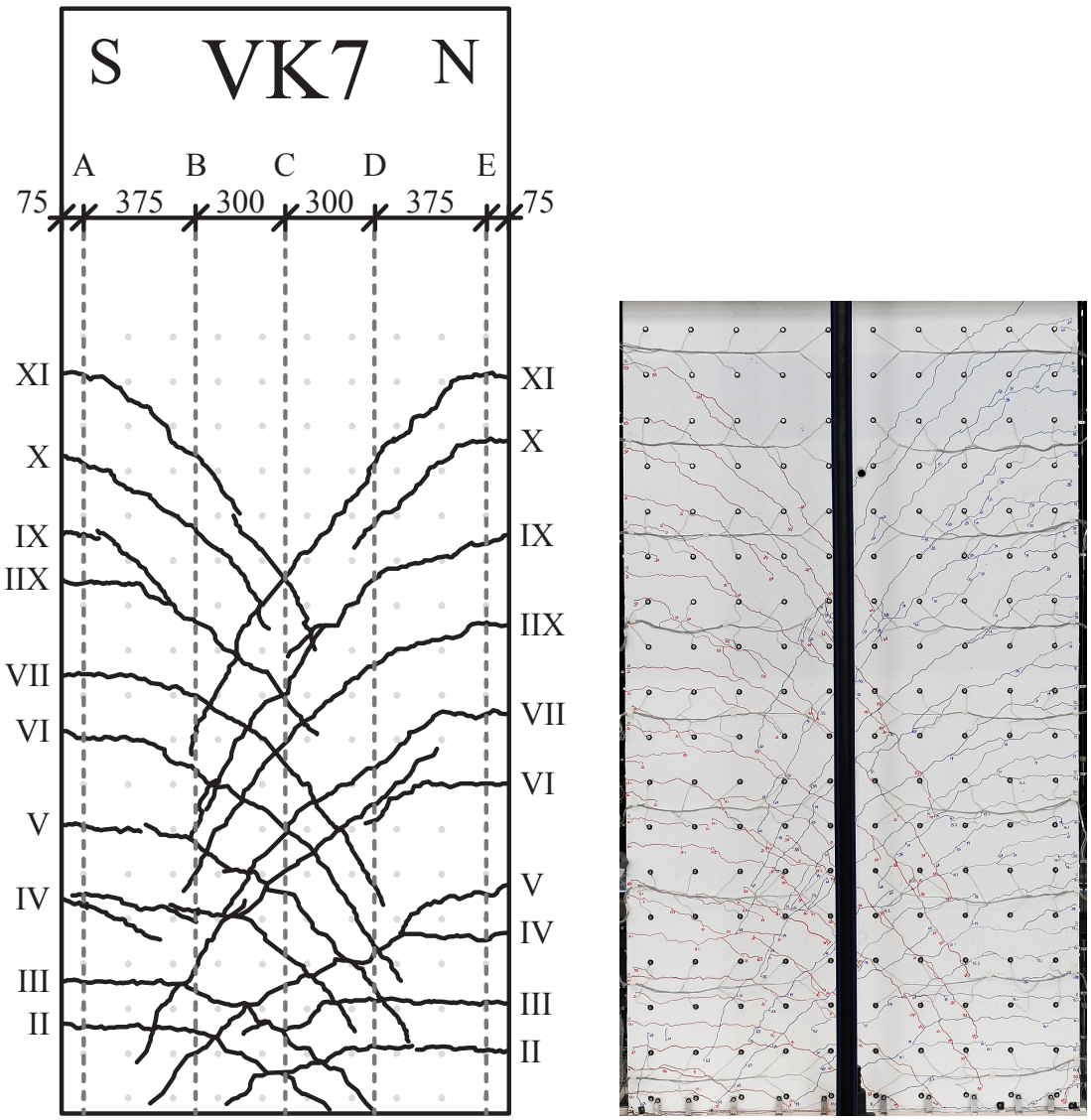

Figure 4.61: Drawing of monitored cracks (left) and picture of complete crack pattern (right) of test unit VK7.

		Crack widths [mm]										
		1^{st} cycles South						1^{st} cycles North				
		A	B	C	D	E		A	B	C	D	E
$1.0F'_y$						0.05		0.1	0.1	0.1		
$2.0\mu_\Delta$			0.05	0.1	0.15	0.05		0.25	0.15	0.25		
$3.0\mu_\Delta$	IV		0.1	0.1	0.25	0.5	III	0.75	0.3	0.35		
$5.0\mu_\Delta$			0.1	0.1	0.55	0.8		1.4	0.9	0.75		
$7.0\mu_\Delta$			0.1	0.1	0.15	0.35		0.4	0.35	0.15		
$1.0F'_y$				0.1	0.1	<0.05		0.05	<0.05	0.05		
$2.0\mu_\Delta$			<0.05	0.2	0.25	0.05		0.1	0.05	0.2		
$3.0\mu_\Delta$	VII		0.05	0.4	0.3	0.25	VII	0.15	0.1	0.35		
$5.0\mu_\Delta$			0.45	0.55	0.4	0.05		0.15	0.1	0.4	0.05	
$7.0\mu_\Delta$			0.4	0.75	0.35	0.1		0.05	0.1	0.35		

Table 4.4: Monitored cracks of test unit VK7 and widths of some of them.

4.6 Comparison of Deformation Components

In Figures 4.62 and 4.63 the ratios of the deformation components of all test units at the end of the shear span a are presented. All ratios were calculated using the corrected top displacement from the LVDT measurements and the deformation components determined from the optical and manual measurements, respectively. Above the measurement grid, a linear curvature profile between the end of the shear span (zero curvature) and the center of the last two measurement rows was assumed. The shear strains above the grid were assumed to be constant and equal to the mean shear strains of the last two rows of the grid. The mean curvature and shear strain of the last two measurement rows were used because the strains are rather small in the upper part of the pier and the accuracy should be increased by averaging the data. In Figure 4.62a the sliding (sl) and the sum of sliding and shear deformation are plotted and in Figure 4.62b the deformation resulting from the base crack (bcr) and the sum of base crack and flexural (flex) deformation are plotted. Both deformation components in Figure 4.62a can be regarded as shear components and those in Figure 4.62b as flexural components. The sum of both was plotted to improve comparability, since the single components are sometimes difficult to separate. If a second crack is opening up under the first row of the measurement devices, its deformation component is ascribed to the base crack, for instance. Up to $0.5F_y'$ the strains were very small, reaching the limits of the measurement systems, therefore especially the shear deformations sometimes seem unreliable (see for instance VK5, where the shear deformation ratio at $0.5F_y'$ is negative). However, for the sake of completeness, they have been included in the graphs. Not included are the measurements of VK4 at 0.5 and $0.75F_y'$ South 1^{st}, because some LEDs in the bottom row yielded questionable results. The displacement components of VK4 are only presented up to the first cycles to $\mu_\Delta = \pm 3.0$, because the lap splice was severely damaged afterwards and therefore determining reasonable components seemed hardly possible.

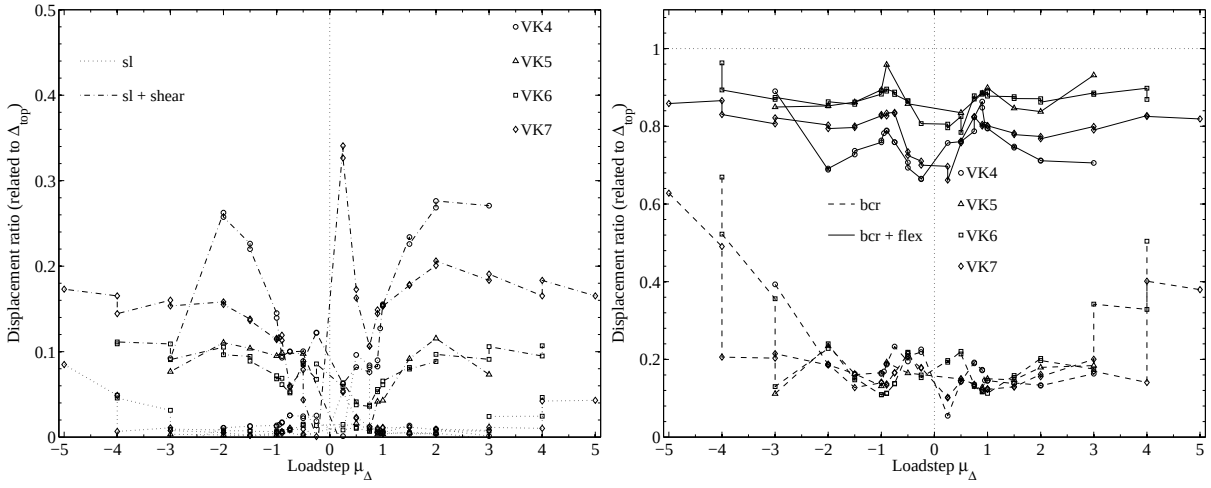

(a) Sliding (sl) and shear deformation

(b) Base crack (bcr) and flexural (flex) deformation

Figure 4.62: Ratio of deformation components related to top displacement at 1^{st} and 2^{nd} cycles (VK5 only 1^{st}) plotted against the load steps. Note that μ_Δ refers to the load steps used in the experiments and not to actual displacement ductilities.

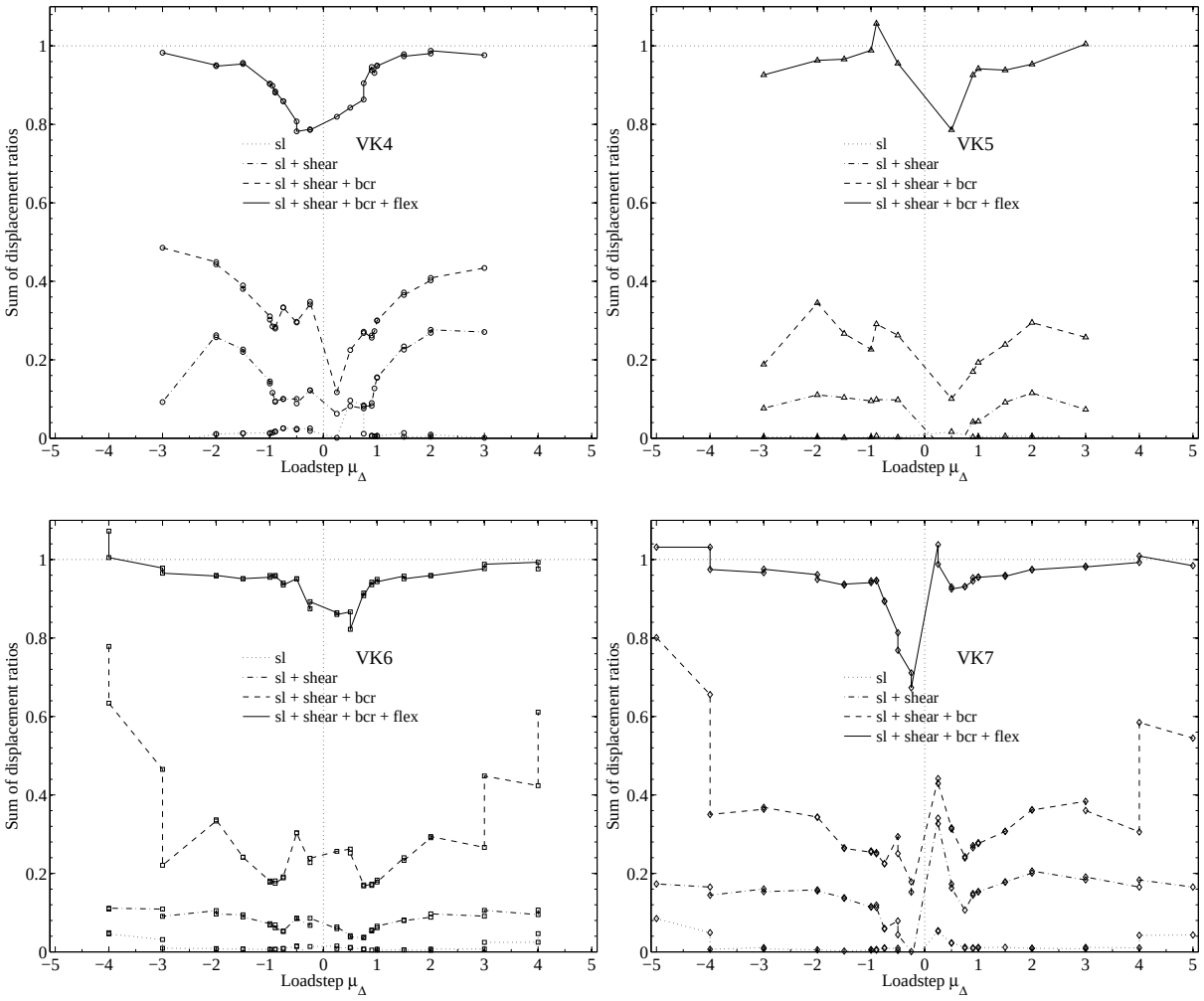

Figure 4.63: Sum of all deformation components of all test units at 1^{st} and 2^{nd} cycles (VK5 only 1^{st}) plotted against the load steps. Note that μ_Δ refers to the load steps used in the experiments and not to actual displacement ductilities.

Summary

Four reinforced concrete piers were tested quasi-statically under reversed cyclic loading in the laboratory of the Institute of Structural Engineering (IBK) at the Swiss Federal Institute of Technology (ETH), Zurich. The piers represent bridge piers with seismic detailing deficiencies, such as lap splices in potential plastic hinge regions and low transverse reinforcement ratios, as they were for instance commonly built in Switzerland before the introduction of modern seismic codes. The piers were constructed in half-scale and tested in single bending until either the axial force bearing capacity was lost or a residual horizontal force resistance was reached. A loading history with two cycles to each target force and displacement, respectively, and small intermediate cycles in the inelastic range was chosen.

Varied parameters comprise the shear-span-to-depth ratio ($a/d = 2.2$ or 3.0), the transverse reinforcement ratio ($\varrho_t = 0.08\,\%$ or $0.22\,\%$) and the detailing of the longitudinal reinforcement (spliced in the bottom region or continuous). The cross section of all piers was 35 cm wide and 150 cm long with 42 longitudinal reinforcement bars $d_l = 14$ mm made of ductile hot-rolled steel, resulting in a reinforcement ratio of $\varrho_l = 1.23\,\%$. Transverse reinforcement was provided by $d = 6$ mm stirrups with 90° hooks that were either spaced 200 mm (VK4 through VK6) or 75 mm (VK7) apart, resulting in $\varrho_t = 0.08\,\%$ and $\varrho_t = 0.22\,\%$ reinforcement ratio, respectively.

In the following paragraphs, the main observations and results are summarized. Note that also here μ_Δ refers to the theoretical displacement ductility used during the tests, which was the same for piers with equal aspect ratio, and not the experimentally determined displacement ductility.

Main Observations

Test unit VK4, with $a/d = 2.2$, $\varrho_t = 0.08\,\%$ and a lap splice at the bottom was able to sustain the full axial load until the end of the test. The maximum horizontal load of 913 kN, corresponding to 3014 kNm base moment, was reached at the first cycle to $\mu_\Delta = 3.0$ South. At this load step, vertical cracks were visible in the compression zone, which led to failure of some splices under reversed loading. Before $\mu_\Delta = 3.0$ North was reached, the horizontal force suddenly dropped significantly due to splice failure. Some vertical cracks were visible in the region where the splice was under tension, the concrete cover had begun to fall off and some regions sounded hollow due to internal cracks in the splice region. During the next four half cycles the horizontal force dropped significantly and the concrete cover above the splice was almost completely loose near the end of the test. Before splice failure initiated, the largest crack widths were measured for the shear cracks in the center of the pier (max. 1.2 mm) and above (max. 2.5 mm) and below (max. 1.6 mm) the splice.

Test unit VK5, with $a/d = 3.0$, $\varrho_t = 0.08\,\%$ and a lap-splice at the pier base was also able to sustain the axial load until the end of the test. Its maximum absolute horizontal force of -639 kN, resulting in -2876 kNm base moment, was applied at the first peak at $\mu_\Delta = 2.0$ North. At this cycle the first vertical crack along a splice under tension at the South face developed and during the second loading towards $\mu_\Delta = 2.0$ North the next one formed. Before $\mu_\Delta = 3.0$ South was reached the first time, the first splices at the North side of the pier failed and the horizontal force dropped. Contrarily to VK4 in this case splice failure was not initiated by visible damage of the concrete under compression. The maximum horizontal force was lower than that of pier VK6 without splice, where the maximum force was applied at $\mu_\Delta = 3.0$ in positive loading direction. Similar to VK4, the horizontal force dropped to a residual level within a few cycles. The observations regarding the cracks were similar to VK4.

Test unit VK6, which was a variation of VK5 with continuous reinforcement, lost its axial force bearing capacity and horizontal force resistance during loading towards $\mu_\Delta = 7.0$ North. The maximum force was reached at $\mu_\Delta = 3.0$ South with 675 kN, corresponding to 3036 kNm base moment. In the following cycles the compression zones were gradually damaged and mainly the inclined shear cracks in the center part of the pier were opening. Eventually there was a triangular concrete wedge left in the center of the pier, shaped by the shear cracks, around which the pier seemed to rotate. While the top displacement was increased towards $\mu_\Delta = 7.0$ North, the reinforcement bars around the cone began to buckle and there was not enough undamaged concrete left to carry the axial load.

Test unit VK7, with continuous reinforcement, $a/d = 2.2$ and $\varrho_t = 0.22\,\%$ abruptly lost its total force bearing capacity during the cycle at $\mu_\Delta = 9.0$. It reached its maximum force of 903 kN, resulting in 2978 kNm base moment, at $\mu_\Delta = 3.0$ South. Compared to VK6, the strains at the bottom of the pier were more evenly distributed and not as much concentrated in a few cracks. The largest crack widths were measured for the flexural cracks in the lower part of the pier. Degradation of the horizontal force was very slow and also the compression zones were initially degrading slowly. From $\mu_\Delta = 6.0$ onwards, degradation of the compression zones increased and finally, while loading to $\mu_\Delta = 9.0$ North for the first time, the concrete was too damaged and both horizontal and vertical load resistance were suddenly completely lost.

Force-deformation envelopes

Figure 5.1a shows the measured force-deformation envelopes of the first and second cycles of all test units with aspect ratio $a/d = 2.2$ and Figure 5.1b those of the units with $a/d = 3.0$.

Failures

In Figure 5.2 pictures of the bottom part of all test units after failure are presented.

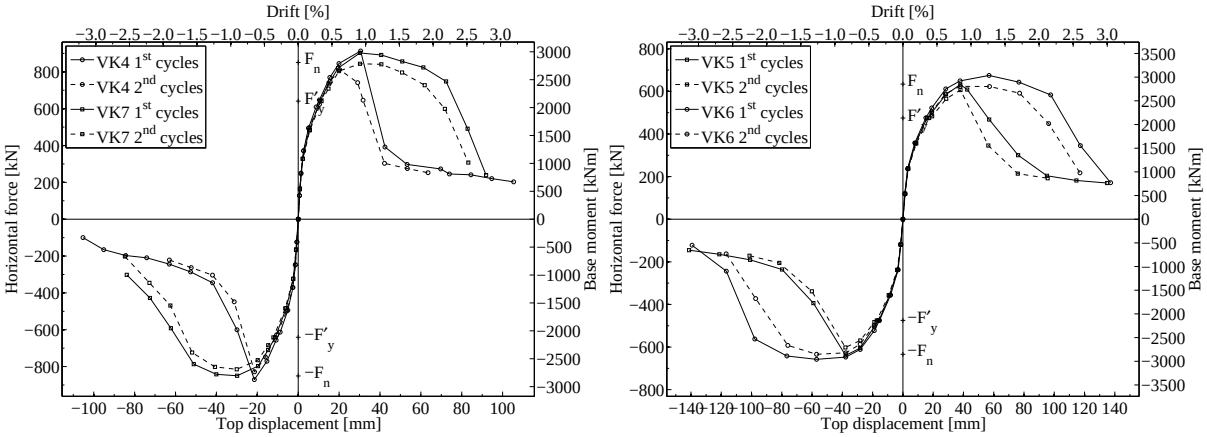

(a) VK4 and VK7 with aspect ratio 2.2 **(b)** VK5 and VK6 with aspect ratio 3.0

Figure 5.1: Measured force deformation envelopes of all test units.

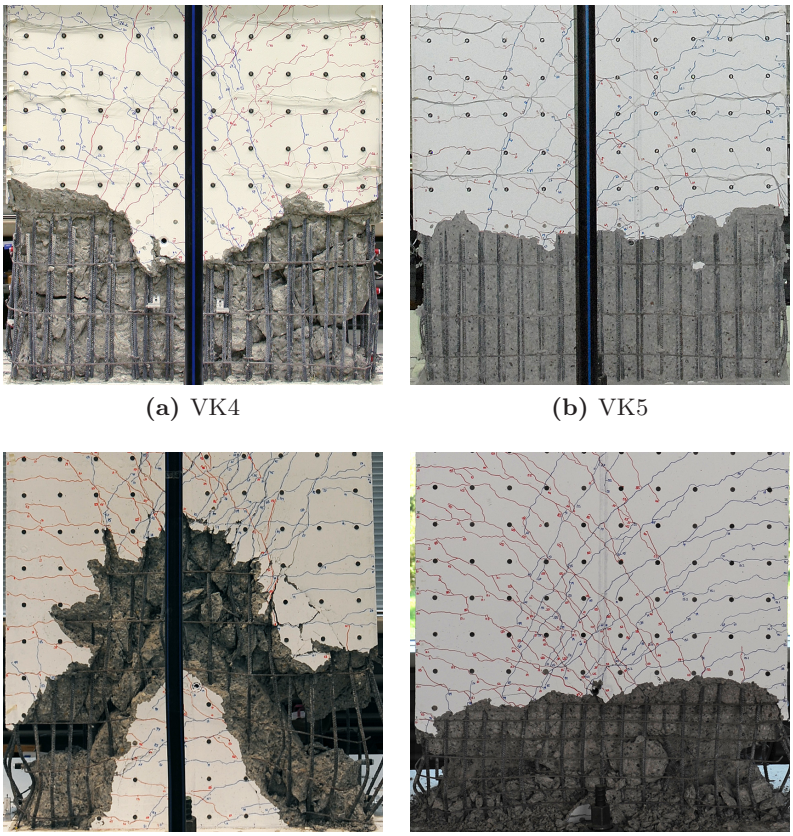

(a) VK4 **(b)** VK5

(c) VK6 **(d)** VK7

Figure 5.2: Pictures of all test units after the end of the test.

Crack patterns

In Figure 5.3 pictures of all test units with fully developed crack patterns are depicted.

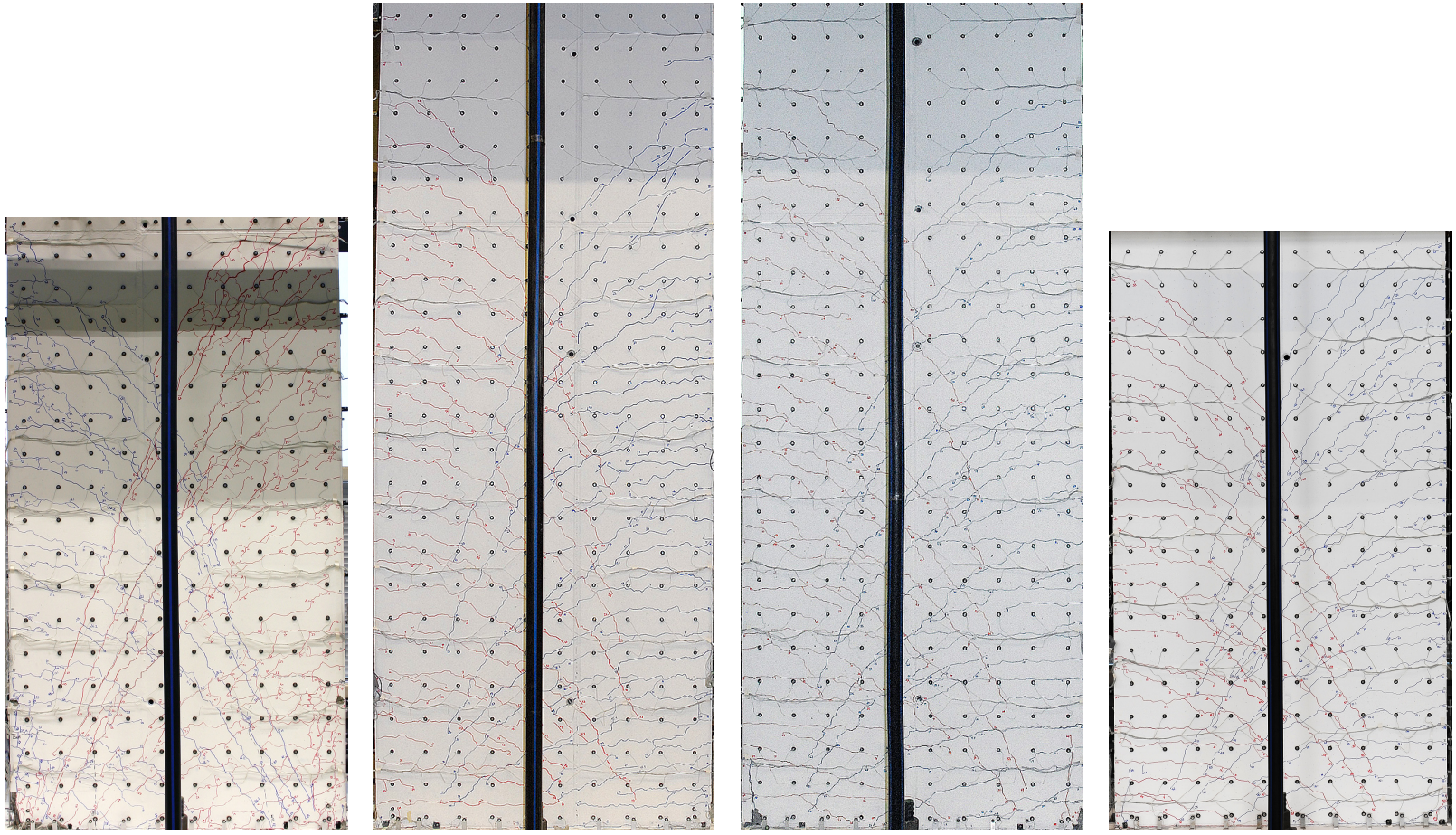

(a) VK4 **(b)** VK5 **(c)** VK6 **(d)** VK7

Figure 5.3: Pictures of all test units with fully developed crack patterns before lap splice degradation and spalling of concrete in the compression zones initiated.

Zusammenfassung

Am Institut für Baustatik und Konstruktion (IBK) der Eidgenössischen Technischen Hochschule Zürich wurden vier Modelle von Brückenstützen aus Stahlbeton im Massstab 1:2 unter quasi-statischer Einwirkung getestet. Die Versuchskörper repräsentieren Brückenstützen mit Konstruktionsdetails, wie beispielsweise Übergreifungsstösse in potentiellen plastischen Gelenkregionen und geringe Querbewehrungsgrade, die bei einer modernen Bemessung für seismische Einwirkung heute vermieden werden. Viele der z.B. in der Schweiz bestehenden Brückenstützen wurden jedoch vor der Einführung neuerer Normengenerationen mit eben solchen Details gebaut. Die Stützen wurden quasi-statisch unter einfacher Biegung getestet, bis entweder die Normalkraft nicht mehr aufgenommen werden konnte oder eine Resttragfähigkeit der Horizontalkraft erreicht wurde. Als Belastungsgeschichte wurde eine zyklische Belastung mit zwei Zyklen je Laststufe und kleineren dazwischen eingeschobenen Zyklen im inelastischen Bereich gewählt.

In der Versuchsreihe wurden die folgenden Parameter variiert: die Schubschlankheit ($a/d = 2,2$ oder 3,0), der Querbewehrungsgehalt ($\varrho_t = 0,08\,\%$ oder 0,22 %) und die Ausführung der Längsbewehrung (durchgängig oder mit Übergreifungsstoss am Stützenfuss). Alle Stützen hatten die gleichen 35 cm breiten und 150 langen rechteckigen Querschnitte sowie die gleiche Längsbewehrung. Für die Längsbewehrung wurden 42 Stäbe aus hochduktilem, warm gewalztem Stahl mit 14 mm Durchmesser verwendet, was einem geometrischen Bewehrungsgehalt von 1,23 % entspricht. Die Bügel hatten 6 mm Durchmesser und wurden mit 90°- Haken geschlossen. Bei VK4 bis VK6 betrug der Bügelabstand s = 200 mm und bei VK7 s = 75 mm, was Querbewehrungsgehalten von $\varrho_t = 0,08\,\%$ bzw. $\varrho_t = 0,22\,\%$ entspricht.

In den folgenden Abschnitten werden die wichtigsten Beobachtungen und Resultate der Versuche zusammengefasst. Dabei ist zu beachten, dass sich μ_Δ auch im Folgenden auf die für die Versuche gewählten Laststufen und nicht auf die aus den Experimenten ermittelten Verschiebeduktilitäten bezieht.

Beobachtungen während der Versuche

Versuchskörper VK4 mit $a/d = 2,2$, $\varrho_t = 0,08\,\%$ und einem Übergreifungsstoss am Fuss der Stütze konnte die gesamte Normalkraft bis zum Ende des Versuches tragen. Die horizontale Maximalkraft von 913 kN, aus welcher ein Biegemoment von 3014 kNm am Fuss der Stütze resultiert, wurde bei der ersten Auslenkung nach $\mu_\Delta = 3,0$ Süd erreicht. Bei dieser Laststufe waren an der Südseite am Fuss der Stütze vertikale Risse im Druckbereich zu sehen, was zum Versagen einiger Stösse in der entgegengesetzten Belastungsrichtung führte. Die Horizontalkraft fiel auf Grund dessen vor dem Erreichen von $\mu_\Delta = 3,0$ Nord deutlich ab. In dem zugebanspruchten Bereich des Bewehrungsstosses waren vertikale Risse sichtbar, die Bewehrungsüberdeckung war teilweise abgefallen und einige Bereiche des Stosses hörten sich beim Daraufklopfen hohl an, was auf innere Risse zwischen den Längsbewehrungsstäben hindeutete. Während der folgenden vier Halbzyklen

fiel die Horizontalkraft weiter deutlich ab und die Bewehrungsüberdeckung über dem Stossbereich war schlussendlich nahezu vollständig lose. Bevor das Versagen des Stosses einsetzte, wurden die grössten Rissweiten bei den Schubrissen in der Mitte des Versuchskörpers (max. 1,2 mm) sowie oberhalb (max. 2,5 mm) und unterhalb (max. 1,6 mm) des Stosses gemessen.

Versuchskörper VK5 mit $a/d = 3,0$, $\varrho_t = 0,08\,\%$ und einem Übergreifungsstoss am Fuss der Stütze konnte ebenfalls die gesamte Vertikalkraft bis zum Ende des Versuches tragen. Der absolute Maximalwert der Horizontalkraft trat mit -639 kN bei der ersten Belastung nach $\mu_\Delta = 2,0$ Nord auf und entspricht einem Biegemoment von 2876 kNm am Fuss der Stütze. Bei dieser Laststufe bildete sich auch der erste Vertikalriss entlang eines Stosses unter Zug an der Südseite der Stütze, bei der zweiten Belastung nach $\mu_\Delta = 2,0$ Nord bildete sich auf der gegenüberliegenden Seite der Nächste. Bevor die folgende Laststufe $\mu_\Delta = 3,0$ Süd erreicht wurde, versagten die ersten Stösse auf der Nordseite der Stütze und die Horizontalkraft fiel ab. Im Gegensatz zum Versuch VK4 wurde in diesem Fall das Versagen des Stosses nicht durch eine sichtbare vorhergehende Schädigung des Betons unter Druck eingeleitet. Ähnlich wie bei VK4 fiel auch hier die Horizontalkraft innerhalb weniger Zyklen auf eine verbleibende Restkraft ab. Die Beobachtungen bezüglich der Rissweiten waren ähnlich denen bei VK4.

Versuchskörper VK6, der eine Variation von VK5 mit durchgängiger Längsbewehrung darstellte, konnte sowohl Horizontal- als auch Vertikalkraft während des Aufbringens der Belastung nach $\mu_\Delta = 7.0$ Nord plötzlich nicht mehr aufnehmen. Die maximale Horizontalkraft von 675 kN, mit zugehörigem Biegemoment von 3036 kNm, wurde bei $\mu_\Delta = 3.0$ Süd erreicht. In den folgenden Zyklen wurden die jeweiligen Betondruckzonen fortlaufend geschädigt und die grössten Rissöffnungen traten bei den Schubrissen in der Mitte des Versuchskörpers auf. Schlussendlich hatte sich mittig am Stützenfuss ein durch die Schubrisse geformter dreieckiger Betonkeil gebildet, um den sich die Stütze zu drehen schien. Während die Belastung nach $\mu_\Delta = 7.0$ Nord aufgebracht wurde, begannen die im Riss um den Keil liegenden Längsbewehrungsstäbe auszuknicken und es war nicht mehr genügend ungeschädigter Beton vorhanden, um die Normalkraft aufzunehmen.

Versuchskörper VK7 mit $a/d = 2,2$, $\varrho_t = 0,22\,\%$ und durchgängiger Längsbewehrung verlor während des Zyklus bei $\mu_\Delta = 9,0$ schlagartig den gesamten Tragwiderstand. Der Versuchskörper erreichte die maximale Belastung mit 903 kN Horizontalkraft und 2978 kNm Biegemoment bei $\mu_\Delta = 3,0$ Süd. Im Vergleich zu VK6 waren bei diesem Versuchskörper die Dehnungen im unteren Bereich der Stütze gleichmässiger verteilt und nicht nur auf einige wenige Risse konzentriert. Die grössten Rissweiten wurden bei den Biegerissen in diesem Bereich gemessen. Der Abfall des horizontalen Tragwiderstandes war relativ langsam und auch die Schädigung der jeweiligen Betondruckzonen schritt nur langsam voran. Ab $\mu_\Delta = 6,0$ war eine deutlicher fortschreitende Schädigung der Betondruckzonen zu beobachten, und während des Aufbringens der ersten Belastung nach $\mu_\Delta = 9,0$ Nord verlor die Stütze auf Grund dessen schlagartig ihre Horizontal- und Vertikaltragfähigkeit.

Umhüllende der Last-Verformungskurven

In Bild 5.4a sind die Umhüllenden der gemessenen Last-Verformungsbeziehungen aller ersten und zweiten Zyklen der Versuchskörper mit Schubschlankheit $a/d = 2,2$ dargestellt, in Bild 5.4b jene der Versuchskörper mit $a/d = 3,0$.

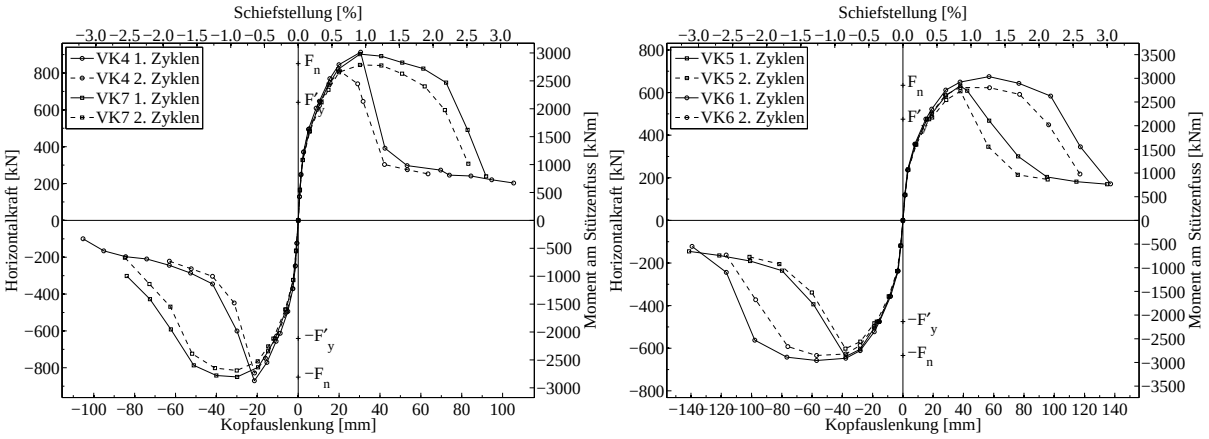

(a) VK4 und VK7 mit Schubschlankheit 2,2

(b) VK5 und VK6 mit Schubschlankheit 3,0

Bild 5.4: Umhüllende der gemessenen Last-Verformungsbeziehungen aller Versuchskörper.

Versagen

In Bild 5.5 sind die Fotos der unteren Bereiche aller Versuchskörper nach dem Versagen dargestellt.

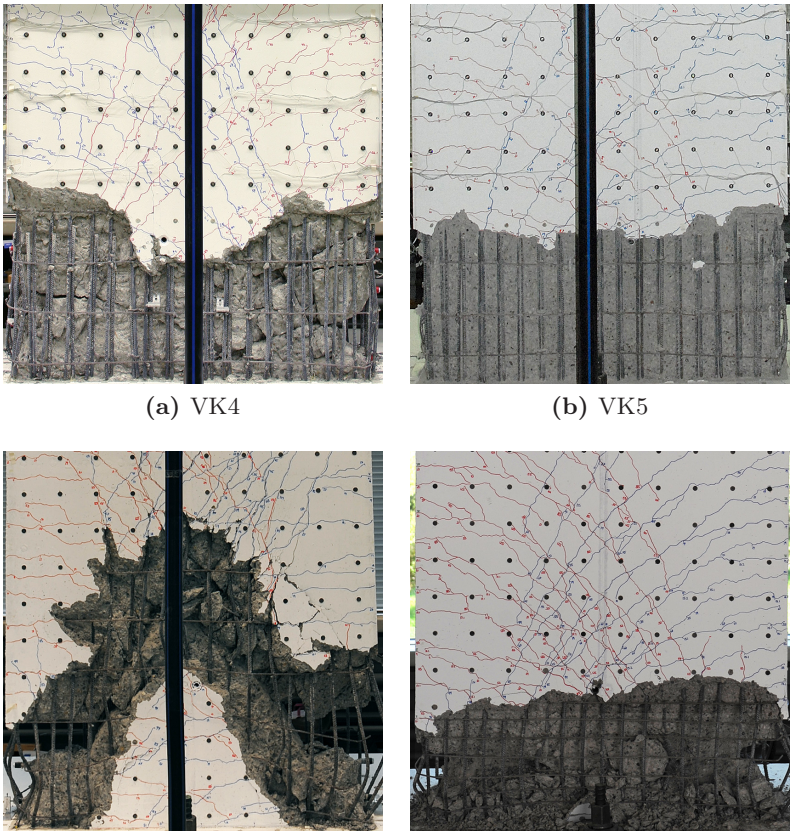

(a) VK4 **(b)** VK5

(c) VK6 **(d)** VK7

Bild 5.5: Bilder aller Versuchskörper nach dem Ende der Tests.

Rissmuster

In Bild 5.6 sind die Fotos aller Versuchskörper mit vollständig ausgebildetem Rissmuster dargestellt.

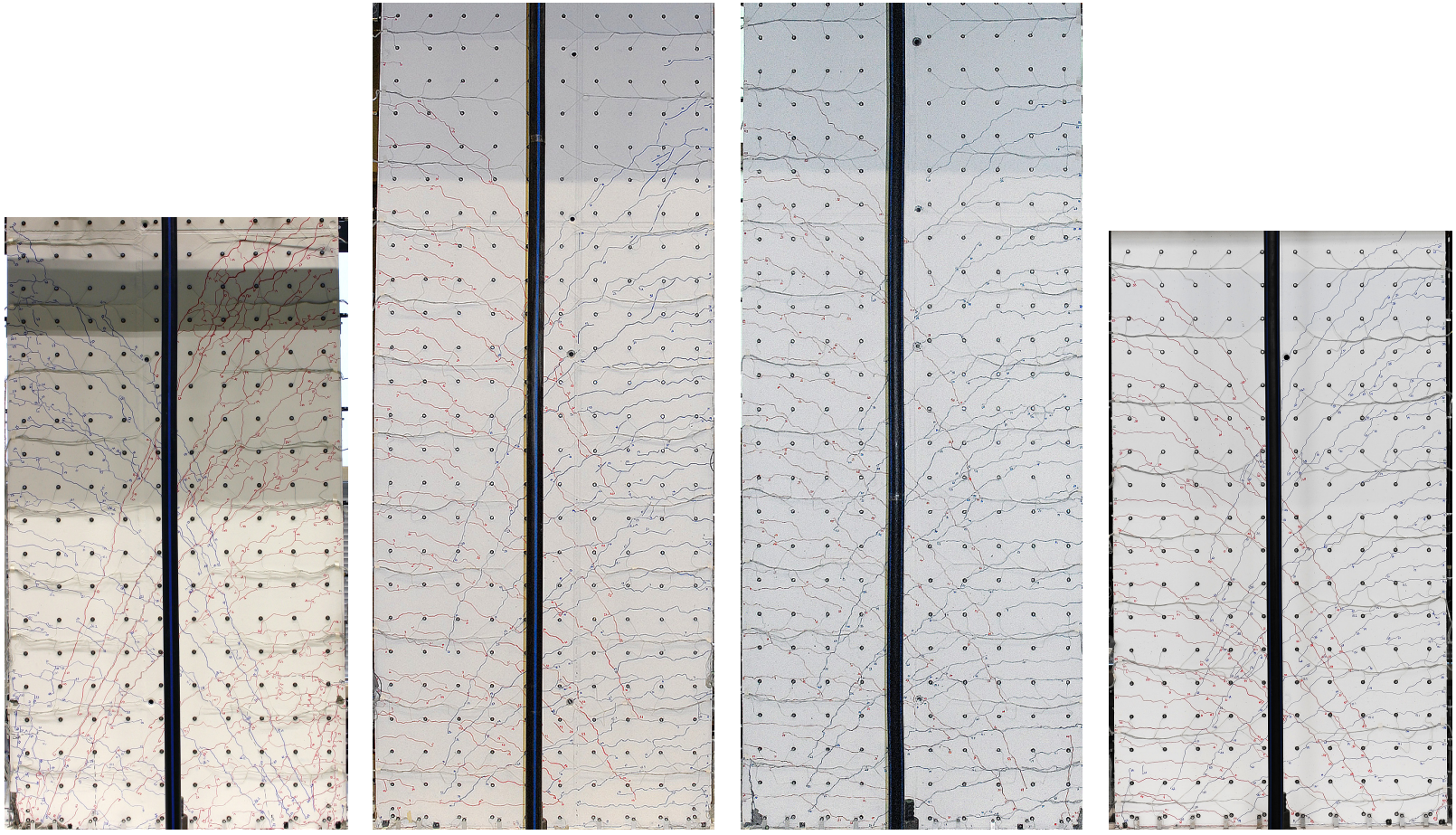

(a) VK4 **(b)** VK5 **(c)** VK6 **(d)** VK7

Bild 5.6: Bilder aller Versuchskörper mit vollständig ausgebildetem Rissmuster bevor die Schädigung der Stösse und der Betondruckzonen einsetzte.

Acknowledgements

The experiments documented in this report were conducted in the framework of the Federal Roads Office (FEDRO) research project number AGB2008/001: "Seismic Safety of Existing Bridges – Cyclic Inelastic Behaviour of Bridge Piers". The financial support as well as the informed advice and interest of all members of the FEDRO advisory committee BKC is gratefully acknowledged.

Stüssi AG (Dällikon, Switzerland) built all test units, Holcim AG delivered the concrete for the piers and Stahl Gerlafingen AG the longitudinal reinforcement. NDI Europe lend a second position sensor for testing the taller piers. All these companies are thanked for their good collaboration.

The assistance of the staff of the laboratory of the Institute of Structural Engineering (IBK) at ETH Zurich during the preparation and testing was essential for the successful completion of the tests. Especially noteworthy are Dominik Werne, who provided invaluable help with all measurement instrumentations as well as Thomas Jaggi and Christoph Gisler, who helped assembling the test setup and the test units. Matthias Wielatt, Seraina Burger, Katrin Zimmermann, Maja Messerli, Adrian Pöllinger, Xiaoshu He and Jörg Donau helped with measurements and preparation of the test units. Sincere thanks are given to them all.

Notation and Abbreviations

Upper case Latin letters

A_{gt}	percentage elongation at maximum force
A_t	percentage total elongation at fracture
E_c	modulus of elasticity of concrete
E_s	modulus of elasticity of steel
F'_y	first yield force
F_n	nominal yield force
M'_y	first yield moment
M_n	nominal yield moment

Lower case Latin letters

c_{nom}	cover of reinforcement
$f_{c,cube}$	cube compressive strength of concrete
$f_{c,cyl}$	cylinder compressive strength of concrete
$f_{ct,3Pb}$	tensile strength of concrete from three point bending test
$f_{ct,dp}$	tensile strength of concrete from double punch test
$f_{s,u,dyn}$	dynamic tensile strength of reinforcing steel
$f_{s,u,stat}$	static tensile strength of reinforcing steel
$f_{s,y,dyn}$	dynamic yield strength of reinforcing steel
$f_{s,y,stat}$	static yield strength of reinforcing steel

Lower case Greek letters

Δ'_y	first yield displacement
Δ_y	nominal yield displacement
Δ_u	ultimate displacement
$\varepsilon_{c,cu}$	strain at compressive strength of concrete
$\varepsilon_{s,h}$	reinforcing steel strain at onset of hardening

$\varepsilon_{s,y}$	yield strain of reinforcing steel
ε_x, ε_y	strain in x- and y-direction, respectively
ε_1, ε_2	principal strains
ϕ'_y	first yield curvature
ϕ_y	nominal yield curvature
ϕ_u	ultimate curvature
ϱ_l	geometric longitudinal reinforcement ratio
ϱ_t	geometric transverse reinforcement ratio
ρ	density
γ_{xy}	shear strain
μ_Δ	displacement ductility, OR: in this report mainly used as experimental load step

Abbreviations

LED	Light Emitting Diode, i.e. markers of the optical measurement system
LS	Load Step
LVDT	Linear Variable Differential Transformer

Bibliography

[Bim10] Bimschas, M., "Displacement-based seismic assessment of existing bridges in regions of moderate seismicity", Ph.D. thesis, Institute of Structural Engineering, Swiss Federal Institute of Technology Zurich, 2010.

[CY80] Chen, W.F., Yuan, R.L., "Tensile strength of concrete: Double-punch test", *ASCE Journal of the Structural Division*, vol. 106(8), pp. 1673–1693, 1980.

[NDI09] NDI, *Optotrak Certus HD*, Northern Digital Inc., Waterloo, Ontario, Canada, http://www.ndigital.com/industrial/certushd.php, 2009.

[PCK07] Priestley, M.J.N., Calvi, G., Kowalsky, M., *Displacement based seismic design of structures*, IUSS Press, Pavia, Italy, 2007.

[Sei07] SeismoSoft, *SeismoStruct, Version 4.0.3.*, 2007, http://www.seismosoft.com.

[SIA56] SIA, "SIA162: Betonbauten", *Building code*, Swiss Society of Engineers and Architects, 1956.

[SIA68] SIA, "SIA162: Betonbauten", *Building code*, Swiss Society of Engineers and Architects, 1968.

[SIA89] SIA, "SIA162/1: Betonbauten Materialprüfung", *Building code*, Swiss Society of Engineers and Architects, 1989.

[SIA93] SIA, "SIA162: Betonbauten, Teilrevision 1993", *Building code*, Swiss Society of Engineers and Architects, 1993.

[SIA03] SIA, "SIA262: Betonbau", *Building code*, Swiss Society of Engineers and Architects, 2003.

[Sof10] Sofistik, *Sofistik AG, Oberschleissheim, Germany*, 2010, http://www.sofistik.com/index.php.